Dissertation

zu Erlangung des akademischen Grades eines

Doktors der Naturwissenschaften

der technischen Fakultät Universität Bielefeld

A

High Speed Sensor System

for

Tactile Interaction Research

---

vorgelegt von

Carsten Schürmann

Technische Fakultät,

Universität Bielefeld

November 2013

A

High Speed Sensor System

for

Tactile Interaction Research

von

Carsten Schürmann

Gutachter:
Prof. Dr. Helge J. Ritter
Prof. Dr. Marc O. Ernst

Prüfungsausschuss:
Prof. Dr. Ulrich Rückert
Prof. Dr. Helge J. Ritter
Prof. Dr. Marc O. Ernst
Dr. Thorsten Jungeblut

Vorgelegt am 14. November 2013
Verteidigt am 15. Dezember 2014

Gedruckt auf alterungsbeständigem Papier nach ISO 9706.

Acknowledgements

The work presented in this thesis was carried out in the Neuroinformatics Group, headed by Prof. Dr. Helge J. Ritter, at the Faculty of Technology, Bielefeld University. It was partially supported by the German Service Robotics Initiative (DESIRE) and by the German Cluster of Excellence 277 "Cognitive Interaction Technology" (CITEC).
There is a famous quote by Isaac Newton: "If I have seen further it is by standing on the shoulders of giants."
Likewise, this work would not have been possible without the help and support of many colleagues and friends.
First I would like to thank Helge Ritter, for giving me the opportunity to carry out my PhD in such an extraordinary scientific environment and stimulating group of researchers. Through his visionary ideas his students journey beyond the current frontiers of science and return with discoveries and inventions that bring man and machine closer together.
I want to thank Risto Kõiva, he was the best office mate and project partner that one can imagine, in addition to being a creative resource of unlimited technical knowledge.
I want to thank Gereon Büscher, a friend whose keen artistic eye helps to present *Myrmex* in the best light.
I also want to thank Robert Haschke, who is able to look through data and algorithms and uncover risks and opportunities that others might miss.
Additional thanks go to Jonathan Maycock for his down-to-earth views on good presentation, and all the exciting experiments that he carries out with the *Myrmex* system.
He is joined by likewise eager researchers: Matthias Schöpfer, Qiang Li, Abdeldjallil Naceri, Claudio Castellini - through your ingenious experiments with my *Myrmex* system you prove its utility and create a large scientific impact.
I started with a student job, did a diploma thesis and then a PhD in the Neuroinformatics Group, joined CITEC from the beginning - it was a real pleasure to do research in these enviroments, my thanks go to all present and former members.
I would also like to thank the members of the disputation committee, Prof. Dr. Ulrich Rückert, Prof. Dr. Helge J. Ritter, Prof. Dr. Marc O. Ernst, and Dr. Thorsten Jungeblut, for taking the time to review this work.
Last, but not least, I thank my wonderful family and friends for their support and encouragement during the whole work!

My hands as recorded with the Myrmex sensor.

Contents

Chapter

1

Introduction

1.1 Motivation

The research of tactile interaction is an emerging field in both human and robotic science. The tactile sense is so fundamental and ubiquitous that its importance is often overlooked. We are however suddenly reminded of its importance when it is missing. This has been vividly demonstrated in experiments where subjects were asked to perform manipulation tasks while their tactile sense was disabled by anesthetization, this proved to be extraordinary difficult [1, 2]. This result can also be backed by anyone who has at one point experienced frozen fingers and yet had to perform a manipulation task.

The term 'tactile interaction research' covers a vast field including interaction between humans and objects, robots and objects and also between human and robots. To facilitate research in these areas it is necessary to have the appropriate tools which allow us to monitor tactile interactions.

These monitoring tools come in the form of tactile sensors. The state of the art of artificial tactile sensing shows that it is still a dynamic field with many new developments and with no standard sensor yet which can truly mimic the human tactile sense [3–5]. The currently available tactile sensors are often designed for a very specific scenario, which may not be the scenario that the researcher is interested in. To monitor a tactile interaction it is necessary that the tactile sensor fulfills certain criteria like physical size, spatial and temporal resolution or sensitivity that are relevant for the scenario.

In this work we want to present a tactile sensor system as a tool to monitor tactile interactions in multiple scenarios. The scenarios that the system

should cover are the following:

- Robot grasping with slip detection
- Study of human finger forces, e.g. grasping of an object
- Tactile table for human robot interaction

We have selected these scenarios as in our view they provide good 'basis vectors' in three different directions of tactile interaction research and the corresponding sensor requirements are useful in many other scenarios.

From the three scenarios, we can derive the specific characteristics that the system has to fulfill:
For the robot grasping scenario, the sensors should be mountable on a robot arm and allow for grasping of everyday objects (e.g. a cup or a bottle) while delivering a very high frame-rate for slip detection. It has been found that humans detect slippage of an object through micro-vibrations, which occur when the object slides at microscopic distances and the contact alternates between stick and slip [6,7]. If we take a look at the frequencies that the tactile cells inside our fingertips can register, we find that up to 800Hz [8] are possible.
For the study of human finger forces it should be possible to assemble or attach the sensors in a way that a natural interaction with an object is possible. We argue that for a natural interaction multiple degrees of freedom to move / rotate the object and freedom of choice for the hand posture is necessary. We do not want to limit the subject in his grasp choice by having only predefined locations for placing the fingers on the object. We argue that using a tactile surface on an object allows also the study of the finger placement. To identify the fingers from the tactile data, the sensor system should have a reasonable spatial resolution (5mm or better).
For the tactile table scenario the sensor system should be able to cover an area which is large enough so that both hands can be placed on it, we aim for at least 300x300mm. To recognize objects or fingers on this surface we also aim for a spatial resolution of 5mm or better, which means having at least 3600 tactile elements (tactels) in total. To integrate the system into a robot setup it should also posses real time capabilities, that means with this amount of tactels it should have a frame rate of at least 30Hz.
For all scenarios it is advantageous if even small forces can get detected, so we also aim for a good sensitivity, the system should respond to pressures as low as 20kpA.

1.2 Main contributions of this work

In this work we will describe and implement the first tactile sensor system that combines the properties of modularity with a very high sensing speed, a high sensitivity and a high spatial resolution. This unique combination of features enables researchers to develop novel applications and makes it possible to replace task specific tactile sensors with a single system.

The very high sensing speed of the system allows for slip detection during robot grasping. And as all our sensor cells are sampled with the same high frequency, our system can even enable the slip detection for multiple contact points at the same time. This high speed was made possible through the development of a highly integrated parallel sensor sampling architecture.

The modularity of the system allows it to be employed in a multitude of applications. Tactile sensitive surfaces of various dimensions can be easily realized through a very simple 'plug and use' principle without the need for software configuration by the user. This was made possible by developing a new bus system that allows the relative localization of the participants. Our system can be used to create tactile sensitive table surfaces with a large amount of sensor cells and due to its high speed design still provide for real time frame rates.

The flexibility and high performance of the system enabled us to develop a tactile sensitive object that allows the continuous high speed monitoring of human finger forces. For this we solved the problem of integrating the tactile sensors to allow free movement of the object, while maintaining a constant high rate of data capture and realizing a low latency synchronization to external devices.

The high sensitivity of the system was made possible through technical innovation in the state of the art of resistive based tactile sensors. We did so by creating an optimized sensor cell shape and investigating the behavior of different sensor materials. The knowledge gained in this process was further used to advance the existing method of sensor normalization into a real time method.

1.3 Relationship to previous work

A precursor of the system presented in this work has been published by the present author in [9]. There were two parts that were used as a basis for our current system, one is the implementation of the USB Video protocol (see section 3.5.1) in the 'central unit' device (see section 3.5) and the circuit design of the sensor top PCB (see section 3.3) where the sensor electrodes have been redesigned.

1.4 Organization of this work

In this chapter we have laid out the motivation and the scientific impact of this work. In the next chapter we will look at the background and related work: how tactile sensing unfolds in nature and what advances have been made in the creation of artificial tactile sensing.
Our ideas for a high performing tactile sensor system will be realized in form of the *Myrmex* system, which will be described in detail in chapter 3.
In chapter 4 we will present with the 'tactile book' a tactile sensitive object made with this system which can be used for manipulation research.
The sensor response of the *Myrmex* system under various conditions will be evaluated in chapter 5.
In chapter 6 we will present several scientific applications that have been successfully realized with our tactile sensor system.
Finally in chapter 7 we will recapitulate our work and give a conclusion and outlook.

Chapter

2

Background and Related Work

2.1 Tactile sensing in nature

Tactile cells

The tactile sense in its broadest definition can be considered to be the most ancient of all senses. The capability to detect mechanical stress caused by contact with other objects or due to external pressure is such an important feature, that it is present in the cells of almost all organisms, in prokaryotes, eukaryotes and even archaebacteria [12–14]. A very basic method of such sensing is a mechanosensitive channel as found in the bacteria E. Coli (depicted in Fig. 2.1). For the bacterium it acts like an emergency release valve and allows the regulation of cell volume as a reaction to stress occurring from osmosis and thus prevents lysis of the cell. If such stress is detected, e.g. the medium of the bacterium is diluted, the bacterium releases its solutes. Otherwise the diffusion of water into the cell would stretch the membrane beyond its capabilities. If the medium returns back to normal, the channel closes and protein synthesis is restarted in the cell. It is argued that this may be the evolutionary basis from which higher forms of mechanosensation have evolved. [13–15]

In multicell organisms there are highly specialized cells for detecting even the tiniest intendation, vibrations of different frequences or stretching in various angles. These mechanoreceptor cells can be found inside the skin, attached to hair follicles or inside the body in the muscles or joints for proprioception. The detailed molecular processes that convert the external force into an electrical or chemical signal in most of these specialized cells are still not thoroughly explored. But the involvement of transduction channels, similar to those of the bacterium, is considered highly likely for most. A general model

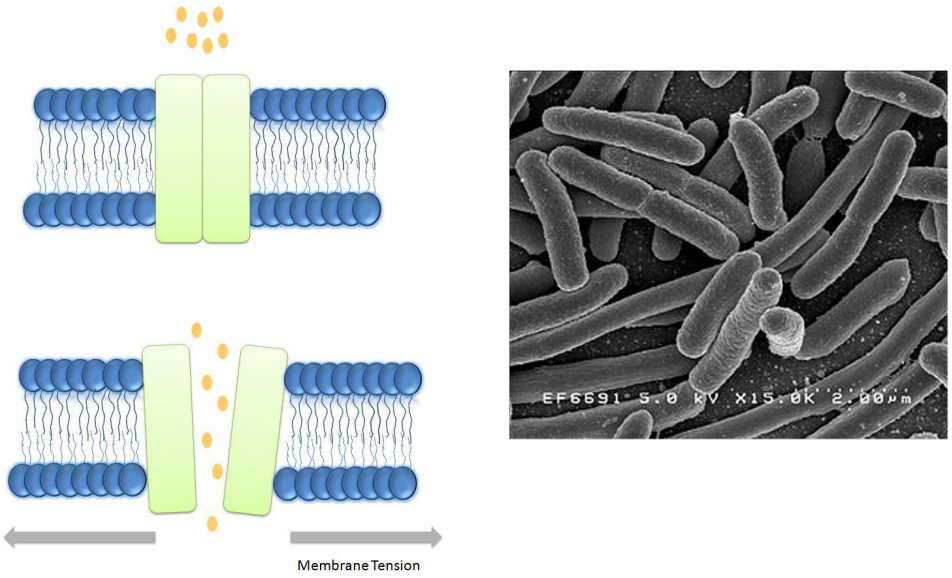

Figure 2.1: Scheme of a mechanosensitive ion channel in the bacteria Escherichia Coli. When the cell membrane is under tension, the channel opens and allows the passage of ions. Image sources: [10, 11]

of mechanosensory transduction which is found in many mechanoreceptors is shown in Fig. 2.2. In this model, the opening of the ion channel depends not so much on the tension of the cell membrane, but on the displacement of an extracellular anchor that is connected to the channel. The variability in the properties of this anchor, together with the variable length and elasticity of the intra and extracellur links allow the creation of cells that are sensitive to different forms and a wide range of force input. The force input on the anchor leads to an opening of the transduction channel, which allows the passing through of ions, which then leads to a change in the potential of the cell. From this follows a cell response such as an action potential being created at the cell membrane and the subsequent release of an electrical signal, like into the nervous system of vertrebraes. Through this method, the mechanoreceptors can respond to mechanic stimulus within a few milliseconds. [15, 16]

Tactile sensing in plants

As the sense of touch is of such importance, even stationary organisms like plants are equipped with tactile cells. The cells in a plant have to sense turgor and wall integrity, and sub-cellular organelles can translocate in response to

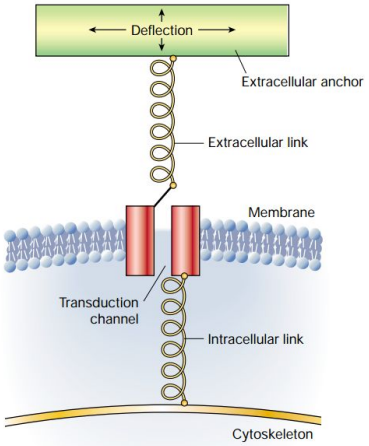

Figure 2.2: General model of a mechanosensory transduction channel in a mechanoreceptor cell. A transduction channel is attached to the cytoskeleton and to an extracellular structure by intracellular and extracellular links. The force acting on the extracelluar anchor changes the tension of the intracelluar and extracelluar links. Through this, the opening of the transducer channel is regulated. Image source: [15]. Reprinted by permission from Macmillan Publishers Ltd: Nature vol. 413, copyright 2001.

mechanical perturbations. Touch responses of plants can even be surprisingly fast, as in the famous venus flytrap, where the repeated stimulation of one or more of the trigger hairs (the repetition filters for living objects) leads to a snap response and traps the insectoid prey inside the plant. A similar fast, but defensively oriented response is known from the mimosa plants (Fig. 2.3), which fold their leaflets inwards within seconds when touched. This touch response is not restricted to the stimulated leaflet, but can propagate to all the neighboring leaflets of the leaf. The goal of the fast folding of the leaflets may be to scare away predators and make the plant appear as a smaller meal. [17, 18]

An area of intense tactile sensing in all plants are their roots, the investigation of this property was pioneered by Charles Darwin [21]. The caps of plant roots are equipped with special mechanoreceptor cells to register touch and gravity. Through these stimuli their growth is guided downwards while avoiding obstacles encountered in the soil. It has been shown in experiments with the plant Arabidopsis Thaliana, that an encounter with an obstacle leads causes the root to form 90° bends and proceed in a step wise growth. [22]

Figure 2.3: The plant mimosa pudica uses small mechanoreceptor cells (red) to detect touch and subsequently folds its leaflets inward for protection within seconds. Image sources: [19, 20]

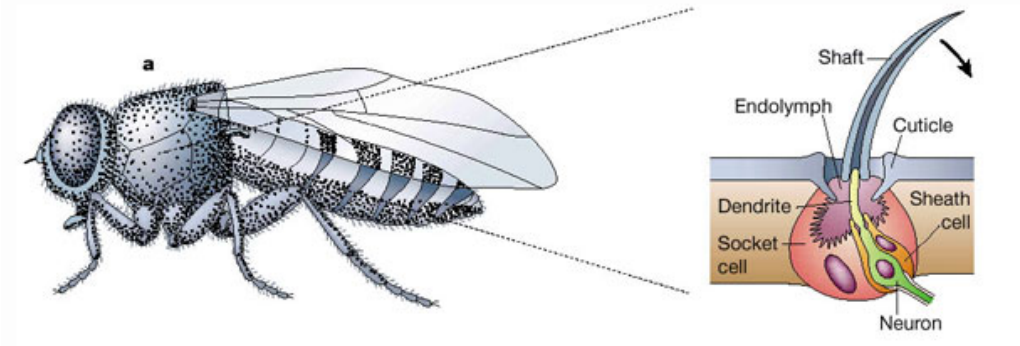

Figure 2.4: Lateral view of the fly drosophila melanogaster. Its body is covered by hundreds of bristles which allow for tactile sensation. Image source: [15]. Reprinted by permission from Macmillan Publishers Ltd: Nature vol. 413, copyright 2001.

Tactile sensing in insects

A further step in natures development of tactile sensing was the usage of hairs which protrude out of the organism and are bended by external force. This external force can be detected by mechanoreceptors located at base of the hairs inside the organism. This is the secret by which insects, which normally have a rigid chitin exoskeleton, can detect touch along their body. Figure 2.4 shows how a fly is equipped with bristles which allow the detection of touch.

In addition, insects can have also other mechanoreceptors in their body to monitor the strain of body parts as a mean of properioception (campaniform sensilla, chordotonal organs). The hair principle also allows an organism to

Figure 2.5: The motor controlled vibrissae of felidae and canidae are highly sensitive tactile organs. They allow them to hunt prey with fast reactions and to navigate even with little light [24, 25]. Image source: [26]

detect forces that act parallel to its surface (and can also provide amplification as the hair acts as a lever). Arthropods like spiders and crickets have specialized hairs (trichobothria) to monitor vibrations in air, which helps them to hear incoming prey (with the response frequency tuned to the insect species that they hunt) or the presence of conspecifics. [15, 23]

Tactile sensing in mammals

Mammals have especially sensitive facial hair, commonly called whiskers (or vibrissae, see Fig. 2.5), in addition to their regular body hair (with the exception of man, which we will discuss later). These are important sensing organs across all mammals, their functions include navigation, locating food as well as facial expressions and intraspecies communication. After birth, many mammals are blind and deaf for the first days and have to rely on their olfactory and tactile sense. For mice it has been shown that the vibrissae are most important for locating food sources in this post natal period. Newborn mice under a reduced food supply actually showed a faster growth rate of vibrissae then their contemporaries, which is interpreted as the reaction of the organism to improve the food localization capability. The role of vibrissae for the acquisition of food stays prominent through the whole life. Horses and other large herbivores use their vibrissae to determine length and texture of the grass that they are eating, as their eyes are located outwards and do not allow for closer inspection. Analogue to this, whales can use the information from their vibrissae to steer towards the maximum density of plankton. For terrestrial and aquatic mammals the vibrissae also allow them to keep a cor-

Table 2.1: Physical properties of the mechanoreceptors in the human skin, adapted from [8]

Receptor	Receptive Field (mm²)	Frequency Range (Hz)
Merkel receptor	2-100	0.4-100
Meissner corpuscle	1-100	10-200
Pacinian corpuscle	10-1000	40-800
Ruffini cylinder	10-500	7

rect head position when swimming. Mice with defunct vibrissae have been unable to keep their head over water. Similar important are the vibrissae for locomotion on land. Night active mammals make extensive use of their tactile information for navigation, like noticing corners or holes in darkness, or triggering protective eye blinks when navigating through woodwork. [25, 27]

Tactile sensing in humans

Although the vibrissae are such important tactile devices, there has been a mammal which managed to completely lose its vibrissae during evolution: man. It is suspected that this change occurred along with the miniaturization of the rest of the human body hair and is connected to the switch to bipedal locomotion. Most of the human body hair now appears as near invisible vellus hair (through this humans seem naked, but still have a body hair density that matches primates). When compared to primates, human non-vellus hair follicles however show an increased innervation which may compensate the loss of vibrissae. Other major changes to the human skin during evolution include a thicker epidermis and a fatty layer below the skin, the appearance of fingerprints (which are also present in primates, but more elaborate in man), and an intense vascularization of the human skin. [28–31]

In general, the human skin contains the four kinds of mechanoreceptors as other mammals, which respond to stimuli such as pressure, stretching and vibration at different depths.

- The Merkel receptor is a disk shaped receptor which is located between the epidermis and dermis.
- The Meissner corpuscle is a stack of flattened disks in the dermis below the epidermis.
- The Ruffini cylinder consist of a cylindrical capsule with branched fibers inside and is located below the Meissner corpuscles.

- The Pacinian corpuscle is another, more onion shaped capsule located much deeper in the skin.

Along with their different shapes and locations, they exhibit different responses to mechanical stimulus. The area in which they react on stimulation (receptive field) and the maximum frequency of excitation is listed in Table 2.1. The merkel and ruffini receptors have so called slowly adapting (SA) fibers, their electrical output signal is continuously fired as long as pressure is applied. Merkel cells are densely present in both the hairy and hairless friction surface (glabrous) skin (ca. 100 per cm^2 in the fingertip of humans and primates). They respond to pressure with a slowly adapting output signal, that is linearly related to the indentation depth. The ruffini receptor can also be found in the hairy and glabrous skin, it is very sensitive to skin stretch and allows to sense the direction of object motion. It also plays a role in the proprioception of hand posture and thus is densly present in the skin on the finger joints. The meissner receptor and pacian corpusle contain rapidly adapting fibers (RA), they fire at onset and offset of stimulation. The meissner corpuscle is only present in the glabrous skin and on the proximal nail folds, in the finger tip it is the most present mechanoreceptor, with ca. 150 per cm^2 in the fingertip. It is insensitive to static pressure, but very sensitive to dynamic skin deformation. It is therefor used for slip detection and to provide feedback for grip control. The pacian corpuscles are very sensitive, responding to as few as 10nm of skin deformation. However they only react to high frequency excitations. They have a very large receptive field, which may include the whole hand. There are about 350 per finger and 800 in the palm. In addition the skin also contains various free nerve endings which react to force as well as damage (pain) and temperature (thermoception). [32–35]

Tactile perception

As the mechanoreceptors and nerve fibers make up the basis for human tactile perception, the other important part is the neural processing of these signals. This is the part that is responsible for picking up the signals from the various mechanoreceptors and creating the tactile sensation. All mechanoreceptors in the human skin are connected to nerve fibers which travel in bundles to the spinal cord and then into the brain. The receptors, the nerve fibers and the brain areas associated with them form the somatosensory system (together with the receptors for pain, temperature muscle-spindle and joints). The electrical signals from the mechanoreceptors go through the nerve fibers through the thalamus and into the so called somatosensory cortex. This is an area of the brain which handles the processing of the tactile stimuli. In

this area, the mechanoreceptors in different body parts can be distinguished in different subareas of the cortex [36]. It is said that humans have the most elaborate somatory system [37].

In general, the tactile acuity can be correlated to the population of the receptive fields of the mechanoreceptors [38]. Some of the highest density is found in the fingertips, the lips and the tip of the tongue. But the actual tactile acuity also depends on the neural configuration in the somatasensory cortex. For example all fingers have the same density of mechanoreceptors, but the acuity decreases from the index to the little finger. This correlates with the size of the area that represents the finger in the somatasensory cortex, so the acuity apparently also depends on the 'wiring' in the brain [39]. This wiring can be influenced as it has been shown that blind people have acquired a higher spatial acuity through training [40, 41]. It has also been shown that the tactile acuity of the fingertips decreases with age, the reason is suspected to be a reduction in the density of mechanoreceptors over time, neurological processes or a combination of both [42]. There is also a big variance in acuity between humans of the same age, this is attributed to differences in skin conformance, where a higher conformance is correlated with a higher sensitivity [43].

Also in the same individual and in the same location, tactile acuity is non constant. For example the temperature of the skin can cause a lower (when the temperature is below normal) or even a higher acuity (when the skin is slightly heated) [44]. Analogue to this, it was found that when the skin temperature is normal an either cold or hot object can sharpen tactile acuity [45].

Tactile acuity is also improved when combined with the visual sense. The so called visual enhancement of touch effect allows subjects to have a higher tactile acuity when the stimulated body part is observed. It is suggested that this is caused by the multimodal information leading to enhanced processing inside the somatosensory cortex [46]. The tactile sense also plays a role in the multimodal processing of thermal sensing. As the spatial acuity of thermal effects is much coarser then the tactile acuity, it has been found that the localization of thermal sensation relies greatly on the tactile feedback [47]. Due to this complexity, it is not outright possible to infer the exact tactile spatial resolution from the mechanoreceptor density in the skin of various body parts. To create a map of tactile acuity of the human body, various experimental designs have been used. A tactile resolution map of the human using the two point discrimination technique is depicted in figure 2.6.

As with the spatial, also the temporal acuity depends on the processing of the tactile data in the cortex. The time to separate two successive somaesthic

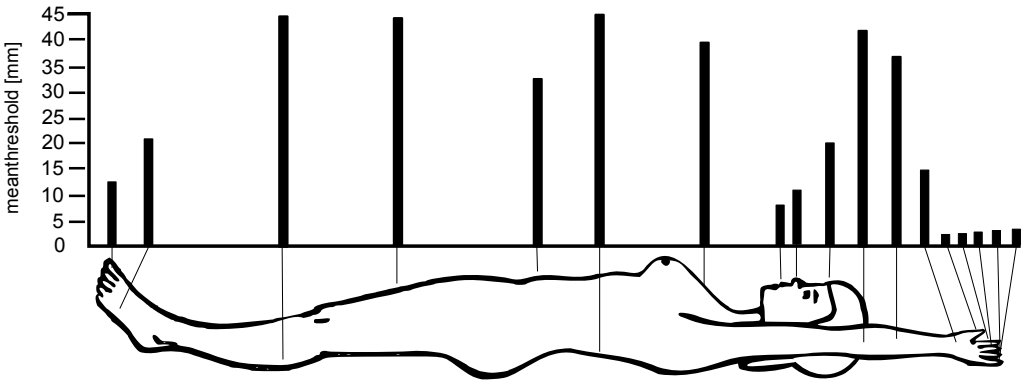

Figure 2.6: Tactile spatial resolution along the human body. Shown are the mean values of two-point discrimination tests, which record the smallest distance where two stimulus points are recognized as separate. Adapted from [48]

simuli, called somaesthic temporal discrimination, was measured for a range of people with normal and damaged somatosensory cortex in [49]. For this test two electrical stimuli were applied to the index finger with increasing and decreasing time intervals, and the subjects had to tell when they could recognize a double stimulation. The mean threshold was around 31ms for the control group and about 173ms for the patients.
In a similar experiment between two groups of older (65-75 years) and younger (21-34 years) subjects [50], the mean threshold for separation was measured at ca. 33ms for the younger and ca. 48ms for the older group. Analog to the spatial acuity, the temporal acuity can be improved through training as an experiment with experienced and inexperienced subjects shows [51].

A correlation between spatial and temporal acuity can also seen when comparing the temporal acuity of different body parts as in [52]. There the lowest threshold is found for the index finger and the highest one for the foot. It is likewise argued that central processes have the most contribution on these differences.

Apparently the cutaneous temporal acuity can also be influenced by changes in the body configuration, in [53] it is investigated that the threshold for discrimination increases from 34 to 124 ms when the subjects hands were placed in a crossover position. These values however describe only the time until the stimulus is perceived consciously, in [54] a first activation in the somatasensory cortex is observed after 14ms. In their experiments the activation time

of different cortical areas to the stimulus is compared, and from this it is concluded that the signal processing in the somatasensory cortex operates in a serial fashion.

We have now seen that tactile sensing in nature is of greatest importance, for the interaction of organisms with the environment and each other. Consequently it has been under development for millions of years.

We will now look at what advances have been made in the field of artificial tactile sensing, which one day wants to be able to handle the same diverse scenarios as natural tactile sensors, but has been under development only for a few decades.

2.2 Artificial tactile sensing

Artificial tactile sensing is the attempt to emulate or even surpass the tactile capabilities found in nature. As the field of devices that have been developed for this purpose is large, we have applied a broad categorization on the application level as shown in figure 2.7.
This should provide the reader with some orientation of where the modular *Myrmex* system, that is presented in this work, is located in the landscape of artificial tactile sensing. The whole distinction between the application areas should be seen as more of a general guideline, as e.g. there can be fingertip sensors that can do slip detection and could also be used to interact with a human.
The first basic distinction we have applied is between robotic and human applications. The robot applications are further grouped into grippers and general purpose devices which includes modular systems. For grippers we have the subcategories of fingertip sensors and tactile sensors for slip detection.
Tactile sensors for human-machine interaction are sensors that have been developed with the focus on interacting with the human, mostly the fingers or the whole hand. Here we separate between tactile sensors that were developed as an input modality to a computer and those that have been developed to study human manual interactions in a more scientific context.

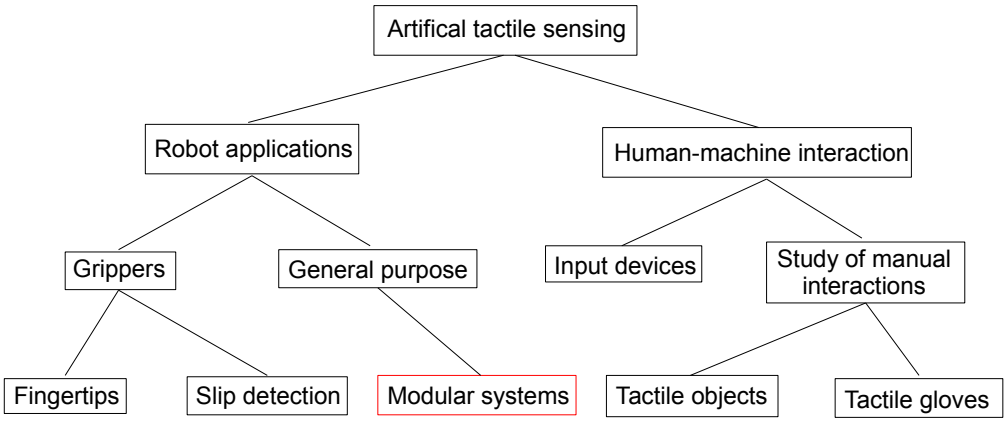

Figure 2.7: A categorization of tactile sensors by the different applications that they are constructed/used for. The class of the *Myrmex* system presented in this work is marked in red.

The placement of the modular systems in the middle is no coincidence, as they can be used for various tasks. The applications of gripper/slip detection, input device and tactile object have been realized with the *Myrmex* system

and will be shown in section 6. In the following pages we will first introduce the reader to the basic general purpose tactile sensors.
Then we will look in more detail at modular systems that are comparable to the *Myrmex* system which we present in this work.
After this we look at tactile sensors that are used for grasping and slip detection. Next we look at the tactile devices that are used as input modalities for computers.
In the later parts of this work we also present a 'tactile book' made with *Myrmex* modules (Sec. 4) that is designed to acquire motion data from humans. Consequently we will introduce the reader to comparable devices in the last part of this section.

2.2.1 General purpose tactile sensors

General purpose tactile sensors are characterized by being flexible in the roles that they can take in connection with robot/computer systems.

A type of sensor that is used for general robotic purposes and which can be easily related to biological tactile sensing is the artificial whisker.
Such a whisker is usually constructed by using a string of flexible material which is anchored to a sensing unit. If the string is bended from its initial position, the sensing unit produces a corresponding output signal. The material of the string can be artificial like a plastic or piano wire, or natural like a human hair or a real animal vibrissae.
The sensing unit can make use of mechanical switches, piezoelectric, resistive or capacitive elements to convert the bending of the whisker into a signal. Figure 2.8 shows an example for a mechanical and a resistive based whisker. A whisker which uses the capacitive effect can be created by attaching a whisker wire to a microphone capsule.

In [56] artificial and natural whiskers are attached to such a microphone capsule and their output while stroking over different surfaces is compared. The most stable data was produced by a real rat whisker, which is attributed to its damping properties.

It has been argued that artificial whiskers should be curved like the ones found in nature, as this has two advantages: the whisker will bend in a predictable manner when large forces are applied and the tip of the whisker is the most likely part of the whisker that will touch the external object [57]. Different whisker morphologies (length, stiffness and curvature) are evaluated in [58] using a Khepera robot and evolutionary simulations. Its is found that the morphology most suited for a wall following task is the one that is com-

monly found in nature.

We have seen that in biology whiskers play an important role in navigation during limited visual feedback and they can take an equal role for mobile robots. In [55] it is argued that ultrasonic or light based sensors may not be robust enough for mobile robot navigation, as ultrasonic sensors can give incorrect distance readings with respect to inclined or very close surfaces and infrared sensors can give incorrect output depending of surface material and color.

A mobile robot with 16 whiskers is used in [59] for shape recognition using the deflection amplitude or deflection velocity of the whiskers. The deflection amplitude changes whether the sweep of whiskers experiences a point or surface contact along the surface of the target object. The vertical shape of an object can be determined when whiskers are stacked vertically, a conically shaped object will result in a time-shift in the whisker signals. A whisker array mounted onto a remote controlled car has been used in [60], the frequency spectrum of the whisker response is used to determine the ground and surface texture and also the speed of the car.

A pneumatically retractable whisker for industrial applications is presented in [61]. It is argued that this type of sensor is very good for searching applications as in checking for the presence or absence of objects in an assembly line. The arguments are that optically based sensors can be fooled by the properties of the sensed object, its reflectivity and surface roughness. While other tactile sensors that touch the objects may stop or relocate them, a light and

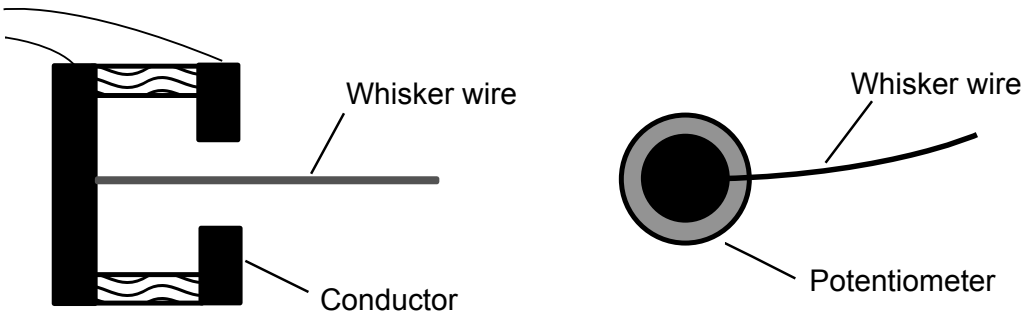

Figure 2.8: Simple designs for artificial whiskers. Left: A binary whisker which closes an electrical contact when bended. Right: A whisker attached to a rotary potentiometer, the flexion of the whisker changes the resistance. Adapted from [55].

flexible whisker bends over the object and springs back when it has passed.

While whisker sensors have proven themselves effective in mobile robot application and surface discrimination, they are however not used for friction surfaces that have strong or constant contact with objects. Because of this they seem not to be a good basis for our robot gripper scenario.

Another class of general purpose tactile sensors are semi-flexible elements which can be attached to hard surfaces. One example is the strain gauge, which is manufactured from a resistive element (foil, wire, or resistive ink) or from semiconducting material.

A typical resistive strain gauge consists of a resistive grid bonded to an epoxy backing film (see Fig. 2.9 left). Due to the pattern layout it is only really sensitive to strain in one direction. The strain gauge is attached to an object, and when the object is deformed it will change its resistance. The change in resistance is caused by the change in the geometry of the resistive pattern. When it is stretched, it will become narrower and longer which increases its electrical resistance, on the other side, when it is compressed it will broaden and shorten and that decreases its resistance.
If the strain gauge is pre-stressed prior to the application of the medium, it is possible to measure both tensile and compressive stresses.

In most applications the object will be hard, so no visible deformation occurs. The reaction of the strain gauge will be very small and needs to be properly amplified. A factor that influences these small changes is the temperature, because of this strain gauges are often used in pairs. The second strain gauge is mounted in a strain insensitive position, so that it only experiences temperature related changes which are used to compensate the main strain gauge.

Another type of such general purpose semi-flexible sensors is the force sensitive resistor (FSR). A typical FSR consists of two flexible membranes which are separated by a thin air gap which is created by spacer at the edge of both membranes. One of the membranes has a set of metal electrodes which are placed close to each other in an inter-weaving pattern. The second membrane is covered with conductive ink that is carbon based [63]. When the two membranes are pressed together, a current can flow from one electrode to the other through the ink.
These two basic sensors can be used to create single tactile sensor devices for various purposes, or even devices with multiple tactile elements (tactels).

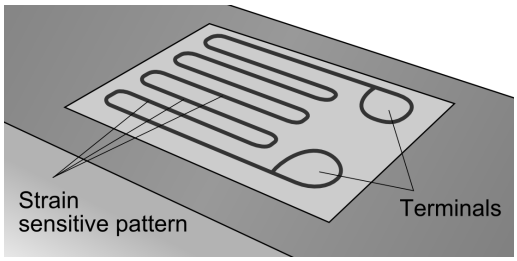

Figure 2.9: A schematic strain gauge. The resistance between the terminals increases when the pattern is stretched. Image adapted from [62]

Such constructions suffer however from the space consuming integration and wiring of the individual sensors elements. To create more compact or versatile tactile sensor arrays, there have been more sophisticated projects to create integrated arrays with multiple tactels based on resistive sensing.

Such tactile sensors arrays are commercially offered by companies like Tekscan. They offer standard and custom designs of various dimensions for specific applications [64]. Their sensors work with a resistive principle very similar to FSRs. To create a sensor matrix, electrodes are etched in rows and columns onto two flexible plastic sheets. The sheets are then and placed onto each other. At the intersections of a row and column from the two sheets pressure sensitive ink is printed to form a tactile sensor cell.

A forces that acts on this cell causes a change in resistance of the pressure sensitive ink between the two electrode sheets [65]. To measure the resistance of a cell a special control circuit is used to activate a row and column and induce an excitation voltage. The response of the sensor cell is then measured by an 8-Bit analog digital converter (ADC). A scanning frequency for the arrays of up to 500Hz is possible, in special designs even up to 20kHz are possible [66, 67].
A tactile sensor array designed as an artificial skin for robots is presented in [68, 69]. It operates on a similar resistive matrix principle. Its uses conductive fabrics to achieve flexibility to cover the curved surfaces of robots. A special shock absorbing layer is used to cushion collisions and at the same time provides mechanical support to the tactile sensor cells.

There are however also general purpose sensors that realize multiple tactels without using multiple sensor elements. One is presented in [70] and uses a flexible and stretchable rubber material. It is based on a form of piezoresistive sensing and uses an algorithmic approach known as electrical impedance

tomography (EIT).
The conductive material is equipped with 16 electrodes at its edges, which function as a voltage source or a sensor electrode in an alternating fashion.
In turn the resistance between the electrodes is measured and then the resistance distribution of the whole material is calculated, which changes on pressure or stretch. The distribution is calculated using inverse problem analysis as in computed tomography [71].

EIT based sensors are useful for covering complex 3D shapes as they are very flat as wiring is only need at the edges of the contact region. However to sense activation it is necessary that a minimum of 1% of the total area has to be contacted. Also the materials have the disadvantage of changing their resistance during stretch.

Modular tactile sensor systems

Modular systems are characterized by having multiple modules with tactile sensors that can be added to or removed from the system. Through this they have a special flexibility in their physical configuration.
Some sensor systems do not form a continuous surface but the modules can be distributed along an object as e.g. in the realization of tactile skin areas for robots. Depending on their implementation modular systems can also be used as a robot gripper or an input device for a PC.

As the *Myrmex* system presented in this work is a modular tactile sensor system, we will present a wider range of comparable systems here, and provide a summary table with the most important parameters at the end of this section.

A modular system that uses an optical measurement method with an urethane foam cover is presented in [72]. It uses tactile sensor cells that consist of a light emitter and receiver as shown in the figure 2.10.

This system was developed to be used as a skin for humanoid robots. It consist of tactile modules which can be connected to each other through direct soldering or small cables. A module can also be reduced in size by cutting of branches with a scissor.
Each module has 32 tactile sensors which are organized in eight H shaped branches (see Fig. 2.11 left). Each branch has four sensors consisting of a LED and a photo-transistor.
The photo-transistor circuit outputs a voltage corresponding to the indenta-

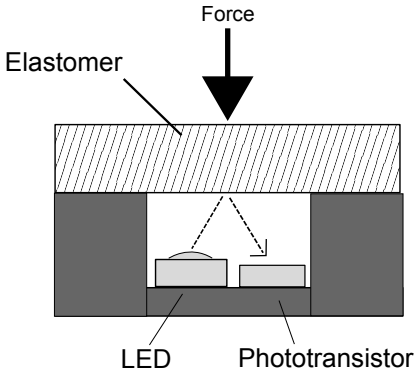

Figure 2.10: Optical tactile sensor. LED and Transistor are located next to each other, the light is reflected by the elastomer cover. When it is compressed, the light intensity at the photo-transistor increases. Adapted from [73, 74]

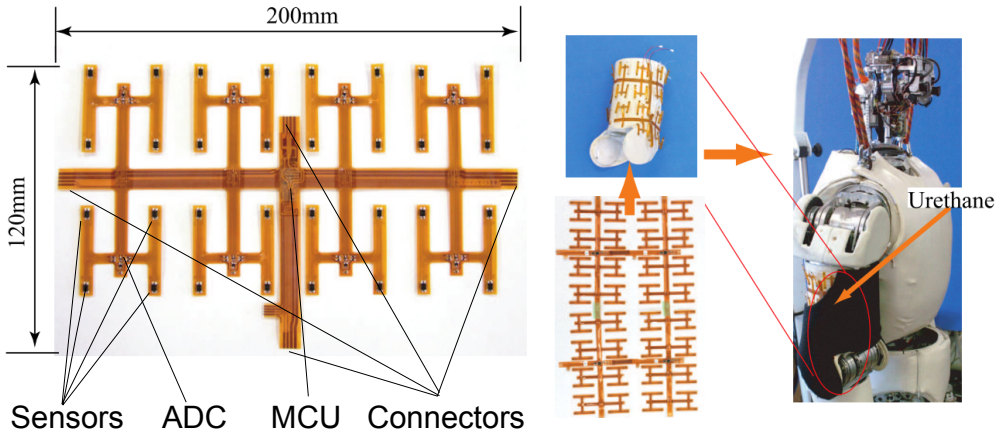

Figure 2.11: An optical based modular tactile sensor system. Left: a module consists of several branches which are equipped with tactile sensors. The data is collected by a MCU in the center. The modules can be interconnected by connector pads that are available at four sides. Right: As the system is realized with a flexible PCB, it can be wrapped around parts of a humanoid robot. For operation it is covered with a black urethane foam. Adapted from [72], ©2006 IEEE.

tion of the elastomer cover. Two branches share an analog digital converter (ADC) to digitize this voltage.
This digital value is then readout by an 8-Bit microcontroller (MCU) located in the center of each module. The microcontroller is connected to an I²C serial bus [75], which leads to the four edge connectors which can connect to other

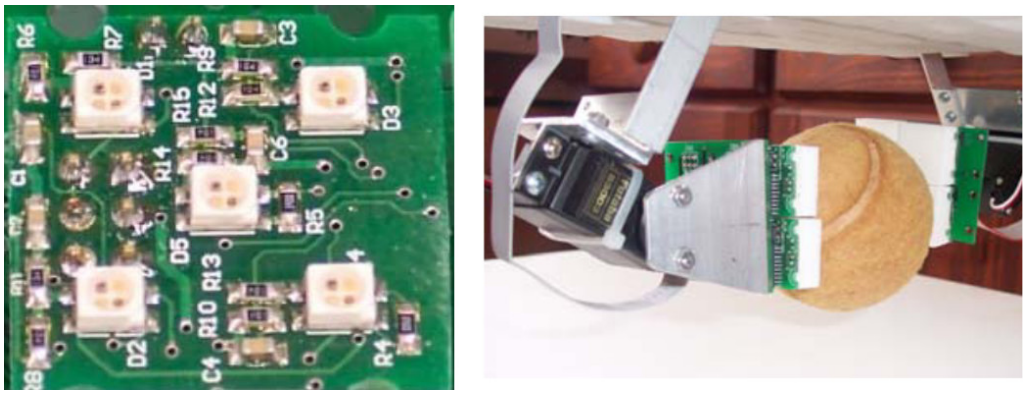

Figure 2.12: Left: The top side of the optical tactile sensor module with five optical sensors [76]. On the bottom side an 8-bit microcontroller is located. Right: A servo based robot gripper with 2x2 tactile modules on each side. The elastomer cover (white) is mounted on top of the optical sensors, which allows to grasp a ball with tactile feedback. Image sources: [74]

modules. Adding more modules increases the amount of participants on the bus which degrades the signal quality, so it is advised to use bus repeaters.
To transfer the tactile sensor data to a PC, a master unit is used. This master unit reads the module tactile data via the I²C bus and forwards it via LAN to a PC.
Due to the flexible substrate of the modules, they can be bended over curved surfaces and used as a tactile skin for robots (see Fig. 2.11 right).

Another optical tactile sensor system is presented in [74]. The modules of the system were designed to be used in a big array to create a tactile surface, but also to be mounted onto a robot gripper.
For tactile sensing the optical reflection principle as previously shown in figure 2.10 is used. The sensor thereby consists of a LED, phototransistor and elastomer cover. The LED and the transistor are placed next to each other as they are both integrated into a single chip.

The elastomer is an open cell foam, which scatters the light exerted by the LED back to the phototransistor. As the foam is compressed the scattering cells come closer to the detector and light intensity increases.
Each module has a size of 22x22mm and contains five optical emitter/receiver chips (as shown in in Fig. 2.12 left) and an 8-bit microcontroller.

The spatial resolution is increased by interpolation. The simulated values are calculated by averaging the output from the 3 adjacent sensors. This re-

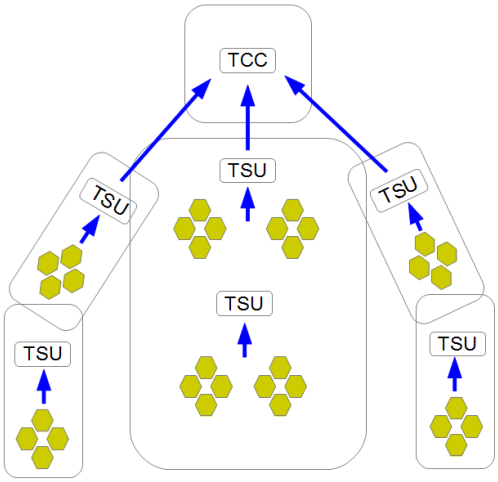

Figure 2.13: The HEX-O-SKIN is designed to use a hierarchical organization on a humanoid robot. Individual modules (yellow) are interconnected with each other and a tactile section unit (TSU). The tactile sections units bundle the data from the modules and forward it to a tactile computing cluster (TCC). The usage of multiple TSUs is necessary for a good performance and also protects, to a certain degree, against hardware faults of the tactile system through their redundancy. Adapted from [77]

sults in 9 total tactels with a spacing of 7.5mm.
The modules can be connected together to form an array of 8 by 10 sensor modules. The whole array can be sampled in 800ms.

The microcontrollers of the modules are connected to a SPI bus, which is directly accessing by using the parallel port of a PC. A tactile gripper has been realized by mounting 2x2 sensor modules onto a SIR 1 robot arm (Fig. 2.12 right).

A system to be used as multimodal tactile skin for robots is presented in [77] and named HEX-O-SKIN. Each module is a small hexagonal PCB which includes sensors for temperature [78], acceleration [79] and proximity [80]. The tactile sensing is realized through the optical proximity sensors, which are single chip sensors with a light emitter and receiver (as in Fig. 2.10).
The sensor gets covered with a transparent elastomer, through this the optical sensor can also work as a pretouch sensor. Each module has an area of 5.1cm² and is equipped with four proximity sensors spaced 1.4cm apart.

The modules are also equipped with a 32-Bit microcontroller. This microcontroller collects the data from the sensors and transfers it via a serial USART

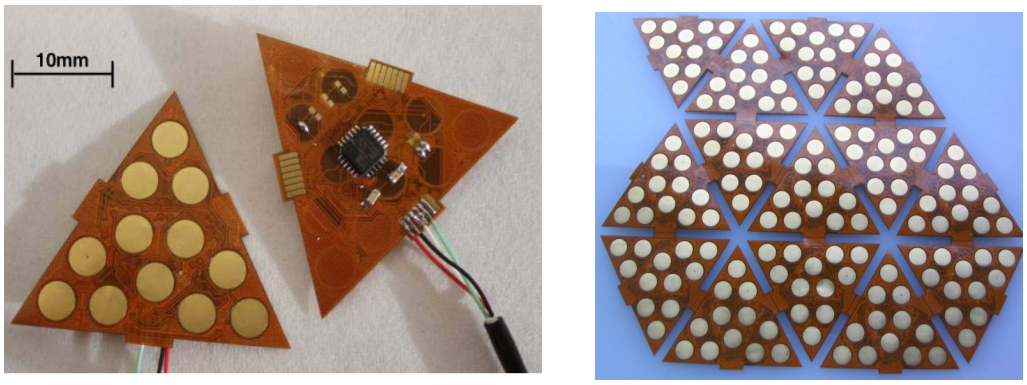

Figure 2.14: Left: The capacitive based sensor modules of the iCub system. They have a triangular shape with 12 tactile cells. On the reverse side of the flexible PCB is the capacitive sensor chip. Right: Multiple modules can be connected together to cover larger areas. Image sources: [81], ©2008 IEEE.

bus. Connections for power and USART are available on 4 sides of each module, adjacent modules have to be soldered together via small cables.

The USART communication for each connection is handled by four separate USART drivers inside the microcontroller. Because of this there exists no common USART bus, only local connections between two modules. This means that each data packet that passes through a module has to be read on one connector and put out on another connector by the microcontroller.

This provides protection against signal degradation that would occur with multiple modules and long wire lengths. It has however the disadvantage of adding an extra delay for each module that is in this chain. With the maximum number of 8 modules this delay is 6.3ms for the last module, while the data generation frequency of each module lies at 1kHz.

To cover a robot body with multiple modules, the system is designed to work in a hierarchical organization (see Fig. 2.13).
A number of interconnected modules connect to a tactile section unit (TSU). A tactile section unit is a FPGA board with integrated Gigabit-Ethernet. Multiple of theses TSU are attached to the Ethernet.
Each tactile section unit converts the UART data of its modules to UDP packets. The data is collected by the tactile computing cluster (TCC), which in the current state is a PC.

Another flexible skin, which was designed for the iCub robot, is presented in [82]. It consists of triangular shaped modules with 12 tactels each (see Fig. 2.14).
The sensor uses capacitive sensing based on the AD7147 capacitive sensor chip [83]. This chip is capable of detecting changes in the capacitance of external electrodes. The chip is originally designed to create input sensors for human touch in consumer devices, through the human finger changing the capacitance of an electrode when it is in a certain range.

This type of capacitive sensing can sense objects even before they make contact (pretouch), but it also has the problem of not being able to sense non conductive objects like ceramic, plastic or wooden objects. So to use this method for the robot skin an addition to the sensor was necessary.

This addition comes in the form of a two layer silicone foam, where the upper layer silicone has been mixed with conductive particles.
Through this a capacitor is formed with the PCB electrode in a 'sandwich' design as depicted in figure 2.15. The measured capacitance now depends on the distance between the upper foam layer and the PCB - and thus on the compression level of the foam. Through this the contact with an object can be registered regardless of its conductivity.
A drawback that still exists is that the sensitivity is correlated to the area of the electrode [83] and thus very small sensor cells are not practical.

Each module has 12 round sensor cells with a diameter of 4mm spaced 5mm apart. The modules can be connected with each other through soldering, several modules together form a patch. From this patch, one module has to connect to a microcontroller board. The microcontroller can read out the digital values of the sensor chip via a serial SPI bus [84].
The maximum amount of modules in a patch is 16. The microcontroller board itself is connected via CAN Bus to a PC.
The maximum transmission rate for twelve tactels lies at 50 Hz, however also a faster mode can be used where a single averaged value is transmitted at 500 Hz. Although the capacitive sensor chip offers a 16-Bit resolution the transmitted sensor data is 8-Bit [85].

The BIOTACT sensor is a modular system based on whisker sensors. It was developed in the european project called Biomimetic Technology for vibrissal Active Touch [86]. It is inspired by the head of a mouse and consist of a conical base with an array of 24 actuated whiskers at the side (see Fig. 2.16). Inspired from biology, the whiskers are moved back and forth to make repeated con-

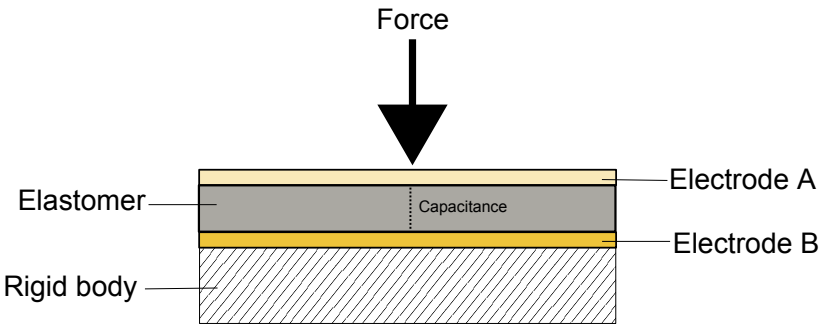

Figure 2.15: Tactile sensor design using two electrodes in a sandwich design, with the electrodes being separated by an elastomer. The elastomer is non conductive. The capacitance between the electrodes is measured and changes with the distance of the two, which is turn changes due to compression of the elastomer.

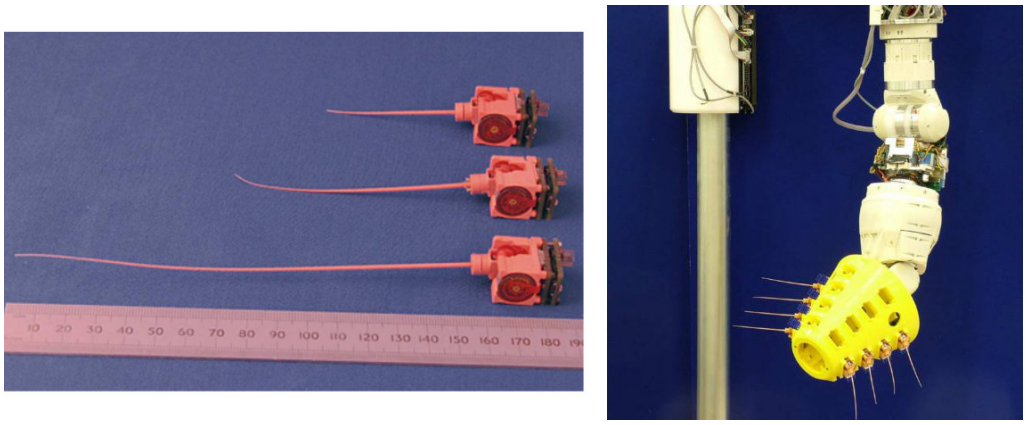

Figure 2.16: Left: The BIOTACT sensor modules are whiskers attached to a sensing base with integrated actuator and microcontroller. Right: The modules get attached to a conical base unit (yellow), here mounted onto a robot arm. Image source: [86], ©2012 IEEE.

tacts with the surface of interest.

The whiskers are modular units that can be put into sockets in the cone. This allows whiskers of different length and curvature to be used, and the number of whiskers can vary. Each whisker wire is made out of a polymer material and can have a fine tip as small as to 0.25mm. Every whisker is attached to a miniature brush-less DC motor, which allows it to be whisked at up to 10 Hz, which matches the dominant whisking frequencies of rats which

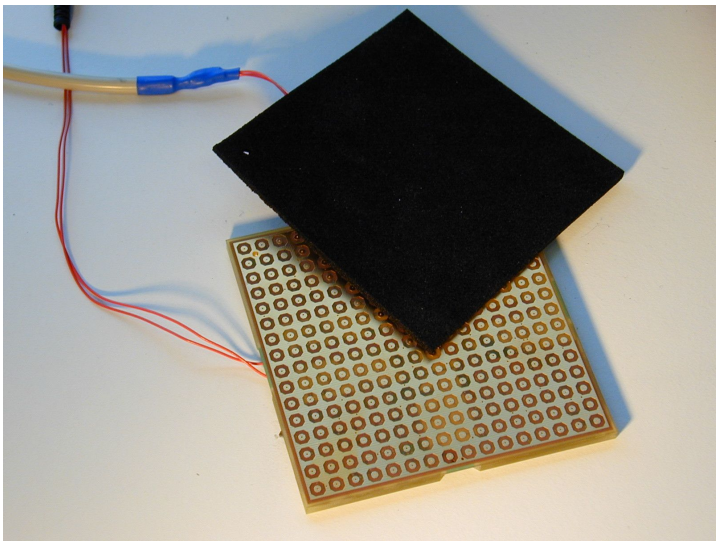

Figure 2.17: A module of a Weiss DSA100-256IS system. The surface is covered with 16x16 round electrodes, surrounded by a common ground eletrode. The black foam is placed on top to form the complete sensor.

lies at about 8 Hz [87].

The sensing of whisker curvature is based on the hall effect, at the base of each whisker is a small magnet and a triaxis hall effect sensor. The motor and the sensor are controlled by a 16 Bit microcontroller in each module. These are connected through their sockets to a SPI bus which connects to a base unit which contains a FPGA for data processing and an USB2controller.

The whole system is connected via USB to a PC, it uses the USB bulk mode (as used for storage mediums) to transfer the data to the PC at a rate of 2 kHz.

A modular tactile sensor system that is commercially distributed is the DSAMOD family by Weiss Robotics [88]. The (now discontinued) DSA100-256IS system uses modules with a size of 100x100mm. On their upper side is a 16x16 grid of tactels with a distance of 6mm to each other (see Fig. 2.17). On their lower side they contain measurement electronic which is controlled by a 16 Bit microcontroller.
The sensors work by employing the piezoresistive principle with a single sided, parallel electrode design as shown in figure 2.18. The resistance between the sensor and the ground electrode is converted to a voltage by using a voltage divider circuit. The output voltage of this circuit is sampled by a 12 Bit ADC.

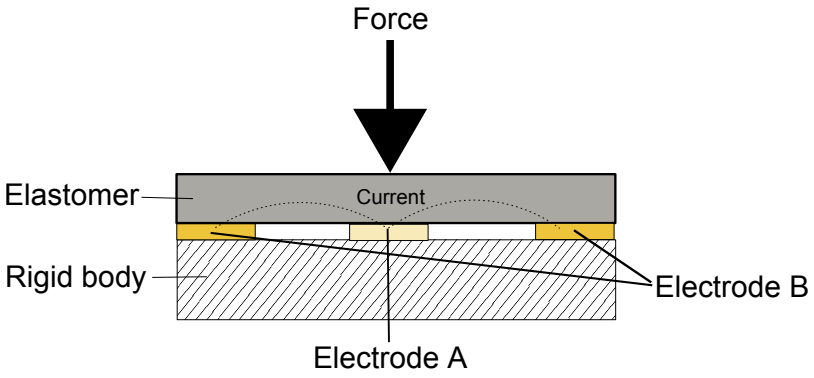

Figure 2.18: Tactile sensor design using two electrodes in a parallel design. Electrode A is surrounded by electrode B, both are separated through a gap. A conductive elastomer is placed on top through which current can flow between electrode A and B. The resistance between the electrodes changes on compression.

Each module has a RS232 and a CAN connector and can deliver frame rates of up to 30 Hz. It is possible to connect multiple modules via CAN bus and place them close to each other so they form a continuous sensor surface. The modules then have to be connected to an extra sensor-controller unit which collects the data and transmits it to a PC.

As the DSA100-256IS is now discontinued, a replacement system is available in form of the DSAMOD-6 system. This system offers modules with different sizes, ranging from 12x16 up to 64x32 tactels. The frame rate ranges from 100 to 35 Hz depending on the amount of tactels. The modularity of the system was greatly reduced, as now only two modules can connect to a sensorcontroller via a proprietary bus. The sensorcontroller now offers additionally USB as connection to the PC [89, 90].

Now we will look at the Myrmex precursor system which was developed in [9]. Similar to the DSA100-256IS system it uses rectangular modules with a 16x16 tactel surface. The size of a module is 80x80mm and the tactels are spaced 5mm apart. The modules can be connected together to form a larger continuous sensor surface, the data transmission to the PC is handled by a so called central unit which connects to the modules and the PC.

Each module consists of two PCBs, a sensor PCB with the tactels on its surface and a connector PCB (see Fig. 2.19). The sensor PCB is mounted onto the connector PCB using 6 connectors that are distributed on the PCB. The sensor cells function through the resistive principle and a parallel electrode

design, where the second electrode is realized by a common ground plane for all sensor cells (as depicted in Fig. 2.18).
The resistance between the electrodes is converted to a voltage using a voltage divider circuit. On the bottom side of the PCB there are 16 ADCs with 16 inputs each to sample the voltages of all 256 tactels. The ADCs are connected to a common SPI bus.

The connector PCB contains an 8-Bit microcontroller and voltage regulators. The microcontroller controls the chip select lines of the SPI bus for all ADCs. Through this it can decide which ADC is active on the SPI Bus. The microcontroller itself is attached to a 2nd SPI bus which together with the ADC SPI bus and power lines is connected to sockets and pinheaders at the edges of the connection PCB. The sockets and headers allow the modules to get connected with each other and the central unit.

The central unit is made up by a NGW100 board, which is a small evaluation board manufactured by Atmel for the AP7000 microcontroller [91].
This microcontroller is capable of running at a speed of 160Mhz and has integrated support for USB, ethernet and several dozen IO ports. It also features

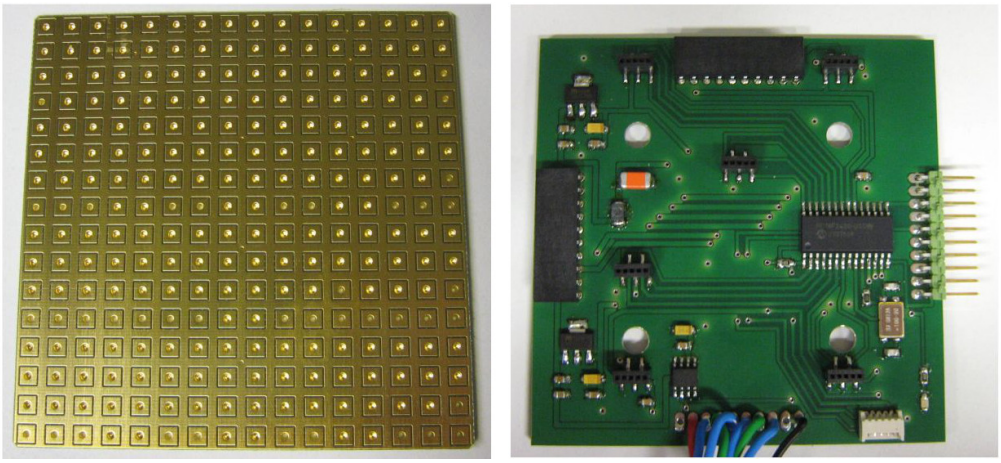

Figure 2.19: A module of the precursor *Myrmex* sensor system. Left: The upper sensor PCB contains a 16x16 array of rectangular electrodes, surrounded by a common ground electrode. The round area in the center of each electrode is a electrical connection (Via) to the other side of the PCB, where the measurement circuit is located. Right: The connector PCB onto which the sensor board is mounted. It contains voltage regulation electronic, an 8-Bit microcontroller and connectors.

two SPI buses, which connect to the buses of the modules.
The central unit acquires data directly from the modules via the ADC SPI bus. For selecting the different ADCs on the bus the central unit instructs the 8-Bit microcontroller on the individual module. Employing the microcontrollers as mediators allows the system to be extended without limits in theory. Because with a normal SPI bus design one would need one chipselect (CS) line for each ADC for addressing - with 16 ADCs per module this would lead to a large amount of connection lines required even when using only one module. But with the mediator design, this bottleneck is removed.

To avoid the usage of CS lines also for the 2nd bus that communicates with the microcontrollers we modified the SPI bus programming of the microcontrollers. The microcontrollers are not activated anymore by the CS line, but by an address sent on the SPI bus. The unique address for each module is stored in the permanent memory of the modules microcontroller. This address is used to by the central unit to select the modules when acquiring data.

The central unit is also able to discover how many modules are on the bus. For this, it issues a discover command that requires the corresponding microcontroller to respond. This is done once on system startup for all possible module addresses (0..127). Through this the amount of modules and their addresses can be gathered, but no information about their physical layout.

To send the tactile data to the PC, the central unit uses its USB connection. As protocol the USB video format was used. This has the advantage of being supported by all major operating systems. The implementation of the USB video device protocol registers the central unit as a webcam to a PC. The data from the modules is packaged in video frames where the pixels correspond to tactels. The USB video parameter for the frame size is adjusted by the central unit on startup, depending on how many modules have been discovered.

Although the system was designed to support multiple modules, it turned out to work only with one module reliably.

The reason for this was found to be degradation in signal quality of the ADC SPI bus, because all ADCs on all modules are on the same physical bus. The additional module adds another long section of traces and ADCs, which increases the parasitic capacitance to a point where the voltage levels of the data signals take too long to stabilize. Through this errors are introduced which cannot be compensated.
The new *Myrmex* system uses a different bus system (presented in Sec. 3.4)

which does not exhibit this problem.

We have now presented a range of modular tactile sensor systems, their quantitative parameters are summarized in table 2.2. This should allow the reader to quickly compare the results of the tactile sensor system developed in this work.
We can see from the parameters that none of the comparable systems can truly fulfill the requirements we laid out in our motivation.

We aim to create a system that allows to use a bigger number of tactels to cover larger areas with a good spatial and temporal resolution for a tactile table scenario, while at the same time being able to reach very high speeds that enable slip detection.

Table 2.2: Properties of the modular tactile systems

Name	Maximum tactels	Maximum update rate	Spatial resolution	Data resolution	Pressure range	Interface	Sensing method
Optical Skin [72]	1024	4 tactels @ 500Hz	20mm	8-Bit	10 to 500 kpAs	LAN	Optical
Optical Modules [74]	720	9 tactels @ 100Hz	7.5mm	8-Bit	0.6 to 9kpA	SPI	Optical
HEX-O-SKIN [77]	32	4 tactels @ 1kHz	14mm	10-Bit	-	LAN	Optical
BIOTACT [86]	24	1 @ 2kHz	15mm	14-Bit	-	USB	Whisker/Magnetic
iCub Skin [82]	192	1 tactel @ 500Hz	5mm	8-Bit	-	CAN	Capacitive
DSA100-256I [92]	-	256 tactels @ 30Hz	6mm	8-Bit	-	RS232/CAN	Resistive
DSAMOD6 [88]	2048	256 tactels @ 100Hz	6mm	12-Bit	20 to 150 kPa	USB/CAN	Resistive
Myrmex precursor [9]	256	256 tactels @ 350Hz	5mm	12-Bit	5 to 300 kPa	USB	Resistive

2.2.2 Tactile grippers

The *Myrmex* system presented in this work has also been used for grasping - as a tactile gripper/fingertip and for slip detection. These applications will be presented in section 6. Because of this we will here briefly describe alternative tactile devices that have been used for these applications.

The most basic form of grasping for robots can be realized by using a gripper, where two opposing planar surfaces are used to grab an object. Tactile sensitive grasping can be realized if one or both contact surfaces are equipped with a tactile sensor. One of the earliest tactile grippers was the one used in the IBM 7565 assembly system in 1983 [93]. It was a parallel jaw gripper with strain gauges that measured the contact force. Apart from strain gauges, a simple method to upgrade an existing gripper with tactile sensing capabilities is to attach a force sensitive resistor to its contact surface as done in [94].

In grasping, it is often advantageous to have feedback from multiple tactels. For this, various tactile sensor arrays for grasping have been developed. One of the first ones was the Lord Corporation LTS100 sensor module in 1984. It had 64 tactels arranged in a 8x8 matrix [73] which was increased to 10x16 tactels in the LTS200 version [95]. The sensors work with a mechano-optical method as depicted in figure 2.20. A sensor cell consists of a LED and a phototransistor. The LED projects light that is received by the phototransistor and converted into electrical current, the light is blocked by a part of the elastomer cover when it gets compressed.
This sensor employed in a parallel jaw gripper was used for object exploration in [96].
A parallel jaw gripper for use in teleoperation is presented in [97]. It is equipped with a 16x16 tactile array consisting of FSRs. The spatial resolution is 1.54mm and the maximum sampling rate 125 Hz. The measurement electronic is made small enough to be mounted at the side of the gripper.

Fingertips

Tactile fingertips are tactile sensors that have a shape similar to the human finger. They are mostly developed for use in humanoid robots. They often contain multiple tactels to gather spatial information about the contact - analogue to the human fingertip which also has a multitude of tactile sensors concentrated in the fingertip.

A fluid based tactile fingertip is presented in [98]. It consists of a rigid core,

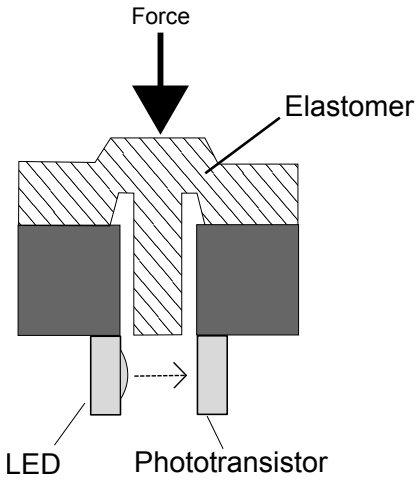

Figure 2.20: A mechano-optical sensor. When the elastomer is compressed, a pin-like projection gradually blocks the light going from emitter to receiver. Due to its construction, this sensor is advantageous when only reaction to normal forces is desired.

which is surrounded by a conductive fluid and is covered by a silicone elastomer.
The surface of the core is equipped with electrodes, where one is a reference electrode and the others are sensor electrodes. At each sensor electrode the impedance between the electrode and the reference is measured.
This value changes when the finger is pressed and the conductive fluid is pushed away from the vicinity of the electrode, changing the volume conductance. It is argued that impedance measurement is used because low alternating currents do not lead to corrosion of the metal contact and electrolysis of the electrolyte. An upgraded version of this fingertip is commercially available as "BioTac" sensor [99]. It contains 19 electrodes and the spatial resolution is given as 3mm.
Apart of the tactile sensing, it also features measurement of the overall fluid pressure and temperature. The overall fluid pressure can be sensed much faster then the impedance, the impedance is sampled at 100hz and the pressure at 1040hz, both are 12 Bit values [100].

A capacitive tactile fingertip for the iCub was realized by modifying the modular system shown in the previous section 2.2.1.
The same AD7147 capacitive sensor chip as used in the modular system is employed with a flexible PCB with 12 sensor electrodes. The PCB has been redesigned to it can be folded around a rigid fingertip core made with a 3D

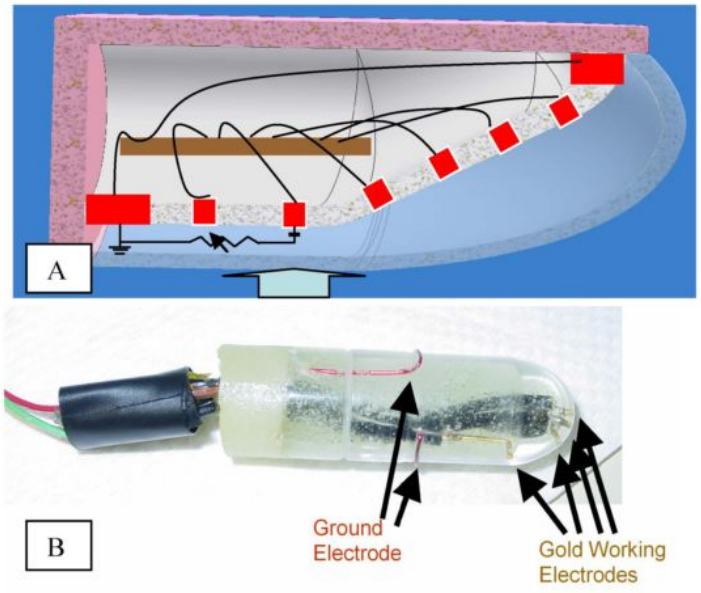

Figure 2.21: A: Schematic of the Biotact fingertip. The rigid core (white) contains the electronics (brown) which is connected to sensing electrodes (red). The electrodes are covered by a weakly conductive fluid under a elastic skin (light blue). B: A prototype of the fingertip. Image source [98], ©2007 IEEE.

printer.
To make the capacitive sensing work with non conductive objects, again a dielectric silicon is used as cover material where the upper layer is connected to ground potential. When the finger touches an object the silicon is compressed, and the capacitance a sensor electrodes measures is changed [101].

A piezoresistive tactile fingertip in the shape of a human finger is presented in [102]. In contrast to other tactile fingertips it consists of only one base shell which contains all necessary parts. The fingertip is designed to fit onto the shadow robot hand [103]. It has 12 tactile cells, employing the single sided resistive measurement design as known from Fig. 2.18.
The sensor cells are on the outside of the shell, and the measurement electronic is on the inside (see Fig. 2.22). Both the tactile sensor electrodes as well as the pads for the measurement electronic and corresponding tracks have been structured by a laser onto the shell.

This process is called Laser-Direct-Structuring (LDS) [104]. For this process a special thermoplastic material has to be used. This plastic gets molded

Figure 2.22: A 3D shaped piezoresistive fingertip. Left: The sensor side with the M shaped electrodes. In the upper right one can see the foam cover that is put onto the fingertip for operation. Right: The electronics are inside the fingertip and soldered right onto the processed plastic. Image source: [102]

into a form, here the shape of a fingertip. The shell is then processed with a laser, which draws the tracks and electrodes on the surface. The plastic contains a special additive which changes its molecular structure under the laser beam. The processed shell is then placed into sequential chemical baths, which builds up copper and a final gold coating on the activated regions.

The sensor electrodes are drawn over the curved surface of the shell, and the pads and traces for the measurement electronic are be drawn seamlessly onto the inside. The advantage of this construction is that it needs less space as the components are directly soldered onto the activated plastic.
The shape of the electrodes was chosen to be the one that has been developed and evaluated during the course of this work, as the results of section 3.3.4 have shown that this design is very sensitive to first touch.
The average spatial resolution is 5.5mm. The measurement electronic consists of an 8-Bit microcontroller with integrated ADC that can sample the tactels at a speed of about 1kHz.

Slip detection

As slip detection is an important skill for the proper manipulation of objects, there have been multiple attempts to create tactile sensors that are optimized for this task.

A slip sensor that works by measuring temperature changes is presented in [105]. It is not capable of detecting incipient slippage, but it is good at detecting small amounts of slippage.
It consists of a polyamide film on which a microheater is printed. The microheater is an electrode patterned in a small rectangle (1.5 x 1.5mm). The microheater is warmed by the Joule effect, current is sent through the electrode by a control and sensor circuit so that the temperature of the heater is constant.

The sensor circuit measures the current and resistance of the microheater and can deduct the temperature of the heater through Joules law. When an object contacts the sensor, the heat is conducted at a material specific rate, which can be sensed by the control electronic as the current that is needed to hold the temperature changes. Through this the sensor is able to discriminate different materials through their thermal conductivity. When slippage occurs this is also detectable, as the power needed to heat the structure suddenly increases.

A fingertip for robots with slip sensing capability is shown in [106]. The slip detection is realized via an accelerometer integrated into the tip.
The fingertip consist of a rigid core with an outer rubber skin and a foam in between. The accelerometer is placed inside the finger and attached to the rubber skin. Due to the foam, the skin can be compressed when a object is touched. The accelerometer can measure the microvibrations which occur when an object is beginning to slip.

In this regard also the preferred surface structure for a slip sensor is discussed. It is argued that a smooth surface (roughness less then one micron) produces a very large coefficient of friction, which causes large scale stick -slip motions as the object slides over the surface.
A mat finish on the surface (roughness of a few tens of microns) allows for better (smoother) slipping, but does provide only minimal vibrations to the sensor. The best texture is similar to human fingerprints, having parallel ridges a few hundred microns wide and up to a few hundred microns high. This skin texture does not show the adhesive behavior of very smooth skin, and as ridges catch and snap back from the object during sliding, strong enough vibration signals are produced.

A material that is often employed to create slippage sensors is polyvinylidene fluoride (PVDF). PVDF shows a very strong piezoelectric effect, it generates a voltage under strain. The strain cause a change in the surface charge

density of the material so that a voltage between its surfaces is created. The amplitude and frequency of the signal is proportional to the deformation of the PVDF material. When the deformation is reversed, the output voltage is of opposite polarity.
The voltage output can be enhanced using a very thin PVDF film, as relatively small forces create very large stresses within the material. This voltage is large enough so it can be directly sampled by an ADC. PVDF however allows only dynamic sensing, a static force does not produce a voltage.

An artificial finger skin for slip detection based on PVDF sensors is shown in [107]. Multiple small PVDF strips are embedded in ridges of a silicone block. The setup is made to resemble the rapidly adapting (RA) tactile cells in the human finger. The output of the PVDF sensors is recorded during slip and an artificial neural network (ANN) trained to recognize incipient slip.

A sensor which is modified to detect lateral dynamic force and its direction is presented in [108]. A PVDF film is modified by adding a silicone rubber column which is mounted orthogonal onto the film. Below the column are electrodes. When the column is pressed laterally, it acts as a lever and compresses the PVDF on one side and lifts it on another side. By comparing the voltages of the electrodes, the slip direction can be determined.

We have now seen that slip detection for robot grasping is possible using special tactile sensors. However the usage of dynamic sensors does not allow to monitor static forces, and single tactile sensors allow no tactile spatial information.

2.2.3 Tactile input devices

One of the first tactile input devices for a computer was the RAND graphic tablet which was introduced in 1963. It had a tactile surface of 26cm x 26cm and 1024x1024 tactels, yielding a resolution of 2.54mm. It functions together with a special pen, which is tracking its position on the tablet. The tablet contains a grid of electrodes in X/Y arrangement. The lines get pulsed with an electrical signal that codes their line number. The pen has a high input impedance electronic, which picks up these pulses when placed in close proximity over a line. It converts the pulses back to digital coordinates, and transfers this information via cable to the PC. The pen has a small switch at its tip, so that the position tracking is only active when the pen is pressed onto the tablet [109].

Graphic tablets with pens are still widely used today. They now operate with a wireless pen that is powered through the tablet via induction. To determine the pen position, most modern tablets make use of electromagnetic induction, using a grid of wires to operate as both transmitting and receiving coils (in contrast to the wires of the RAND tablet which only transmitted data). An electromagnetic signal is sent through the wires and picked up by the pen. The electronic inside the pen picks up the signal and sends data back. With analog tablets, the pen contains a coil/capacitor (LC) circuit which resonates with the excitation signal on the grid, this resonance signal is picked up by the tablet and the pen position is calculated via interpolation and fourier analysis [110]. In digital tablets the position is transmitted in discrete values between pen and tablet, optionally along with a pressure value, tilt angle or button status of the pen. Pens which offer pressure sensing usually contain a small strain gauge [111] or force sensitive resistor [112] in their tip.

Another tactile input device for computers which is widely used today is the touch screen. The first touch screen for a computer can be traced back to 1965. There a touch display was presented which was used in air traffic control and consisted of thin wires placed on top of a monitor surface. When a finger was contacting a wire a change in capacity was registered. The information which wire was touched was fed into the computer and used to select menu items. In this regard it was an one dimensional touchscreen, as it did not return X/Y screen coordinates but the index of one of 16 horizontal lines [113].

In 1972 the PLATO IV system was built by the University of Illinois and was used for the education of students. It was a computer system which had terminals connected in a proprietary network and an advanced graphical output terminal (see Fig. 2.23). It was using a plasma display with a resolution of 512x512 pixels, onto this display a 16x16 touch grid was mounted. This grid worked by using opposing infrared diodes and sensors. When a finger was touching an item, it blocked the light from reaching the sensors in X and Y dimension and thus the screen coordinate was given [114, 115].

The capacitive principle is still widely used in the touch screens of today (as in mobile phones, pads and monitors). Thereby the so called surface capacitive touch panels consist of a uniform conductive coating on a glass layer. Electrodes in four corners of the panel create an uniform electric field across the conductive layer. As an conductive object approaches (like a human finger), the electric field gets disturbed by the parasitic capacitance of the object. Current is drawn from each corner of the panel, the amount is be measured

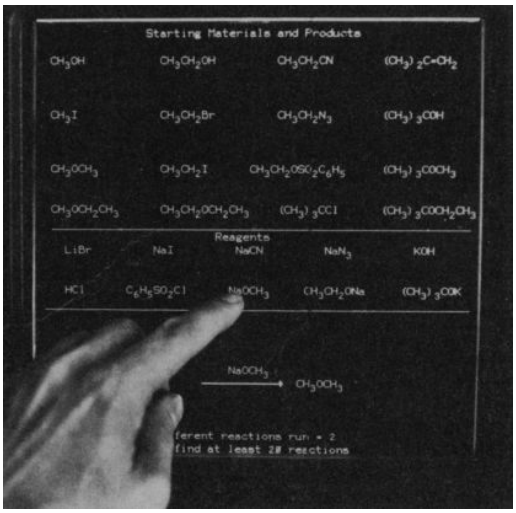

Figure 2.23: The 1972 PLATO IV was a computer for educational purposes which featured a high resolution display and a 16x16 touch grid infrared panel. Image source: [114]. From Science, vol. 192, 1974. Reprinted with permission from AAAS.

and the contact position interpolated [116]. This however does not allow the usage of non conductive objects for contact, or provides a measurement related to contact force.

An alternative to capacitive sensing is using a resistance based method for touch screens, this is often employed in mobile devices, PDAs and cameras. Thereby two glass or acrylic panels are integrated into the screen. Each has a special coating that creates a resistance gradient between two sides. When mounted onto each other, the position of a contact that connects both planes can be determined through measuring the resistance values for the X and Y directions.
Due to the conductive coating, the screens have a lower clarity then capacitive based designs. Also they require a higher contact force, as the panels must be physically pressed together. However they are the most affordable type of touch screen. [116, 117].

Tactile sensing for larger areas, as in multi-touch tables is often realized by optical methods. One way to realize a multitouch table is to use a (partly) transparent table, IR emitters and a video camera. Methods that use this setup are frustrated total internal reflection (FTIR) [118], diffuse illumination (DI) [119] and diffused surface illumination (DSI) [116]. The video camera is

mounted below a transparent table surface, and the IR emitters highlight the fingers on the table, the camera sees IR blobs at the position of the fingertips.

The conventional optical methods require quite bulky constructions as a camera is needed in some distance under the table, and a PC for image processing is used to determine the contact blobs.

Alternative methods make use of LCDs with integrated sensors, which allows a much slimmer construction. The PixelSense table [120] by Microsoft uses optical sensors that are embedded with every pixel. For this an IR emitter and receiver is employed at every pixel. The emitter measures the amount of light that is reflected back and this data is collected and combined by an internal processor.

A multitouch table that works with capacitance is the DiamondTouch table [121]. This table was designed for interaction with multiple people and it can distinguish which person is touching which position. This is done by using special chairs that are part of the system. The touch sensing works by using a transmitter array under the display surface which transmits small radio-frequency signals to the fingertips of the users. Each chair is equipped with receiver electronic which reads this signal after it has been transferred through the human body.

The technology in touchpads, as common in laptops or keyboards, is mostly based on capacitance. One of the most common type of touchpad works by using two grids of electrodes which are separated by an insulation layer, thus forming a capacitor when the lines are charged. As third layer, a sensor electrode is mounted below the other layers and measures the capacitance of the upper layers.
The lines are alternately charged and the capacitance measured. A fingertip placed above the sensor disturbs the capacitance from the normal level. The position of the fingertip is interpolated by using the capacitance values for all grid points, and thus can be higher then the grid resolution [122, 123].

We have now seen that there exist quite a few technologies (resistive, capacitive, optical) to realize tactile sensitive surfaces. However the currently available implementations hardly excite us. As in our tactile table scenario we want to use information about contact position and strength and the currently available tactile surfaces are made to provide only location and hardly any force information. Furthermore we want to realize tactile tables in various dimensions, whereas touchscreens come in fixed sizes. It might be possible to

create a camera based system where the table size can be more easily altered, but these solutions are bulky and again do not give real feedback about contact forces.

2.2.4 Tactile objects

The study of human fingers forces is a topic of interest for scientists from diverse fields such as biology, psychology and robotics. In the course of this work we have developed a tactile object which allows to record such forces, which is presented in section 4.

There are already approaches that measure human finger forces which provide very accurate results. However they are static and require the hand to be fixated in a specific position. One example is the device used in [124]. There the forearm is fixated on a block and the palm lifted to a certain degree. The fingers are free to move in the vertical direction. Steel wires hanging from a structure above the hand are attached to the fingers. The wires in turn are attached to force sensors, so when the fingers press downward, the strain on the wires is measured.

The finger-force linear sensor (FFLS) device is another device that was built to measure forces applied by the human fingertips [125]. The device consists of a plate onto which the human hand gets strapped at the wrist. The fingers are attached to metal blocks with strain gauges using adjustable bands. The strain gauges can measure the force exerted by the fingers either through pushing or pulling. The thumb is placed into a cylinder that is custom shaped for each participant. This cylinder is attached to a 2D strain gauge sensor, through this the thumb forces can be recorded regardless of its rotation. The design allows for a very precise recording of individual finger forces.
The drawback however is that the scenario is very artificial for the participant and it is not possible to monitor real-world applications with these approaches.

Another approach is to put tactile sensors on the human hand. This has been realized in various implementations to create tactile sensitive gloves [126–128]. However all these gloves have the drawback of interfering with the contact of skin and object and thus change the sensory feedback during manipulation. Also most gloves have a limited amount of sensor cells that are only attached to the most prominent contact locations like the fingers, so not all

possible contacts of the hand with the object surface can be monitored.

Devices that do not change the users tactile sensation are tactile sensitive objects. These allow the user to move his hand and arm freely, creating more natural interacting scenarios. A tactile object that includes also other modalities is described in [129]. The grasp force of the whole hand is registered by a load cell inside the object. Additionally an 3 axis acceleration sensor is integrated, which records data about the movement of the object.
A tactile object with three strain gauges is shown in [130]. The user places his first and second finger on one side of the objects and the thumb on the other, he can then lift the object. Below the object are laser sensors that monitor the movement of the object.

While these devices require the participant to place their fingers onto predefined locations, there are other approaches that allow more freedom. Examples are the cable based Nara-IST cylinder [131], which is a cylinder that is covered with strips of FSR sensors and used to control a robot hand. As the whole contact surface is covered by tactile sensors, the user is free in choosing the positioning of his fingers. Also from the data that is gathered from the multiple tactile sensors, the finger contact location can be derived and compared between subjects.

Another tactile object with multiple tactile sensors is the iObject that is presented in [132]. The iObject is equipped with tactile and motion tracking sensors and was designed for evaluating the actions of a human or an anthropomorphic robotic hand (see Fig. 2.24). The iObject was inspired by the shape of a soda can and has similar dimensions: a diameter of 80mm and a height of 120mm, so it conventionally fits into a human hand.
It enables the measurement of finger contact location and force, the acceleration of the object (linear + rotational 3D) and the orientation relative to the earth (using a 3D magnetometer).

The tactile sensing is realized by using 10 sensor boards which contain 22 tactile cells. The principle of the sensor cells is the same resistive principle as known from figure 2.18. The sensor cells are round electrodes with a diameter of 5mm spaced in 10mm distance from each other. The surrounding surface is the common ground electrode.

The sensor boards are arranged in a circle and covered with a conductive foam. Each sensor board contains two 16 channel ADCs [133] which sample the electrode voltages. They are connected via a SPI bus to a central board

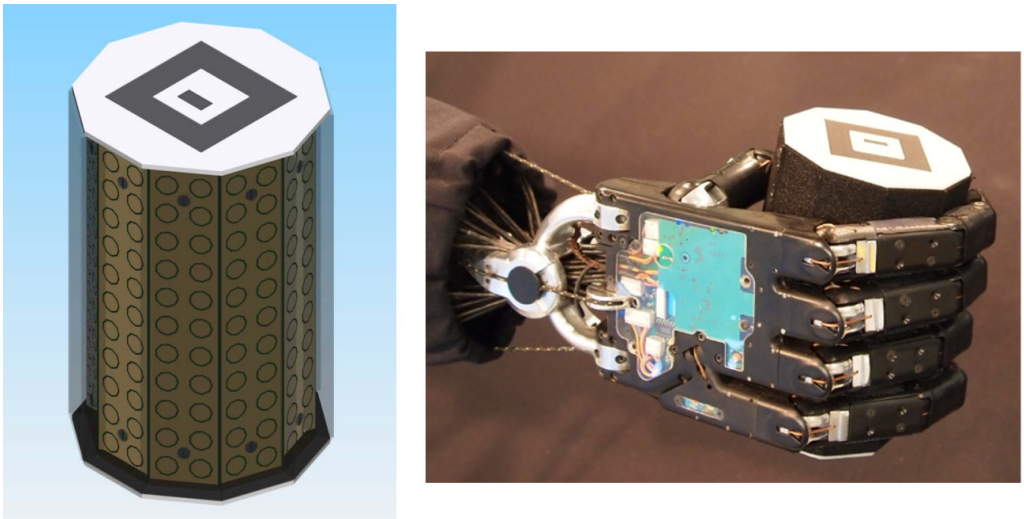

Figure 2.24: Left: A 3D model of the iObject, with the foam cover made translucent. Below the foam the sensor boards with the round tactels are visible. Enclosed by the sensor boards is the central board with blue-tooth unit and battery. The inner and outer support structures were made with a 3D printer. On top and bottom markers for vision systems are integrated. Right: The iObject fits nicely into the anthropomorphic shadow robot hand. Image sources: [132]

which contains an 8 Bit microcontroller. On the central board also a a motion tracker unit is integrated, which contains an 3D accelerometer, a 3D gyroscope and a 3D magnetometer [134].

The data from all sensors is transmitted wireless by an integrated blue-tooth module. This wireless connection is however also the bottleneck of the object, as with the data rate drops with increased distance to the receiver or in environments with electrical noise. In the optimal case, the data can be transmitted at 250 Hz, however in non optimal scenarios the rate can drop to 25 Hz or even to 0 Hz - when the wireless communication is disturbed.

2.3 Summary

In this chapter we have first looked into how important tactile sensing is in biology. We have seen how complex it is and how it works in plants, insects, animals and man. We have found that tactile sensing in biology has evolved over a long time span, and that nature uses a wide range of different tactile

cells among all organisms. The capabilities of tactile sensing are more elaborated in higher level animals and humans. The tactile sensation of our skin is actually created by a multitude of different tactile cells.

After this we looked into what methods exist to create artificial tactile sensors and what their characteristics are.
For this we have grouped the existing tactile sensors according to their applications. We have positioned our *Myrmex* system as a general purpose / modular system. We have shown that tactile sensors can be based on various principles, such as resistivity, capacitance or optical and thermal effects.

We have presented modular tactile sensor systems that are comparable to our *Myrmex* system. Their specifications have been summarized so they can be easily compared with the *Myrmex* system that we will present in this work. We have also introduced the reader to the specialized tactile sensors that are used for the various individual scenarios that the *Myrmex* system aims to fulfill.

We have seen that none of the current systems can combine the features needed to realize all the scenarios that we laid out in our motivation, that is the slip detection for robot grasping and the creation of a tactile table surface as well as the study of human finger forces.

Chapter

3

Myrmex system

3.1 Introduction

In this chapter we will describe the *Myrmex* system that we developed and present the design decisions that were made to achieve its outstanding performance. In the previous section we have seen how various tactile sensors and especially modular tactile sensor systems have been implemented. We have also compared their specifications in table 2.2.

In comparison we have listed the specification of our *Myrmex* system here in table 3.1. Through this we can demonstrate that our *Myrmex* is better suited for large scale and high speed applications then the comparable systems. Also one can see that from the spatial resolution, sensitivity and data resolution it is among the upper range of the comparable systems. We will also see that because of its modularity and granularity the scenarios of the tactile gripper, tactile grasp force analysis and tactile table can all be realized.

In addition our system also has positive usability factors that are not expressed in numbers: an auto-configuration feature and a standard USB video connection which allow for a 'plug and use' like operation of the system.

In the following sections we will explain the design and implementation of the *Myrmex* system. We start with an overview of the system layout in the next section.

Table 3.1: Myrmex system specification

Maximum tactels	32512
Maximum update rate	256 tactels @ 1900Hz
Spatial resolution	5mm
Data resolution	12-Bit
Pressure range	3-300kpA
Interface	USB video
Sensing method	Resistive

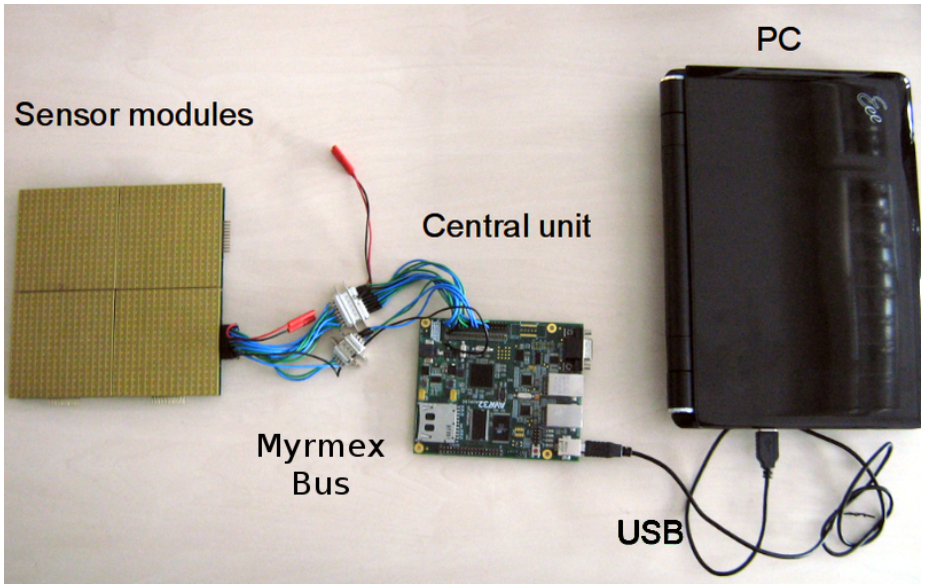

Figure 3.1: Photo of a *Myrmex* system. An array of sensor modules is connected to a central unit, which transmits the tactile data to a host computer.

3.2 System layout

A picture of our *Myrmex* system can be seen in Fig. 3.1 and a schematic overview of the system is visible in Fig. 3.2.
The organization of the system is similar to other modular systems shown in section 2.2.1. We use sensor modules that get connected to a separate unit (here called the central unit) that collects/converts the tactile data for the final transmission to a PC.

The modules are the building blocks that realize the tactile sensing capability. Due to their design and implementation they provide a high spatial

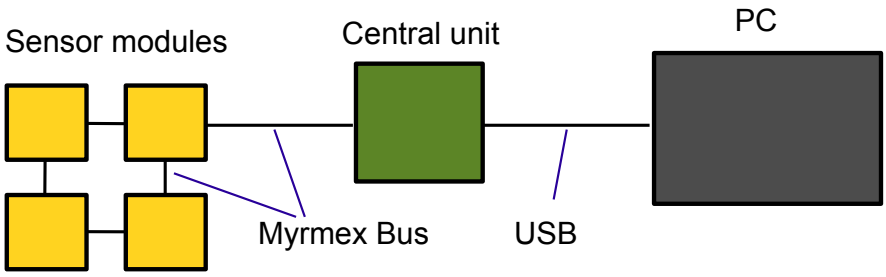

Figure 3.2: Overview of the system layout. The amount of modules can vary, but the organization is always the same. Sensor modules are connected with each other and the central unit via the proprietary *Myrmex* bus. The central unit is connected to a PC via USB.

resolution, sensitivity and outstanding speed. They will be described in detail in the following section 3.3.

Compared to the other modular systems, we can also realize a higher number of total tactels with our system, and also employ a convenient auto-configuration of the system. This was achieved by developing a proprietary *Myrmex* bus to connect the modules with each other and to the central unit. This bus will be described in section 3.4.

The central unit is responsible for collecting the tactile data and presenting it to a PC for further processing. It does so via an USB connection and registers as an USB video device - realizing a tactile camera. The central unit will be described in section 3.5.

3.3 Sensor Modules

The modules of the *Myrmex* system are the units that realize the tactile sensitive surface. Here we will first describe their implementation, then we will discuss important design decisions such as the sensing technique and the granularity of the system. Finally we show the steps that we took to optimize the sensor cell structure for this type of sensor to increase the sensitivity to low forces.

3.3.1 Implementation

A schematic overview of one *Myrmex* module can be seen in figure 3.3. A module consists of two hardware pieces: the top printed circuit board (PCB) and the bottom PCB, additionally a conductive elastomer is used as contact material.

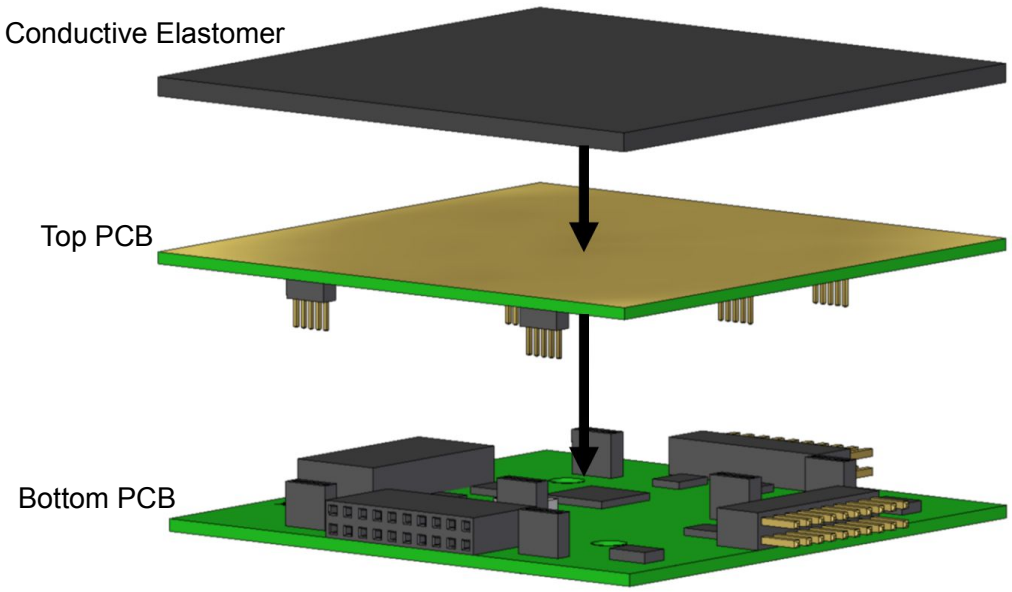

Figure 3.3: Schematic of a single sensor module: The 80x80mm bottom PCB contains control and power circuits, the top PCB contains the electrode surface and analog circuits to measure the tactile cells. The top PCB is of the same size as the bottom PCB and gets covered with a conductive elastomer.

Top PCB

The top PCB contains the sensor cells and the measurement electronics. As we choose to use the resistive approach for tactile sensing, we realized the tactile sensing functionality by creating a matrix of tactels using the parallel electrode design as known from Fig. 2.18 in section 2.2.

Fig. 3.4 shows a photo of the upper and bottom side of the top PCB. As a 4-layer PCB is used for implementation, the uppermost layer is free to be used as sensor surface. The lowest layer is used to hold the electrical components as well as the connectors to the bottom PCB. The electrical connections between the components and the sensor electrodes are done in the inner two layers.

On the top layer of the board the sensor surface is realized by a big ground electrode and multiple sensor electrodes. Inside the ground electrode are 16x16 sensor electrodes spaced 5mm apart, separated from the ground electrode through a gap. This gap gets bridged by the conductive elastomer that is placed onto the module. The elastomer acts as a variable resistor between the sensor and the ground electrode, as the resistance between the two electrodes changes when it gets compressed.

To acquire a digital value that is representative for the foam compression / tactile activation of the sensor cell, we convert this resistance to a voltage which can be sampled by an analog-digital converter chip (ADC).

This conversion is done through a voltage divider circuit. In Fig. 3.5 we see a schematic of such a circuit as used in the *Myrmex* modules. Is consists of two potentials (in our case a supply V and the ground level GND) as well as two resistors R1 and R2. In our design, R2 is the resistance between the sensor and the ground electrode through the elastomer and R1 is a fixed resistor. Between the two potentials there is the voltage U_{in}. This voltage is available in a 'divided' form between the two resistors as voltage U_{out}. This voltage is then converted by an ADC. The U_{out} voltage in relation to the input voltage and resistor values can be calculated by the formula:

$$U_{out} = \frac{R_2}{R_1 + R_2} * U_{in} \tag{3.1}$$

As already stated we wanted to make the system sensitive to even low forces. For a resistance based sensor an increase in sensitivity can be achieved

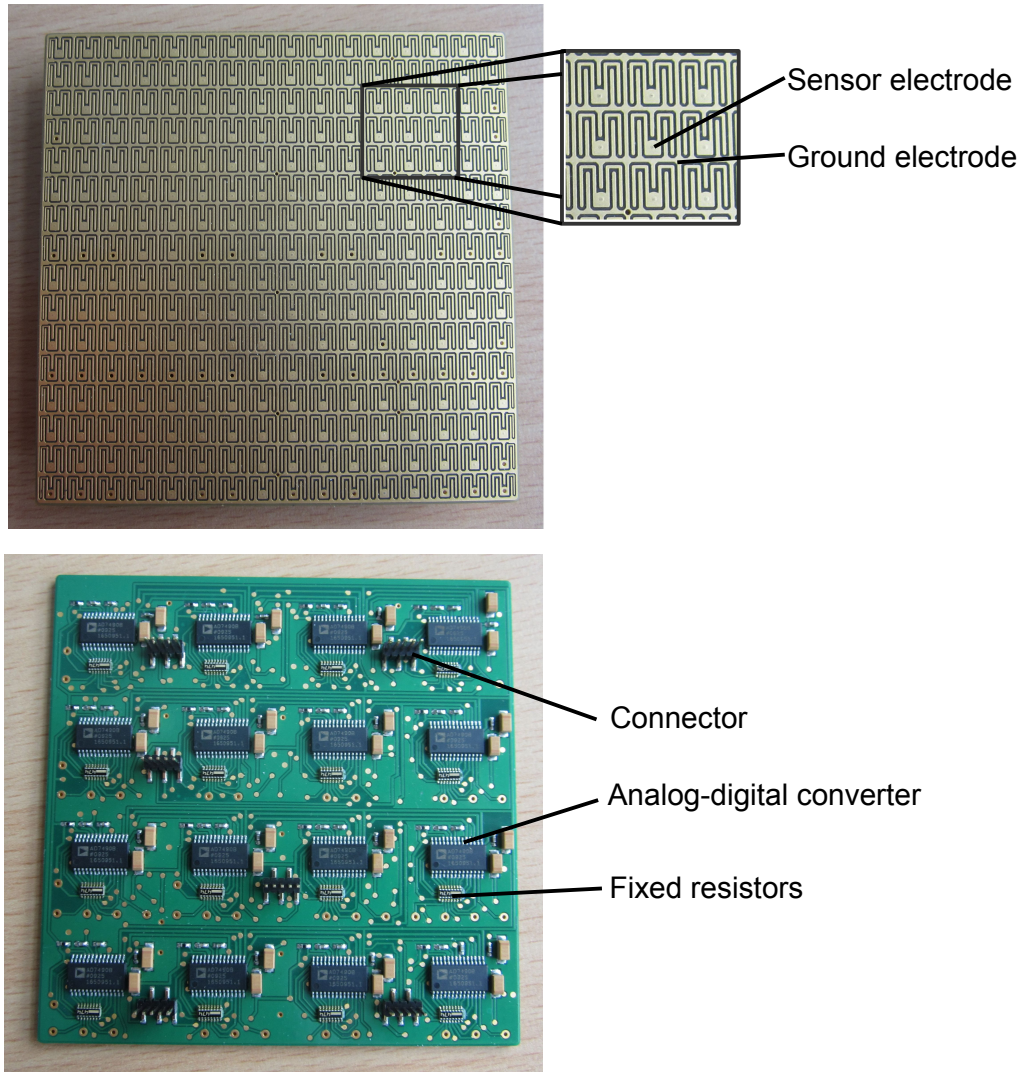

Figure 3.4: The top PCB. On its upper side is the matrix of sensor electrodes, consisting of 16x16 sensor electrodes and a common ground electrode. Each sensor electrode has a 'M' shape. The lower side of this PCB contains the analog-digital converters as well as fixed resistors used for voltage divider circuits.

by two ways: use of an appropriate fixed resistor R1 in the voltage divider circuit and a sensor surface structure that is optimized in regard to the conductive elastomer.

We have experimentally measured the resistance range for the elastomer

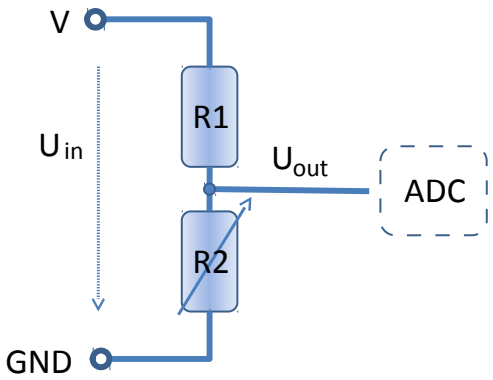

Figure 3.5: Schematic of the voltage divider circuit used for the *Myrmex* tactile sensor cells. R1 is a fixed resistor, R2 is the resistance between the sensor and ground electrode.

(R2) using our prototype *Myrmex* sensor modules. The result was that R2 for the polyurethane foam ranges from 10 MOhm (uncompressed) to 60 kOhm (fully compressed). In Fig. 3.6 we have plotted different values for R1 using this range and the formula 3.1.

We can see that a high value resistor like 1000 kOhm would provide a steep response on low pressure. However such a high value was not available in the required very small integrated chip package, so we settled on the highest possible version that is 470 kOhm.

In regards to using an optimized sensor surface, we performed experiments to find an optimized electrode design which resulted in the M shaped sensor electrode. These experiments will be presented in section 3.3.4. Additionally the sensor response in regard to different elastomers under varying conditions can be found in the sensor evaluation section 5.

Bottom PCB

The bottom PCB contains all the control and voltage regulation electronic that is necessary for a module to function. The heart of the control logic is the PIC32 microcontroller (see Fig. 3.7).

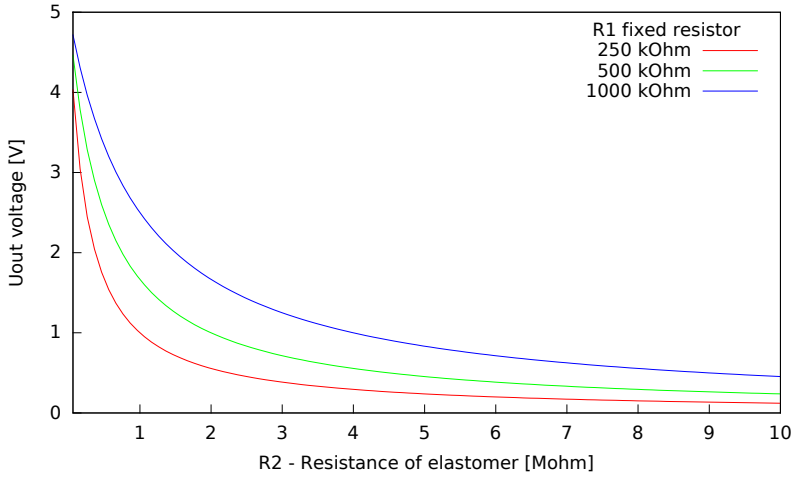

Figure 3.6: The output of the voltage divider according to formula 3.1 in relation to the elastomer resistance R2 and the fixed resistor R1. The elastomer resistance gets lower as it is compressed. When the foam is lightly touched, R2 is high and here a steep response is preferred for a good sensitivity.

This chip is connected to the ADCs of the top PCB via a SPI bus. During operation the MCU collects the tactile data from the ADCs. The top PCB is mounted to the bottom PCB through 6 sockets that are distributed over the PCB. Their locations where chosen to create a stable base for the top PCB while preventing a false assembly (there is only one way the top PCB can be rotated to fit into the sockets).

The MCU is also connected to the proprietary *Myrmex* bus via electrical buffers. These buffers are located at the four connectors that allow the modules to get physically and electrically connected. The buffers function as gates for the bus, they can control if the module is connected to the bus. Details about their role in the bus operation can be found in section 3.4.

As the amount of components needed to realize the bottom PCB is much smaller then for the top PCB, we only use a two layered PCB and have all the components mounted on one side.

3.3.2 Granularity

We have now shown that our *Myrmex* modules have a dimension of 80x80mm and use 16x16 sensor cells, resulting in a spatial resolution of 5mm. These numbers were guided by technical limitations but are also the result of design

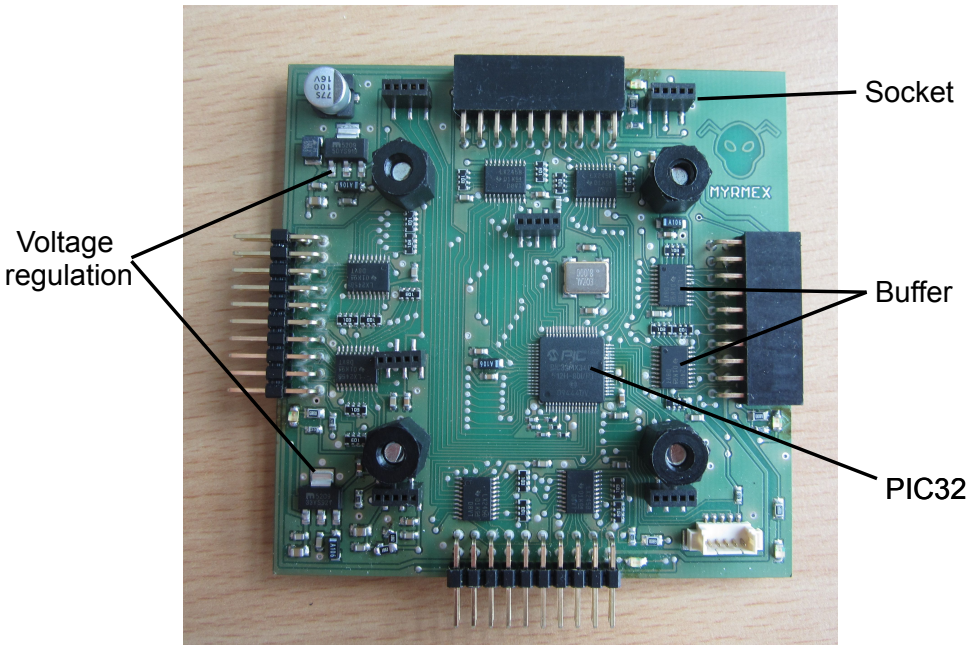

Figure 3.7: The bottom PCB contains the PIC32 MCU which collects all the tactile data from the ADCs of the top PCB. On this board also the voltage regulation electronic for the module is located. At each side of the PCB are the connectors through which the modules can be interconnected with each other. Each connector has two buffer chips through which the *Myrmex* bus runs. The sockets on the board are used to hold the top PCB.

decisions that we will present here.

When designing a modular system the granularity is an important factor as we encounter a trade off situation: larger units are favorable for the economies of scale but smaller units allow a higher variety of application scenarios.

With a large granularity the design of the electronics would require less redundant parts and assembly (which results in lower construction cost and time) and less complex control logic is needed to organize and run such a system. Large modules however are not good for the versatility as some scenarios like the gripper/finger tip would become unrealizable if the modules are too big. To have the widest range of possible application scenarios it would be favorable to choose a small physical size for the modules.

Choosing a too small granularity however creates problems when a larger

area needs to be covered, because of the increased complexity and overhead. On the usability level it takes more effort to physically compose a large area like the tactile table, as in creating the electrical connections. While this is an one time effort each time that the system is used, the more important drawback is that the speed of the system may be negatively affected. A small granularity is likely to create organizational overhead which will affect the overall throughput of the system, e.g. to obtain the tactile data one has to address and communicate with each of the numerous modules.

After weighting these considerations and including the future applications of the system, the size of a single sensor module was chosen such that it covers large parts of everyday objects which are graspable with a human hand e.g. a cup, a bottle, or a pen. Hence, each sensor module has a sensitive area of 80×80 mm which roughly resembles the size of a human palm. In our view the inspiration by the human hand dimensions fits well in the scope of human manual interaction research.
For example, in context of the tactile table, an surface area that is manipulated by a human hand is very likely to have a dimension of at least the size of the human palm. The exception may be very fine object manipulation done with few fingers e.g. picking up a needle.

With a guideline for the overall dimension of a module, the next question is the density of sensor elements, which is dependent on the application requirements and the sensing technique used.

The ideal sensor module would of course have a spatial resolution near infinity, or very small (1mm) as comparable to the human fingertip. Here however practical limitations come into play. With increasing density of sensor elements, the wiring of the sensor electrodes and components gets more and more complex. Also the amount of data that is transmitted would increase and slow down the sensor system, which conflicts with the targeted high speed.

For these reasons we found that the spatial resolution of 5mm together with the surface size of 80x80mm (using 16x16 sensor cells) provides a good balance between resolution, amount of data and challenge of technical implementation.

3.3.3 Measurement technique

The basis of the *Myrmex* system is the tactile sensing technique and as shown we have used the resistive one. Here we will discuss why we chose this technique.

In the related work section 2.2 we have shown a lot of different tactile sensors and sensing techniques. However not all of them are suited to create dense arrays of tactile elements. For a modular system it is desirable that all the tactile elements together with the accompanying measurement circuits can be integrated together on minimal space and do not interfere with each other.

If we recall our comparison of modular tactile systems in table 2.2, we see that most modular systems use either an optical or resistive approach. We have also decided that our system should have a spatial resolution of 5mm or better, this number has only be achieved with the systems that are based on resistive or capacitive measuring. The capacitive measurement principle is however prone to electrical noise if not properly shielded, and requires modifications to handle non conductive objects.

The review of the comparable systems and the higher robustness compared to capacitive sensing have tilted our decision towards the resistive measurement technique.

To limit the wiring effort and to reduce environmental influences on the signal quality we also decided that each sensor module should acquire and digitize its sensor readings locally close to the electrodes, and only transmit digital values to the central unit.

To remove any cross talk between sensor cells and to increase the potential speed of the sensing, we use an individual voltage divider and an ADC input for each sensor cell.
This increases the amount of components needed (1 resistor and 1 ADC input per cell) compared to matrix approaches.

In a matrix approach one would use rows and columns of sensor and ground electrodes. A single ADC input would be connected with multiplexers to the currently active ground / sensor electrode. This however would limit the possible speed of sensing, as each selecting and switching between electrodes needs time.

In our design a single module has 256 tactels and the employed A/D converters (ADCs) provide 16 multiplexed input channels, so we use 16 ADCs per module where each is covering a sub area of 4×4 tactels.

This makes it possible to achieve a high sensing speed by using all 16 ADCs in parallel. The details of this are shown in section 3.4.6.

3.3.4 Optimization of sensitivity

We have already shown in section 3.3.1 that we selected the fixed resistor R1 to have the highest value possible for our implementation to increase the sensitivity of the system to low forces. However there is still another factor that can be optimized for a high sensitivity, that is the shape of the sensor cells.

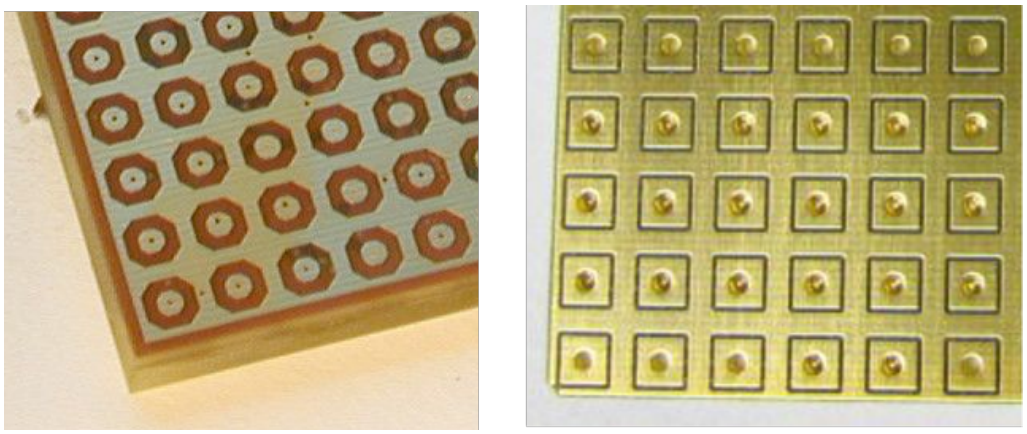

Figure 3.8: The sensor cells of the Weiss Sensor [88] (left) have a round shape and the *Myrmex* precursor used a square sensor shape [9] (right). While the selection of these shapes seems arbitrary, we conducted experiments to create an optimized shape for better sensitivity.

To optimize the sensor shape for a higher sensitivity, we will first look in more detail into how the resistive tactile sensor principle with a conductive foam as elastomer works.
The resistivity between the electrodes of a resistance based tactile sensor cell actually amounts to two components: the internal resistivity R_V of the sensor material between the electrodes and the surface resistivity R_S at the transition from the electrode to the sensor material (see Fig. 3.9).
It has been shown experimentally that the surface resistivity R_S has the main

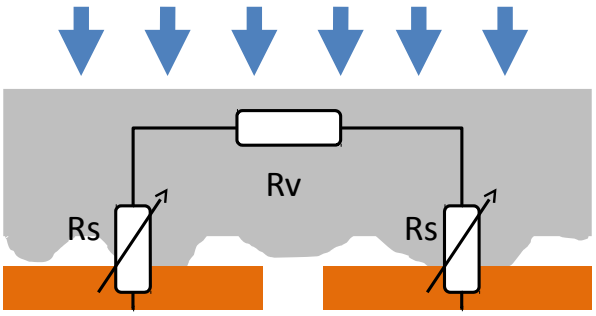

Figure 3.9: Working principle of a resistive tactile sensor: An applied load increases the contact area between the sensor material and the electrodes, thus decreasing the surface resistivity R_S (adapted from [135]).

contribution to the load-dependent variation of resistance [135].

The change in the surface resistivity R_S is primarily caused by an increase of the actual contact area between the electrode and the sensor material: If a load is applied, the rough surface of the sensor material is pressed against the electrode, thus increasing the actual contact area.

To increase the sensitivity to light loads, a simple method is to reduce the distance between both electrodes thus decreasing the material resistivity R_V, as it is proportional to the distance the current has to travel through the material. Through this the influence of the surface resistivity R_S to the combined resistance is increased.

Another powerful method to increase sensitivity when using a conductive elastomer with a rough surface structure (like a foam) is by taking advantage of single bulge contacts. The surface structure of a foam is not planar but consists of a multitude of bulges and indentations.

When the foam is pressed down, at least two contacts have to be created by two bulges on the sensor and on the ground electrode, through which the current flows. If a bulge of the sensor material is located directly above the gap between the inner and outer electrode it can simultaneously contact both electrodes when pushed down, which reduces the distance the current has to travel through the material. Hence, it seems to be a reasonable strategy to increase the probability of such single bulge contacts. This can be achieved by increasing the circumference of the gap between both electrodes. An in-

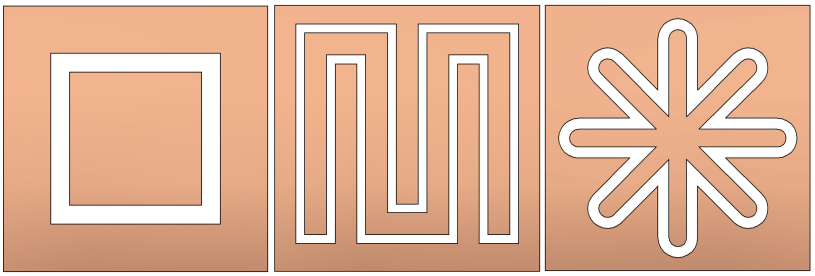

Figure 3.10: Sensor designs that were evaluated: quadratic sensor shape, M shape and star shape.

creased circumference means that the area where a single bulge can contact both electrodes is increased.

As this is possible with various electrode designs, we conducted an experiment with different sensor shapes as shown in Fig. 3.10. For each of these shapes we considered several variations regarding the width of the electrodes themselves as well as the gap between them. The parameters of all tested shapes are summarized in table 3.2. The star- and M-shaped electrodes were more restricted in possible configurations of their parameters, because there are constraints on the width of electrode traces due to PCB production limitations. Because of this the number of quadratic shape configurations that were tested is larger. A photo of the PCB is shown in Fig. 3.11. We created a 3x3 area of each sensor shape and tested the middle cell.

To quantify the sensitivity of the sensor cells we used the measurement setup shown in Fig. 3.12 composed of a 3 DOF CNC linear table and a digital scale weight. The sensor array was stressed with a 5 mm diameter probe mounted to the tool mount. The results of probing each sensor configuration at a fixed load and with a polyurethane foam used as an elastomer are also shown in table 3.2.

The dependency of the sensor output on the distance of both electrodes is summarized in Fig. 3.13. The visible decay supports our hypothesis, that a reduced average electrode distance will increase sensitivity. In Fig. 3.14 we see the sensor output in relation to gap circumference and again our hypothesis seems valid as the output is higher with the designs that have a larger circumference.

Due to these results we selected the M-shaped electrode design (with ID 'K') for our final PCB layout, as it at the same time minimizes the average elec-

Table 3.2: Properties and sensitivity of the various sensor shapes.

sensor shape	ID	circumference of gap [mm]	max. distance of electrodes [mm]	min. distance of electrodes [mm]	avg. distance of electrodes [mm]	sensor output avg. of 10 samples
quadratic	A	12,0	2,40	0,32	0,95	2519,0
	B	9,3	2,02	0,40	0,93	2644,9
	C	8,0	1,91	0,53	1,04	2375,8
	D	7,2	1,98	0,73	1,26	2669,7
	E	6,8	2,09	0,83	1,38	2413,1
	F	8,0	2,55	1,03	1,68	2296,0
star	G	35,9	2,55	0,15	0,59	2787,8
	H	31,6	2,30	0,21	0,61	2680,2
	I	32,7	2,40	0,20	0,69	2662,8
M	J	37,1	1,38	0,21	0,40	2641,8
	K	37,4	1,41	0,21	0,41	2680,8
	L	37,0	1,48	0,30	0,52	2856,4
	M	36,5	1,45	0,30	0,53	2599,0

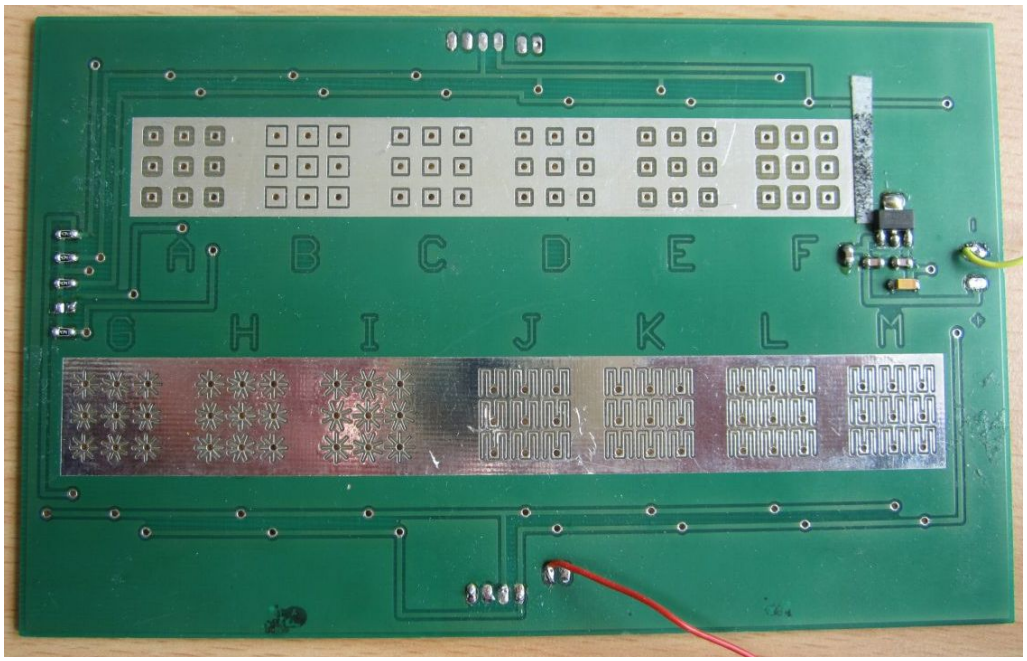

Figure 3.11: Photo of the test board with the different sensor shapes that were evaluated. Each shape / size combination is marked with a letter for identification (A-M).

trode distance (reducing the influence of the material resistivity R_V) and maximizes the circumference (increasing the probability of single bulge contacts).

To verify the improvements we repeated the experiment to compare full modules with 256 sensor cells. One module had a top PCB with square-shaped design and the other had a new top PCB with the M-shaped electrode. To reduce variance, we applied the loads to a stiff plastic sheet covering the whole sensor area, thus uniformly distributing the pressure onto all tactels.

Repeating this procedure 10 times, we finally averaged of all $256 \cdot 10$ sensor readings. As can be see from Fig. 3.15 the characteristic curve of the optimized sensor design is shifted by a constant amount compared to the original sensor design.

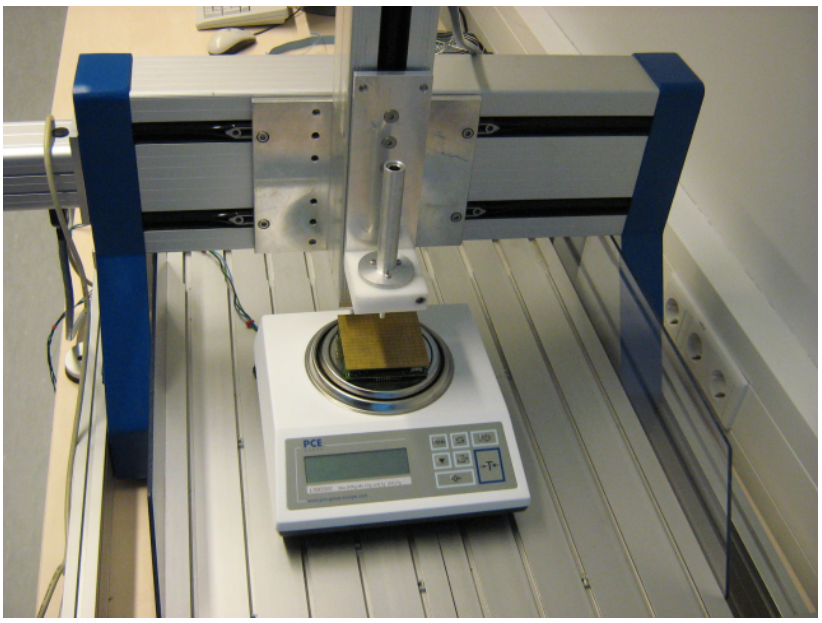

Figure 3.12: Measurement setup with 3 DOF table, scale and sensor.

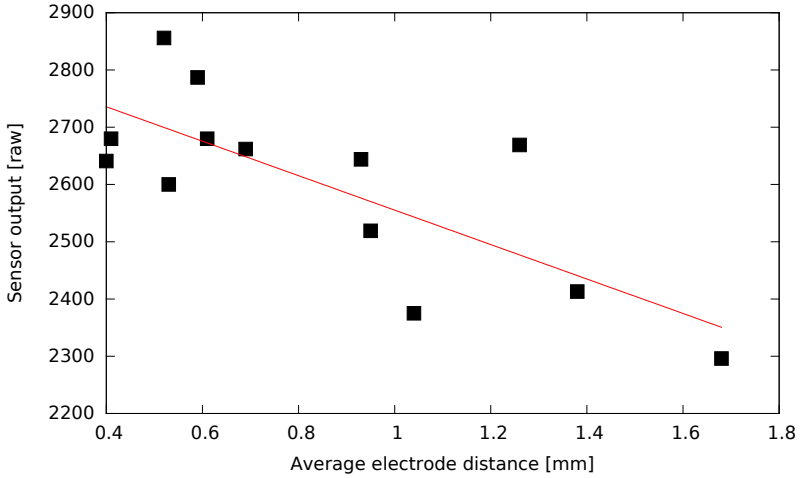

Figure 3.13: Sensor output in relation to the average distance between both electrodes. Sensitivity increases with decreasing average electrode distance.

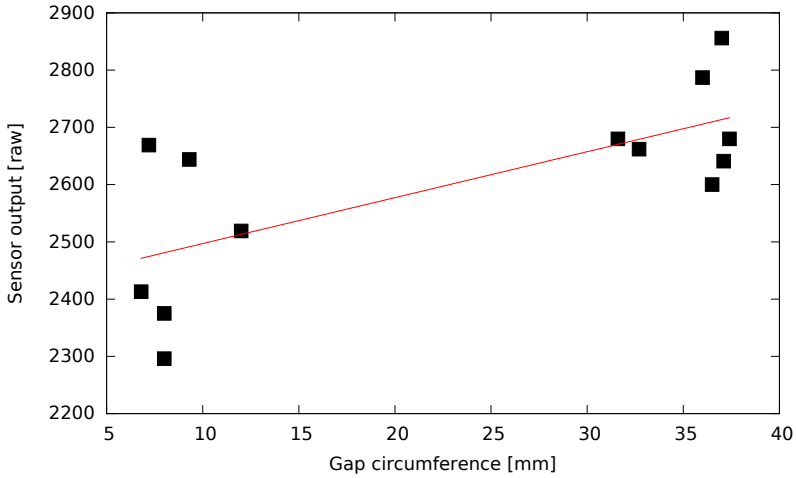

Figure 3.14: Sensor output in relation to the circumference of the gap between the two electrodes. Sensitivity increases with increasing gap circumference.

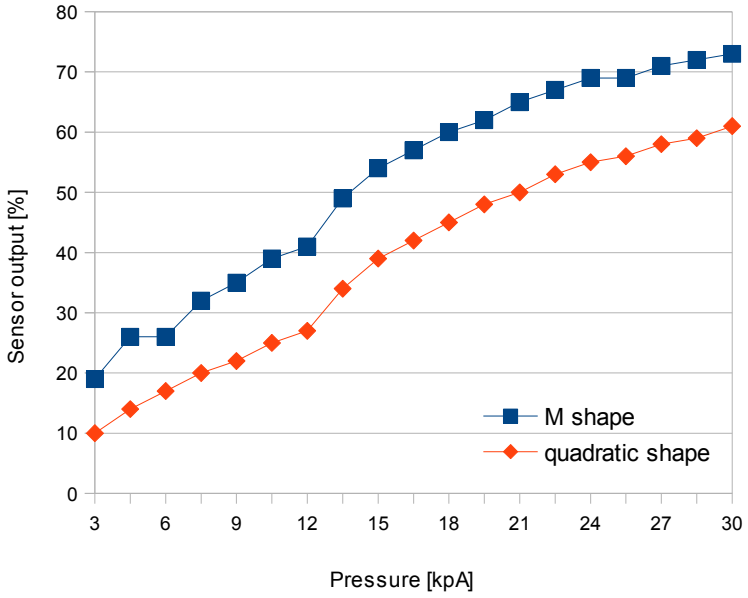

Figure 3.15: Comparison of the sensor output for quadratic and M shape with increasing overall load ranging from 3 to 30 kpA. The characteristic curve is shifted by a constant value, thus increasing sensitivity.

3.4 Myrmex Bus Design

3.4.1 Design Considerations

As shown in the system layout section 3.2, the *Myrmex* system is composed of tactile sensor modules and a central unit. The sensor modules generate tactile data and the central unit collects the tactile data from the modules and sends it to a PC using an USB connection, making the system very compatible. The bus system that is used for the communication between the modules and the central unit however is not visible to the PC and thus has not an effect on the compatibility, allowing us to consider non standard options.

We choose to implement our own bus system for the *Myrmex* system, as this allows to implement features that are not possible using one of the conventional bus systems.
As described earlier, one of the features that sets this system apart from competitors is an intelligent auto configuration. Our motivation for this is that we developed the system to be used in various tactile interaction scenarios, it was made modular so various physical configurations can be achieved. This physical configuration, the amount of modules and how they are connected, however needs to be known by the system, so it can properly collect the tactile data and send it to the PC.

A simple method to solve this problem would be to let the user create the configuration data and send it to the central unit or hardcode it into the source code. This however creates extra work for the user and reduces the accessibility of the system. Because of this we developed an auto configuration algorithm that lets the system figure out its physical configuration by itself after powerup.

To understand the auto configuration algorithm and the *Myrmex* bus operation, we will first give an overview about the *Myrmex* system states in the next section.

3.4.2 System states

To understand the operation of the *Myrmex* bus and the whole system, knowledge about the different system states is essential. The *Myrmex* system uses only two states: configuration mode and full transmit mode. The two states define different behavior of the modules, the bus and the central unit. The transition between the two states is irreversible and controlled by the central unit. A schematic of the different system states can be seen in Fig. 3.16.

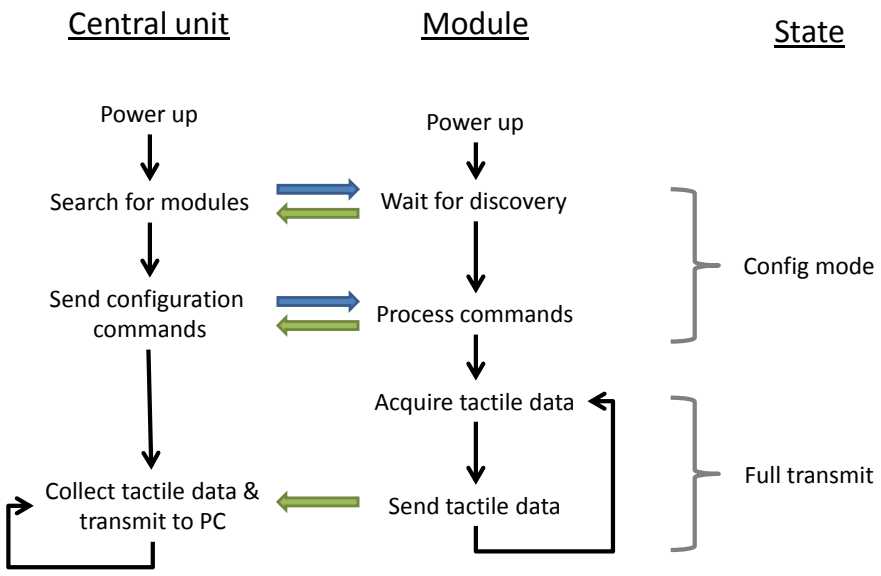

Figure 3.16: The two states and their transition. Depending on the state the modules and the central unit perform different actions. The blue arrow indicates data transmission from the central unit to the modules, which only happens in the configuration mode. The green arrow indicates data transmission from the modules to the central unit.

After powering the system, all modules and the central unit are in the so called configuration mode. This state is defined by the *Myrmex* bus allowing bidirectional communication between the central unit and the modules. This state has two phases, after which the transition to the full transmit mode occurs. The first phase is the so called discovery phase. In this phase the central

unit discovers the modules that are on the bus. The information from this process is then used to determine the physical arrangement of the modules. The discovery process is described in section 3.4.4.

The next phase is the configuration of the modules by the central unit. This phase is characterized by the central unit telling the modules what connections they should use to route the bus through the array, and setting the system parameters for speed and compression. This process is described in section 3.4.5.

After the configuration is finished, the system enters the full transmit mode. In the full transmit mode there is only data communication from the modules to the central unit, that is the data from the tactile sensor cells. The central unit collects the data from all modules and then forwards it to the PC, this process is described in section 3.4.6.

As the *Myrmex* system was designed to deliver very high frame rates, we will look in section 3.4.7 at how this is achieved. How this system speed scales with multiple modules is analyzed and explained in section 3.4.8.

First of all, we will look at how the *Myrmex* bus is physically implemented in the next section.

3.4.3 Physical Implementation

The *Myrmex* bus uses 15 signal lines, of which 12 are used for data bits and 3 for control. The voltages used on the lines are 3.3V for a high signal and 0V for a low signal. The function assigned to each line depends on the state that the system is - configuration mode or full transmission mode.

As introduced in the previous section, the configuration mode is used after the powerup of the system to exchange data between central unit and the modules for the discovery and configuration of the modules. Because of this some lines are configured to allow data transfer from the central unit to the modules. After the configuration phase is finished, the full transmit mode is used to transfer the tactile data from the modules to the central unit using all available data lines.

The function of each line is documented in tables 3.3 and 3.4. Table 3.3 shows the bus line description in the configuration mode. This mode is the default into which all modules go after power up. In this mode 8 of the 12 signal data lines are configured as input to receive command bytes from the central unit, while 4 are used by the module to sent data back. After the configuration, the bus operates in full transmit mode as shown in table 3.4.

The two different configurations of the bus are possible because the direction of the bus lines can be changed by the buffers used on the modules. As shown in section 3.3, a module has two buffers on each of its four sides. One of the buffer chips controls 8 data lines and the other 4 data lines and 3 control lines.

The communication between the modules and the central unit is controlled by the three control lines of the bus: NEW_DATA, INT and RESET.
The transmission of commands in the configuration mode is done by the central unit. It outputs a command byte on its 8 data lines, then toggles the INT line. The module recognizes this and acts according to the command. When the module has finished processing the command or has put requested data on its 4 data lines, it toggles the NEW_DATA line to inform the central unit. If a command requires multiple data transmissions, they are done using the same procedure by toggling the NEW_DATA and INT lines alternately.

The commands used in the configuration mode by the central unit and the modules are shown in appendix A. Table A.1 shows the 8 Bit commands used by the central unit, and the corresponding 4 Bit answers of the modules are shown in table A.2.

The transmission of tactile data in the full transmit mode is handled in the same way. When the central unit is ready to read data, it toggles the INT line. When the module has put new data on the bus, it toggles the NEW_DATA line to inform the central unit. The RESET line is used in this mode to instruct all modules that a new transmission cycle begins. The details for this operating mode will be shown in section 3.4.6.

The usage of buffers is crucial for the *Myrmex* bus. On the one hand they allow us to use very long bus length when many modules are connected with each other and on the other hand they allow for insulation of modules in specific directions. The buffers can be independently controlled by the MCU on a module to one of three possible states: input, output or off. Electrically, the *Myrmex* bus consists of many short connections that only run from the buffers of one module to the buffers of the following module. Because of this the amount of modules that are attached to the bus has no influence on the signal quality.

The buffers on a module are all connected with each other. The MCU is also connected to these buffer lines, which means it can 'read' all signals that run between the buffers. If a buffer on one side of a module is enabled as input, and on another side a buffer is an output, the bus signals that go into a module on one side are forwarded to the other side. If one buffer is enabled as an input and no output buffer is used the bus ends at the module, as the signals can not reach other modules anymore. Also if no input buffer is enabled, the module is not receiving any bus signals.

Using two different bus modes has the advantage that not more electrical lines had to be employed then necessary. As we have seen the communication in direction from the central unit to the modules is only necessary in the configuration mode. After this, the same lines can be reused using the opposite direction in the full transmit mode.

The ability to direct the bus to different sides of a module using the buffers is also a prerequisite for the discovery of module structure, which is shown in the next section.

Table 3.3: Pin functions of the *Myrmex* bus in configuration mode

Pin	Direction	Name	Description
1	I	DATA0-7	Config data from central unit
2	I		
3	I		
4	I		
5	I		
6	I		
7	I		
8	I		
9	O	DATA8-11	Config data from module
10	O		
11	O		
12	O		
13	O	NEW_DATA	Toggled by module if the previous command was executed
14	I	INT	Toggled by the central unit when the new command is ready
15	I	RESET	Not used in configuration mode

(Directions as seen from the module, I = Input, O = Output)

Table 3.4: Pin functions of the *Myrmex* bus in transmission mode

Pin	Direction	Name	Description
1	O	DATA0-11	Pins for tactile data from module
2	O		
3	O		
4	O		
5	O		
6	O		
7	O		
8	O		
9	O		
10	O		
11	O		
12	O		
13	O	NEW_DATA	Toggled by module when new data is ready
14	I	INT	Toggled by the central unit when data has been read
15	I	RESET	Resets all module states to start of data transmission

(Directions as seen from the module, I = Input, O = Output)

3.4.4 Autonomous discovery of Module Structure

A feature that sets the *Myrmex* sensor system apart from other systems is its ability to configure itself each time it is used. The need for this configuration arises from the modularity of the system - one can attach a single module to the central unit as well as multiple ones (up to 127 in the current implementation), and connect them in a row or a square or a rectangle.

Having multiple sensor modules connected to form a larger sensor area like a tactile table, the central unit first needs to discover how many modules are present in the system, so it is able to configure its USB data size parameters correctly for the transmission of the tactile image to the PC. Also it has to configure a path for tactile data transmission with the *Myrmex* bus, as the modules themselves also do not know their position in the system. After all modules have been discovered, the size and connection information of the array is transported to the PC, so the tactile image can be reconstructed to match the physical layout of the sensor array.

We will now look at the auto discovery as it proceeds from powering up of the system. After power-up the modules enter the configuration mode, where the modules configure their buffers to allow bidirectional data transfer as introduced in the previous section.

Right after this they start their discovery procedure. For the modules this means that they enable one of their buffer pairs on one side and output a specific bit pattern. Then they wait until a timeout occurs for a specific answer bit pattern from the central unit. If they did not get an answer, they disable the buffers and enable a buffer pair on another side, showing there their pattern and waiting. This procedure is looped infinitely until an answer is found.

The central unit proceeds in a similar way: After power-up and self initialization, it outputs its bit pattern and waits until it reads the bit pattern of a module.

As we have seen in section 3.2, the central unit is connected at one side of the module array to only one module. This module and the central unit will discover each other. The bit pattern of the central unit will not reach other modules, as the bus is not forwarded yet by the just discovered module.

After the first module is discovered, the module goes out of the discovery phase and accepts configuration commands from the central unit. The first

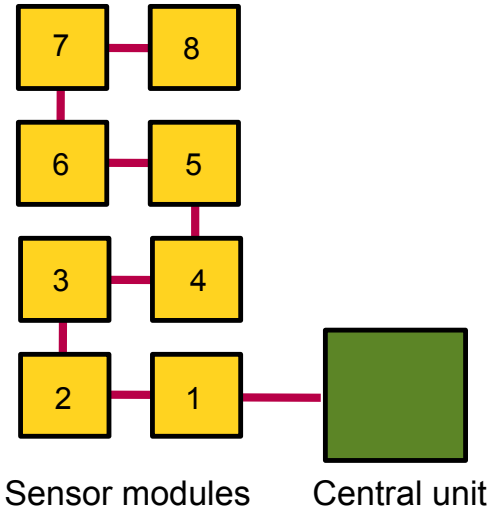

Figure 3.17: A 3×4 module array after the discovery process. The activated bus connections are shown in red. Each module has been assigned a number in the order of its discovery. The same order is later used for reading the tactile data in the data acquisition phase.

command the central unit will use is to assign an address to the module. This address can then be used to direct commands to this module once more modules are on the bus.

The central unit will then proceed to discover more modules. It will do so by instructing the first module to forward the discover bit pattern of the central unit to one of its four sides. Then the central unit will wait until a timeout occurs for the answer of another module. If no answer is received, its instructs the module to direct the *Myrmex* bus to another of its sides. If another module is discovered, the same procedure as with the first discovery is repeated.

Each time a module is discovered it is assigned an address and the central unit notes which address was found at which side of a certain module. The whole discovery process is repeated until no more modules can be found as determined by a timeout on all sides.

Figure 3.17 illustrates how an exemplary 2×4 module layout would be discovered and the active connections for data transmission.

The information about the active connections between the modules is

stored by the central unit and later sent to the PC as part of the USB video frame data (see section 3.5.1). This makes it possible for the PC software to reconstruct the physical layout of the modules (relative to the central unit). It can do so by knowing the relative connections of the modules to each other as well as the order in which they will transmit their data.

In the current implementation, the *Myrmex* system supports module arrays in square or rectangular configurations (that includes single module rows, e.g. 1x5 modules). After the discovery process is finished, the central unit proceeds to the module configuration phase as shown in the next section.

3.4.5 Module configuration

The module configuration is the step after the discovery of modules and the last step before the system enters the full transmission mode. At this point, the central unit has assigned all modules with an unique ID. Also at this stage all modules are attached to the *Myrmex* bus, as seen in Fig. 3.17 there is a single path that goes from the first module to the last module.

The task of the central unit is now to configure the transmission parameters for the modules. After switching into full transmission mode, there will be no more way to configure the modules as the *Myrmex* bus will become unidirectional.

The first step of the central unit is to configure how the *Myrmex* bus will be routed through the array of modules in the upcoming full transmission mode. Currently the system programs the same path that was taken during module discovery, that means that the module that was discovered first will also be the first to transmit its data in full transmission mode.

The next step is the configuration of the speed and compression setting for all modules. The speed setting is a way to slow down the tactile data acquisition of the modules, and therefor reduce the speed system. As we will later see this only has an effect when a single module is used. The impact of the speed setting value on the system speed is shown in section 3.4.8.

The compression parameter allows to enable a simple compression algorithm that can increase the speed of the system when there are many tactels with none or constant pressure. This can be the case when using a larger surface as in a tactile table, where the action is concentrated on a partial area.

The parameters for speed and compression are shown in table 3.5. There are default values for these parameters stored inside the central unit, but these

values can also be set by the user using the USB video interface of the *Myrmex* system.

The optional compression mode that can be activated by these settings can reduce the amount of data that needs to be transmitted from the modules to the central unit and thus speed up the system in some cases.
If the compression is activated, each module sends a 256 Bit flag array prior to the transmission of its tactile data. If a bit is set to 1, a tactile value for this sensor cell will be transmitted, if it is set to 0 this sensor value will be not be transmitted. The flag bits are set according to a comparison of the sensor cell value to the threshold, through this also noise or low force contacts can be filtered. The automatic thresholds work by taking a snapshot of all sensor values and using the highest value as compression threshold, this is done by each module internally if enabled.

This simple compression method can reduce the amount of data that needs to be transmitted if only a few sensor cells are active (=below threshold). If a module with no load normally needs 256 bus transmissions, with the compression active it will just need 22 (as each transmission is 12 Bit wide) to only transmit the flag bit array. However if there are many sensor cells active this effect is reversed: for a module where all cells are active there are 256 + 22 transmissions necessary in this case.

After the modules have been configured with the path and speed / compression setting, the central unit issues a special command that switches all modules into the full transmission mode.

Table 3.5: Module configuration parameters

Name	Range	Default value	UVC video parameter	Description
Speed	0-255	0	Contrast	A higher value lowers the speed of the system
Compression	0-255	0	Brightness	0 = No compression 1 = Automatic threshold 2 - 255 Threshold

3.4.6 Full transmit mode

The full transmit mode is the final operating mode of the system. In this mode the tactile modules measure their tactels and transport these values to the central unit, the central unit in turn transports them to the PC. The operation of the system in full transmit mode has been highly optimized - it is the reason why the system achieves so high frame rates, which we will discuss in the course of this and the following section.

When the *Myrmex* system uses multiple modules, synchronization is required on which module shall transmit on the *Myrmex* bus. To reach high speeds even with many modules, this synchronization shall slow down the system as little as possible, that is why we designed this process to happen automatically without any action from the central unit. In the case when only one module is used, there is no synchronization necessary and the module can operate slightly different to increase the frame rate even further, this will be described in detail in the next section. Now we will the describe how multiple modules behave in full transmit mode.

After the system goes from configuration mode into full transmission mode, all modules use their buffer direction configuration that was sent to them by the central unit in the configuration phase. This configuration contains the information which pair of input buffers and which pair of output buffers will be activated. But at this stage, the modules only activate one pair, the input pair that allows signals to reach the module.

For the first module this means that it is electrically connected to the bus. However it does not activate the buffers yet that lead to the next module, number 2.

All modules begin now to sample their ADCs to acquire tactile sensor values and buffer them in their internal memory. The central unit has, after sending the modules into full transmission mode, activated its USB connection and has been enumerated as an USB video device (see 3.5). It will start to acquire a tactile image from the sensor system.

It does so by toggling the INT line of the *Myrmex* bus. The first module, the only one to receive this signal, outputs the 12 Bit value of the first tactile sensor cell onto the bus, and triggers the NEW_DATA line. The central unit then reads this value, buffers it and toggles the INT line again to read the next value. This procedure is repeated until all 256 tactile data values have been transferred.

After the 256th value, the module activates its outgoing buffer pair, which extends the bus to the second module. The second module notices the toggle of the INT line by the central unit, outputs its first 12 Bit value and the transmission process is repeated as with the first module. Notice how this switch to a new module requires no action from side of the central unit. It just has to perform a simple loop of reading data for all modules, the synchronization is done by the modules themselves. After all modules have been read (the central unit knows the amount of modules from the enumeration) a cycle of tactile data acquisition is complete.

The central unit will now reset the state of all modules to prepare the next data acquisition cycle. It does so by toggling the RESET line of the *Myrmex* bus. All modules go back into the starting state of the full transmit mode, where they have only their input buffers enabled. In the meantime the central unit transmits the collected data as an USB video frame to the PC. After this it will start to read out the modules again.

This concept proves to be very effective, as it minimizes overhead and allows us to achieve high frame-rates even with a greater number of modules, much higher then the competing systems that we have seen in section 2.2. How this is achieved will be shown in detail in the following section.

3.4.7 Achieving High Frame Rates

The high framerates of the system were achieved by optimizing the two factors on which the speed of the tactile system depends: the time needed for the analog data acquisition and the transmission time of the digital data.

Data acquisition

The analog data acquisition time is the time needed by a module to communicate with its ADCs to read the tactile sensor cell values. These are generated by the ADCs through converting the analog voltage from the sensors cells to digital values.

The limiting factor for this process is not the raw sampling and transmission rate of the A/D converters (which is one million samples per second with the AD7490 chips used on the module [133]) but the time needed to charge the internal capacitor of the ADC to reach the actual sampling voltage after

switching the ADC channel.

As we have already heard, the ADCs have 16 analog input channels. But internally they only have one measurement circuit to which the 16 input channels are multiplexed. When a new channel is selected, the internal capacitor of the measurement electronic has to charge to the voltage level of the new channel. This charging process has an exponential characteristic, where the decay factor is determined by the resistivity of the overall system, which is comparatively large (as we use a 470 k resistor for the voltage divider of tactile sensor cells, see Sec. 2.2).

The time needed to reach a constant voltage level was identified in experiments to be approximately 30 µs, in comparison to a theoretical sampling time of only 1 µs of the ADC.
To improve the overall acquisition speed, we take advantage of the fact that each module employs multiple ADCs, and alternately use each of the 16 ADCs - this increases the time available for voltage adaption by a factor of 16. We use the waiting time needed for the charge of the new channel on one ADC to read the other 15 ADCs.

Using a sampling time of 1.2 µs to achieve more robust ADC readings, the time needed to acquire all 256 sensor values of a single module accounts to 308 µs, leaving a time of 15·1.2µs = 18µs for voltage adaption. This reduction of the adaption period is a tradeoff between speed and accuracy in the default operation to achieve the high frame-rate of 1900 hz.

Data transmission to the host

The data transmission to the host computer is a two stage process. In the first stage, the tactile data acquired from the ADCs is transmitted from the modules to the central unit, in the second stage this data is transferred to the host PC. The transmission from a module to the central unit via the *Myrmex* bus takes about 333 µs. This data is then send as part of a video frame via USB to the host PC. This transmission to the host PC via USB takes an average of 32 µs per sensor module.

For single module operation we implemented an optimized data acquisition / transmission scheme. In this scheme, the single module transmits the tactile data to the PC and at the same time samples the next tactel. This is done by using the SPI subunit of the PIC32 MCU which can talk to the ADC

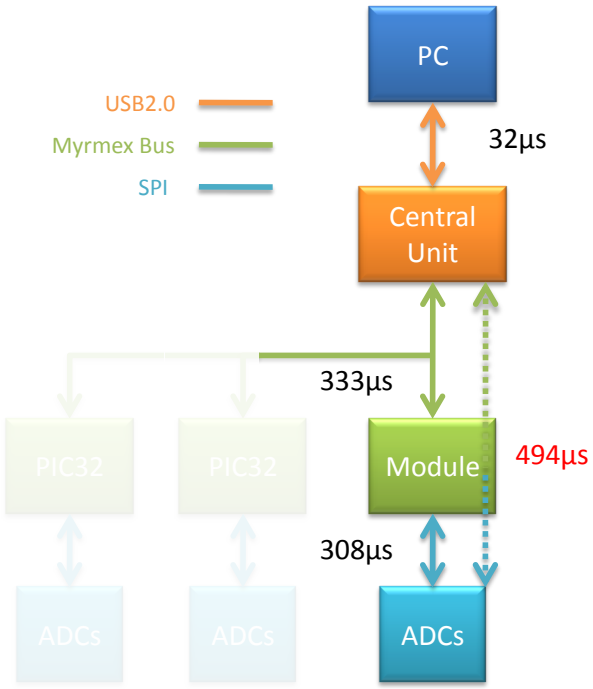

Figure 3.18: Detailed communication diagram of the sensor system including data acquisition and transmission times. If a single sensor module is used (as for the grasping / slip detection scenario), acquisition and transmission can be further optimized, needing only 494 µs combined.

while the PIC32 is busy communicating to the central unit. With this method it takes 494 µs + 32 µs to acquire and transmit a whole sensor image, resulting in an overall frame rate of 1.9 kHz. An overview of the speeds and devices is shown in Fig. 3.18.

When multiple modules are used it is even possible to optimize the data transmission and acquisition to a greater extend. What we have seen in the previous section is that the time needed for data acquisition of a module is 308 µs. As the acquisition and transmission speed are of similar magnitude, we can employing a parallel data acquisition and transmission scheme that greatly increases the system speed when using multiple modules.

A detailed graphic with the speeds for this parallel method is depicted in Fig. 3.19.

There we assume to have at least two modules. Take a look at module #1: while it is sampling its data for the next transmission, module #2 is trans-

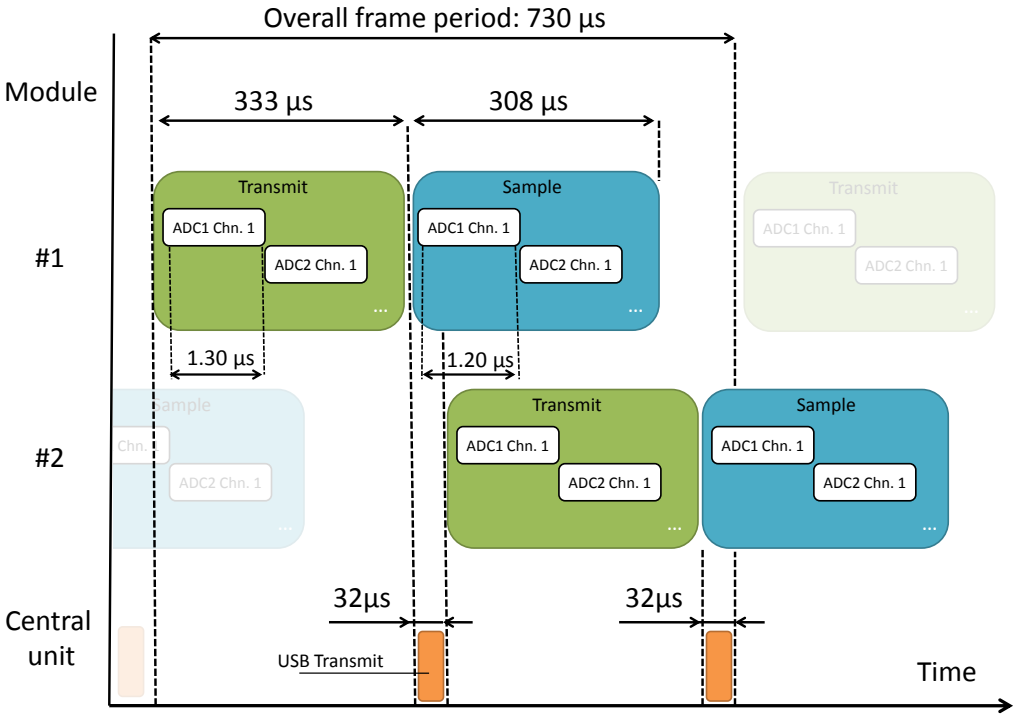

Figure 3.19: Schematic timing diagram which illustrates the parallel data acquisition and transmission phases of two sensor modules. The time axis is not linear to scale.

mitting its data. As the acquisition time is lower then the transmission time, module #1 will have all tactile data ready when module #2 has finished. So while one module transmits its data to the central unit, the other module can already acquire and buffer tactile data from its ADCs. Because of this each module needs only (333 µs +32 µs) to sample and transmit its data on average.

If we would use a sequential operation however it would take (333 µs + 308 µs + 32 µs) for each module to sample and transmit its data. To sample and transmit both modules after each other it would then take over 1200 µs. With our parallel approach however we only need 730 µs including USB transmission, which is only 60% of the time needed for sequential operation.

3.4.8 Overall system speed

As the times needed for the data acquisition and transmission phases are nearly fully deterministic, the overall system speed with a number of N modules can

be calculated by the formula:

$$T_{total} = \begin{cases} N \cdot T_T, & \text{if } N \cdot T_T \geq T_S \\ T_S + T_T & \text{else} \end{cases} \tag{3.2}$$

where T_{total} is the total time needed to sample and transmit data from all modules to the PC, T_T is the time needed to transfer the data from one module to the PC (333 µs +32 µs), and T_S is the time needed for one module to sample its data, which amounts to 308 µs + (0.65 µs $\cdot Speedsetting$). The $Speedsetting$ is a factor known from section 3.4.5 that can be set by the user to reduce the system speed.

How the overall system speed reacts to the amount of modules is shown in Fig. 3.20. For e.g. using a large quadratic sensor area like a tactile table with edge length 480 mm, composed of 6×6 modules accumulating to an overall number of 9.216 tactels, this results in a frame-rate of approx. 75 Hz. It can also be seen that the speed setting has only an effect on the speed when one module is used, as $N \cdot T_T$ gets larger as more modules are used.

In table 3.6 we have shown the impact of the speed setting on the sensor output. The data was recorded from a single sensor cell at various speed and pressure level combinations. The speed setting reduces the speed of the data acquisition of the modules and slightly increases its sensitivity and accuracy. As we use an aggressive timing during the data acquisition to maximize the speed of the system, the tactile data output is slightly higher then it would be with a relaxed timing.

The impact of the speed settings can be seen best by looking at the unloaded (0kpA) case. In the other cases the impact can be overshadowed by other effects caused by the cover material such as hysteresis and change over time. These effects will be evaluated in section 5.

The element in our calculations that is not fully deterministic however is the USB transmission time. While in normal operation it was measured to be 32µs, this assumes that the *Myrmex* systems is the only streaming USB device and the PC has enough CPU time to collect the USB data as fast as possible. If multiple USB devices (e.g. external hard disks) are used and data is transferred the operating system may decide to treat the *Myrmex* video device with a lower priority, or it simply has not enough time to read the data as fast as the central could send it. The central unit does not throw away or buffer multiple images.

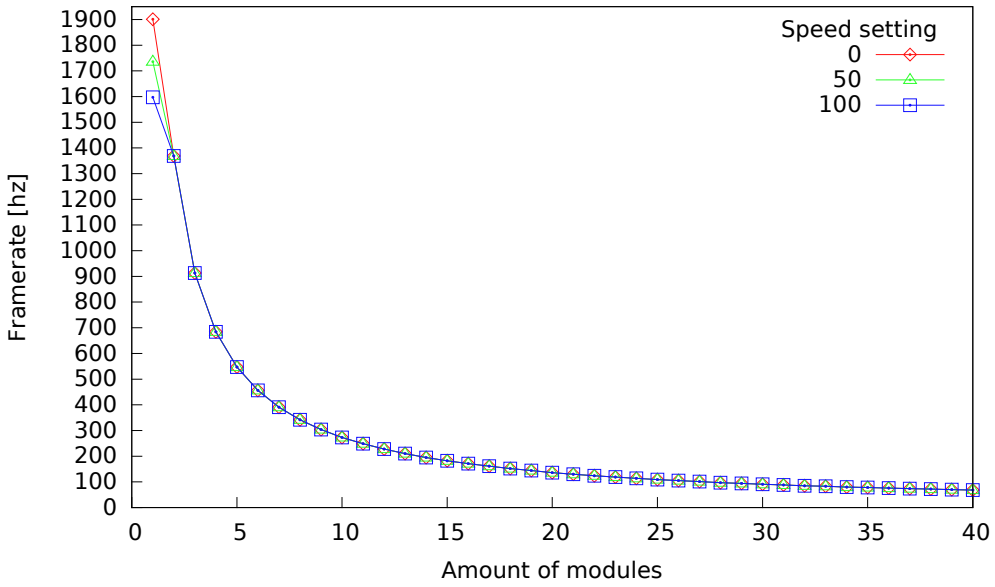

Figure 3.20: Decline of frame rate with number of sensor modules. The frame rate for a single module can also be influenced by the speed setting.

Table 3.6: The impact of the speed setting on sensitivity / accuracy. This table shows the sensor output for different speed settings and pressure levels.

Speed setting	0kpA	50kpA	100kpA	150kpA	250kpA	500kpA
0	40	3663	3815	3929	3977	4025
15	25	3675	3820	3931	3979	4027
25	15	3681	3824	3934	3981	4027
50	8	3689	3827	3934	3982	4029
100	0	3693	3830	3936	3984	4030
150	0	3696	3833	3934	3985	4030
200	0	3704	3834	3939	3985	4030
255	0	3706	3836	3941	3987	4031

3.5 Central Unit

The central unit is the device which connects the array of *Myrmex* modules to the host PC. It acquires the sensor information from the modules and provides a standardized interface to a common PC using a USB2.0 connection. The central unit is an off the shelf evaluation board by Atmel, the NGW100 [91].

This board contains a 32 Bit MCU called the AP7000, which can run at up to 150Mhz with 210 DMIPS. This MCU features an integrated USB2.0 high-speed controller. The NGW100 runs an implementation of the USB video protocol that was developed for the Myrmex precursor system. This protocol and its adaption for the system will be briefly covered in this section, for a detailed reference we refer to the description of the Myrmex prototype system in [9]. To communicate with the *Myrmex* modules the central unit also implements the 12 Bit *Myrmex* bus protocol which was presented in section 3.4. A photo of the central unit can be seen in 3.21.

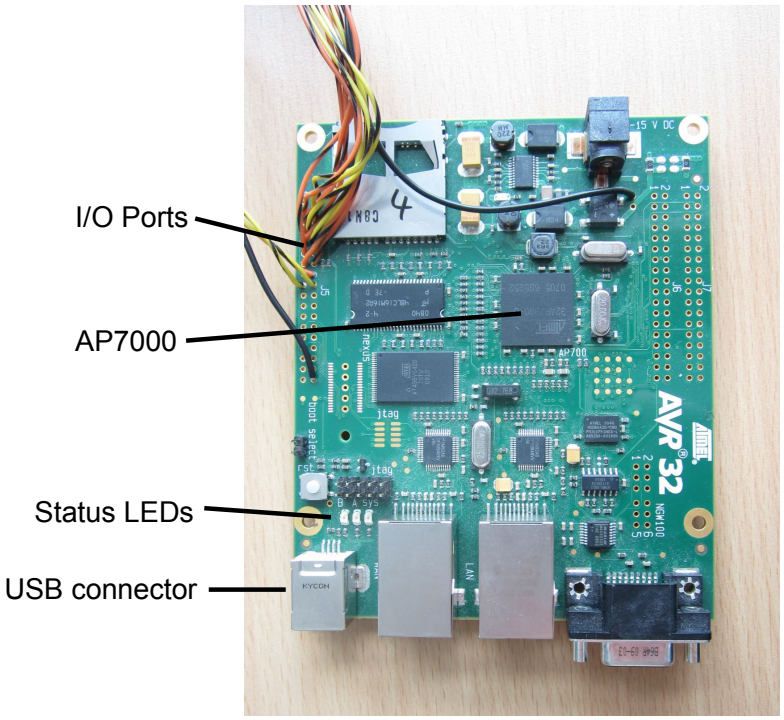

Figure 3.21: The NGW100 board that is used as central unit. The AP7000 MCU features an USB2.0 controller through which the central unit can communicate to a PC. The connection to the *Myrmex* bus is realized through its I/O ports. A number of LEDs indicate the system status to the user.

3.5.1 USB Video Protocol

In [9] we looked for methods to transport tactile data in a way that makes a tactile sensor system compatible and easy to migrate. As the *Myrmex* system provides a matrix of tactile sensor data an image/video format was seen as a intuitive method to package the data.

For transferring a video stream / implementing a video device a range of different methods are possible, like video over Ethernet, USB video or Firewire. We have decided to use USB video as the format is widely supported by different operating systems, has a good documentation and a good hardware platform was available with the NGW100 board (central unit).

The central unit implements an USB video device according to the UVC (USB Video Class) 1.1 [136]. The implementation of this protocol has hardly changed compared to the central unit which was presented in [9]. To maximize the performance the implementation is done without an underlying operating system like an embedded Linux. Here we will describe the basic operation of the central unit as it uses the USB connection to the PC.

After the central unit has discovered all modules with the procedure described in 3.4.4, it enables its USB transceiver subunit. If the central unit is attached to a host PC, this leads to the USB enumeration of the central unit by the operating system of the host PC. After a short exchange of standard identification and configuration data, the *Myrmex* system is identified as an UVC device and the appropriate class driver is loaded by the PC operating system.

This driver then requests the configuration data specific to UVC devices. Here a specialty of the *Myrmex* system comes into play: the video parameters are dynamic as they depend on the amount of modules that are attached. The number of pixels reported for the *Myrmex* video device matches the numbers of tactels in the system. The amount of modules has been determined by the central unit through the module discovery process shown in section 3.4.4.

Also the speed and compression configuration options for the *Myrmex* modules (as known from section 3.4.5) are represented by the video device interface that is created. As there is a limited amount of predefined configuration options offered by the UVC protocol, the brightness and contrast parameters were chosen to represent the speed and compression setting.

Because the *Myrmex* parameters of speed and compression can only be

set during the configuration phase of the modules, the changing of them only has an effect while the system has not switched the modules into full transmit mode. This switch happens after the first USB video image is requested from the *Myrmex* system.

The data format for the video stream is YUV2. It is a packed 16 Bit format and described in more detail in [137] and [9]. During data transmission the tactile image consisting of 12 Bit values from the ADCs is packaged into pixel values which are 16 Bit wide. As the upper 4 bits are not occupied by the tactile data, they are used for the transmission of meta-data to the PC. This meta-data is the routing information acquired from the discover phase of the tactile modules. With this information, the PC software can rearrange the pixel values of the tactile images to match the real world position of the corresponding tactile sensor cells.

3.6 Summary

In this chapter we have presented the design and the implementation of our *Myrmex* tactile sensor system. We have shown the overall system layout and described the single components, starting with the *Myrmex* modules.We have explained the design of the modules and the sensing principle.
Then we have discussed the granularity and measurement technique that is used. The sensitivity of the tactile sensor cells was optimized by selecting appropriate components and developing an optimized electrode design. For this we carried out experiments with various electrode designs and presented the results. The results were so encouraging, that the tactile fingertip presented in [102] uses the same shape for its electrodes.
Next we have looked at the *Myrmex* bus, which we developed mainly to realize an auto configuration of the system. The protocol and operation of the bus has also been optimized to realize a very high frame rate, up to 1900Hz. We have provided detail information on how this is achieved, through parallelization of of tasks as far as possible and a low overhead communication protocol.
We have shown that the interface to a PC is realized by the so called central unit. A high degree of usability is achieved through the implementation of an autoconfiguration algorithm which presents a 'ready to use' system to the user after powerup. This is complemented by using the USB video standard protocol, which can transport the data to PC even with various operating systems.

Chapter

4

Tactile book

4.1 Introduction

In this chapter we present a novel tactile sensitive object, the tactile book. We have seen that due to its modular design, the *Myrmex* system is capable of realizing functions such as a (big) tactile fingertip on a robot gripper, or a tactile table surface for human machine interfaces.
For some scenarios, e.g. capturing the forces a human hand exerts while handling an object, it is however favorable to have a tactile sensor that can be taken into the hand and lifted, shaken and rotated like a natural object. We will show how this can be achieved by using the *Myrmex* system to create a tactile sensitive object. Due to its rectangular shape it was called the tactile book. We have listed its specifications in table 4.1.

In the following sections we will first look at the design considerations for the tactile book. After this we will in the implementation section look at the system layout and hardware design.
We will show how we modified the electronics of a *Myrmex* module to add a cable free operating mode and motion sensing. We present a 3D printed case for encapsulating the *Myrmex* modules and thus forming the tactile book.
We will also present the problems that had to be overcome to achieve a jitter free data storage. Finally we will present our solution for a wireless synchronization for the tactile book with a fixed latency.

Table 4.1: Tactile book specification

Tactels	1024
Update rate	680 Hz with cable / 175 Hz in cable less mode
Spatial resolution	5mm
Data resolution	12-Bit
Pressure range	3-300kpA
Interface	USB video / microSD card
Sensing method	Resistive

4.2 Design Considerations

The motivations that lead the design process for the tactile book were very similar to those of the *Myrmex* tactile sensor system itself - creating a tactile device that is very fast, sensitive, easy to use and versatile in its applications, and now with the additional feature of being mobile. With a tactile sensor like the *Myrmex* modules available, the tactile sensing capability of the book can be realized by a combination of existing electronics and some modifications to implement the additional mobile capabilities.
It should be possible to use the book in a cable free mode, as this gives the user the most freedom for handling the book and makes it truly mobile. Additionally it should still be possible to attach the tactile book to a PC like a regular *Myrmex* system with the same USB video connection as this provides compatibility for existing software. This operating mode provides some degrees of freedom with a long cable and can also allow for high frame rates.

A review of the comparable tactile objects shown in section 2.2.4 and experience gained from the usage of the iObject [132] was used as an aid to design the tactile book. The frame rate of the iObject lies at 0-250hz using its bluetooth connection, which is dependent on the distance to the receiver. This poses a problem as often the distance between the PC and tactile object is dynamic when the object is manipulated by a person during an experiment. This leads to a reduced transmission rate and thus has a negative effect on effective data analysis, as interesting movements can happen too fast to be adequately recorded by the iObject. Even with a close and constant distance, the frame rate can vary depending on electrical noise.

With this motivation we choose to implement an offline recording mode in our tactile book, using a local storage medium integrated in the tactile book.

This allows the recording of data at fixed and precise intervals. Additionally we integrate acceleration sensors in the tactile book to provide information about the overall movement as it is manipulated by the human hand, as these sensors in the iObject have shown to be a useful source of additional information.

The final challenge was then to find a method to synchronize the cable less recording of the tactile book with that of other modalities. The tactile book was also planned to work as part of the Manual Intelligence Lab [138]. This laboratory for example contains VICON [139] and regular cameras and data gloves for the tracking of body motions.
These online recording devices can be synchronized by the PC they are attached to, their recordings can be started and stopped at the same time. To properly integrate the tactile book into this setup, a method had to be found to synchronize the start and end of the tactile book recording as well.

4.3 Implementation

4.3.1 System layout

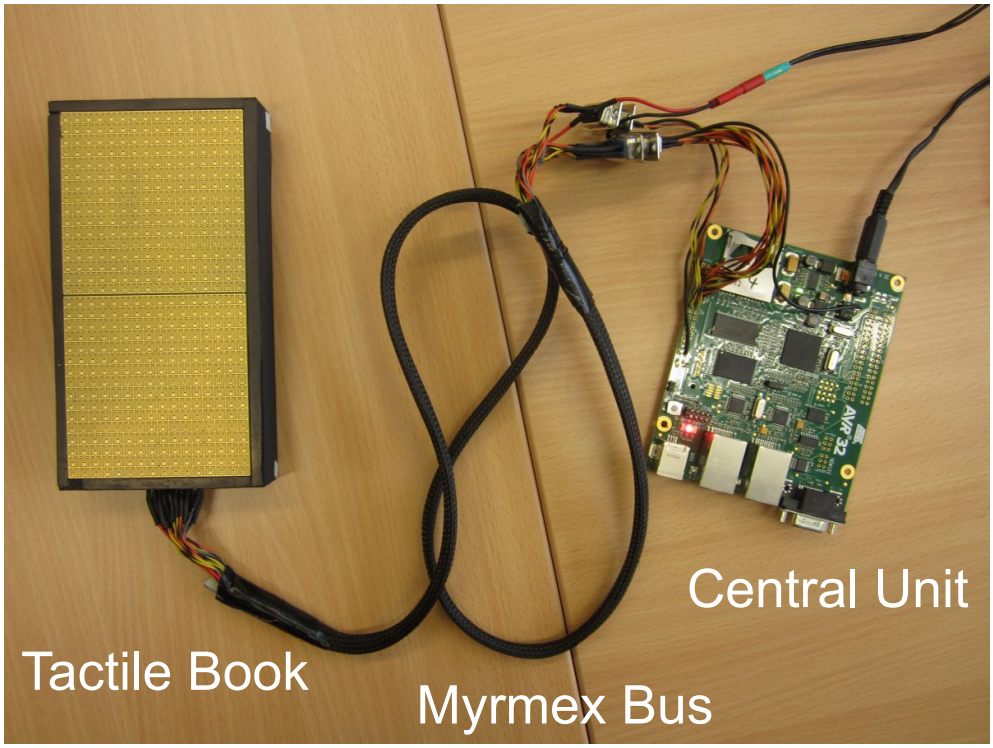

Figure 4.1: Photo of the tactile book in operation. The tactile book can on one side get connected to the central unit through a custom made cable. The central unit in turn can be connected to a PC via USB as known from the regular *Myrmex* system.

A photo of the tactile book as attached to a central unit can be seen in Fig. 4.1. In this photo it uses the cable operation mode, where the data from the tactile book is transmitted online to a PC via USB video.
The connection to the central unit is made via an elongated *Myrmex* bus cable. The tactile book consists of two pairs of *Myrmex* modules stacked onto each other. The two bottom and top module pairs are connected with each other through cables inside the book.

Technically the system layout is identical to a regular *Myrmex* system with a 1x4 module array (see Fig. 4.2). However one of the modules was modified to realize the optional cable-less operation mode. This so called master mod-

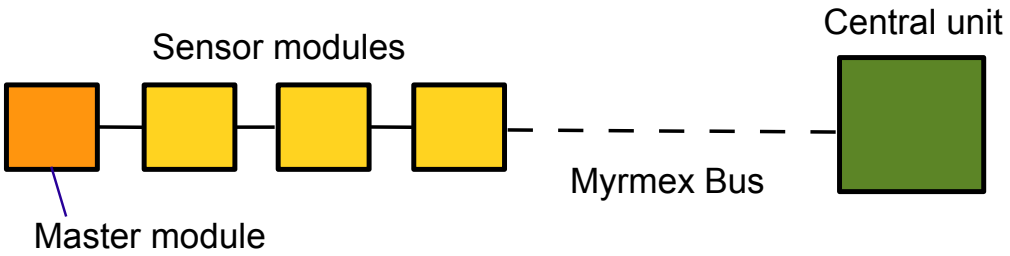

Figure 4.2: Connection layout of the tactile book. Four modules are connected with each other through the *Myrmex* bus. The book can get attached to the central unit to operate as a regular array of 4 modules. However one module is a modified master module which optionally can take the role of the central unit to allow for cable free operation.

ule can simulate the behavior of the central unit. It contains internal storage capabilities to record the tactile data from the other modules and itself. Additionally it contains motion sensors which will be described in the following section.

4.3.2 Sensors

The desired tactile sensing is realized by a 160x80mm tactile sensor area on the top and bottom side of the book. This area is created by the usage of two *Myrmex* tactile modules on each side. Due to the specifications of the modules (see section 3.3), the book has a 32x16 tactile sensor array on each side with a spatial resolution of 5mm. A photo of the book and the *Myrmex* sensor surface can be seen in Fig. 4.3.

The hardware of the *Myrmex* modules was unchanged apart from the master module. The master module is a regular *Myrmex* module where the bottom PCB, that is equipped with a MCU and responsible for the communication, has been strongly enhanced. This was done in order to realize the offline data storage and to integrate additional sensors. The modified PCB can be seen in Fig. 4.4. This master module has received a microSD card slot on which the data can be stored, and in addition two new movement sensors were added. One is a 3 axis accelerometer [140], which is capable to measuring up to +/- 3G and provides information about the lateral displacement. The additional 3 axes gyroscope [141] provides information with a range of ±2000°/sec about the rotational movements.

These sensors improves the motion capture facility even when the tactile book is being used without sophisticated external sensors. The MCU on the master module was programmed to act as a slave in the presence of the *Myrmex* central unit, so the book can be discovered and configured like a normal 1x4 *Myrmex* module array if it is attached by cable. But additionally it was also programmed to act as a *Myrmex* bus master, and do the discovery and configuration of the other modules in the tactile book in the cable-less operating mode.

Figure 4.3: Top: The *Myrmex* tactile book in cable free operation mode. Like the other *Myrmex* modules, it needs to be covered with a conductive elastomer to allow the tactile sensing capability. In this case a black polyurethane foam is used. Bottom: The top side of the tactile book without the elastomer. One can see the sensor surface of two *Myrmex* modules. The tactile surface is surrounded by adhesive magnetic strips attached to the edges of the book. The foam cover is equipped with the same strips, which allows for an easy and secure attachment of the foam to the book.

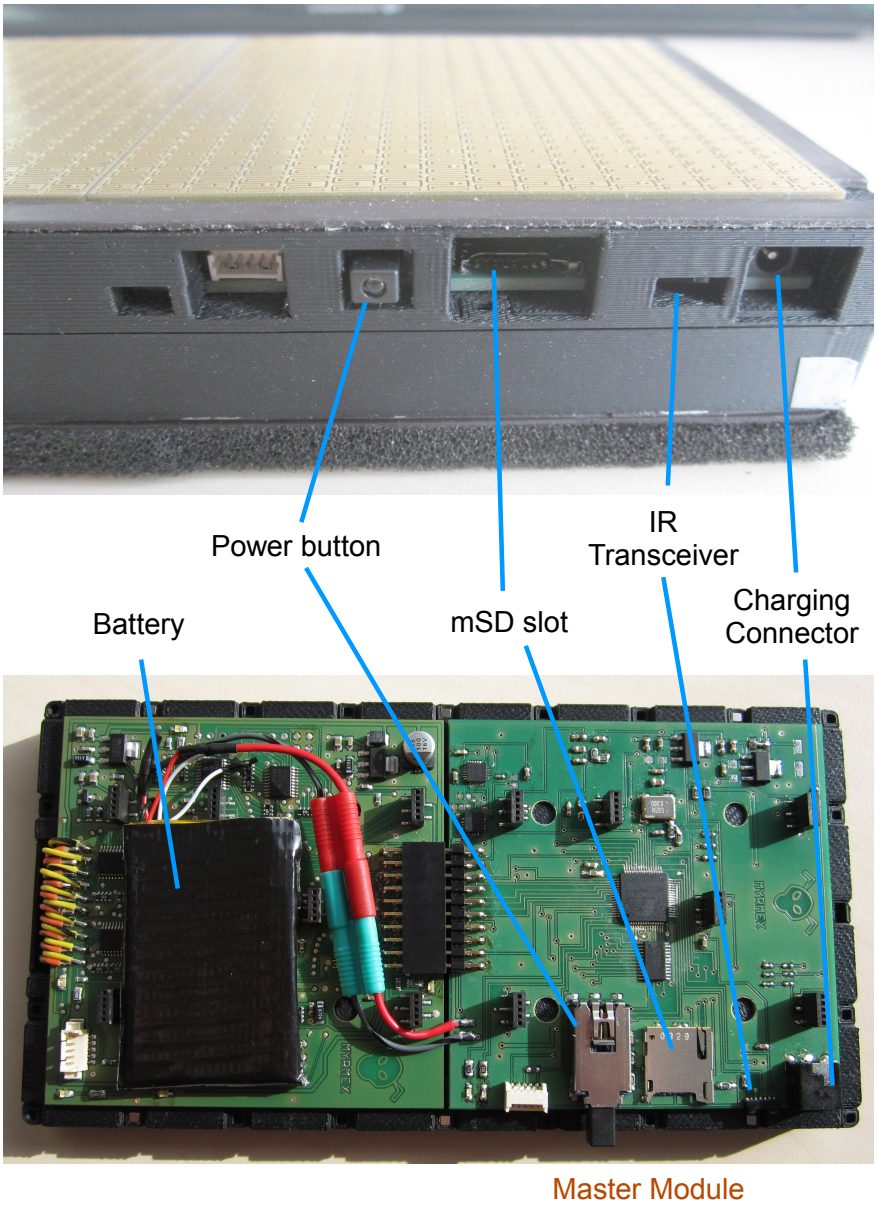

Figure 4.4: The master module was modified with various functions, and a battery was added to allow the cable free operation. Top: Side view of the connectors as seen from outside the case. Bottom: View on the open book with the master module PCB.

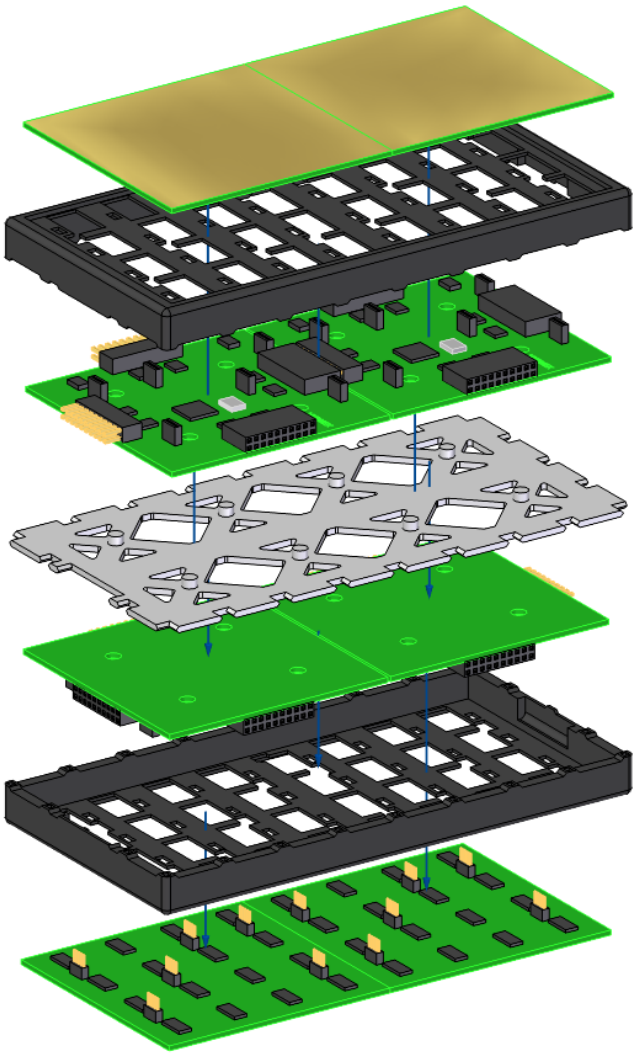

Figure 4.5: Explosion view of the tactile book. The center plate (gray) and the two case parts (black) are made from ABS plastic using a 3D printer. As described in section 3.3 the four sensor modules consist of two parts each.

4.3.3 Case

The case of the tactile book was designed to contain the electronics and allow the attachment of the tactile sensor cover material (conductive elastomer) on top of the sensor surface.

It has a size of 170x90x23mm, which is needed to fit the *Myrmex* modules inside (see Fig. 4.5) and leaves a 5mm frame around the tactile area which is

needed for the attachment of the conductive foam. The case consist of three parts, one center piece on which the 2x2 *Myrmex* modules get clipped and the upper and lower part of the enclosing case.

The upper and lower case parts are kept together by 22 Neodym magnets sized 2x2mm which are integrated into each case part and spaced at regular intervals. These allow the easy dis- and reassembly of the tactile book. The inside of the case contains a rechargeable two cell LiPO battery which outputs 7.4V and has a capacity of 350 mAh, this enables the tactilebook to operate approximately 30 minutes. On one side of the case there are openings for user access to the microSD card, battery charge connector, on/off button, debug connector and the IR transceiver (as shown in Fig. 4.4).

4.3.4 Data storage

The tactile book offers two data transmission methods: one is the traditional method via a central unit and USB connection to the PC. For this purpose a cable can be used for the *Myrmex* bus to connect one module of the tactile book with the central unit. After power up, all 4 modules will be discovered as previously described in section 3.1.

The second method is the cable free operating mode. Thereby the sensor data from both the tactile and the motion sensors is stored locally in the tactile book on a removable microSD card. This allows a cable free operation and a constant rate of data capture, which a transmission method like bluetooth may not guarantee. This solves the problem of having a device with full degrees of free movement that can still record data with precise timing.
The data storage onto the microSD card was optimized by us to achieve the highest frame rates possible. For this reason we do not use a file system to store the tactile book data, but write directly to the SD card in RAW mode.

To store data onto a microSD card with minimal latencies however also requires awareness of the operating structure of this storage medium. The flash memory used in the microSD cards of today operates in a way that a specific block of memory has to be erased first before it can be written. This is normally done by a flash controller chip inside the microSD card, which buffers the incoming data, erases the memory blocks and writes the data subsequently [142].

This behavior however can have an adverse effect on the latency if data is written to the microSD card in a continuous stream, as the flash controller

seems to operate in a 'burst mode', in a way that it collects data in his buffer up to a threshold, and then erases the needed memory blocks and does the writing in a single run. The negative effect we observed is that the flash controller is unable to accept any new data until this erase and write cycle is finished. From our observations the time needed for this process varies between several hundred milliseconds depending on the type of microSD card.

To circumvent this problem the tactile book uses a radical approach to completely erase the whole microSD card prior the start of data recording, and not leaving the write mode of the microSD card after the recording has started. With this method the total time needed to record a frame of data is approximately constant at 5.6ms, with a slight latency spike of ca. 11ms after 2048 frames have been written, which again seems to be attributable to a buffer operation on side of the flash controller.

The time needed to record a frame can be broken down into ca. 1.1ms to acquire the data from the movement sensors, 2ms to gather the tactile data and ca. 2.5ms to write the data onto the microSD card (excluding the latency spike).

One frame stored by the tactile book consists of 2048 bytes, which contain 1024*12 bit of tactile data plus 3*16 bit data from the XYZ gyroscope, 3*10 bit from the XYZ accelerometer and a 32 bit time stamp. We have found that the alignment of the data into a multiple of 512 bytes was advantageous as it causes the latency spike to occur in fixed intervals.

4.3.5 Configuration

As motivated we want to synchronize the start of the data recording in the tactile book with external hardware such as additional motion tracker systems like VICON or Datagloves as used in our Manual Intelligence Lab (MI-LAB) [138]. For this a method was implemented to exchange small tokens of data with very constant latency to communicate start time and duration of the recording. Traditional wireless methods like bluetooth would not be accurate enough, as such a wireless transmission would not have a constant latency. The latency of a wireless transmission is hard to predict as it can be influenced by environmental noise. A non constant latency would hinder the proper synchronization of the data streams.

Because of this we chose to use an optical transmission method to synchronize the tactile book with a host PC. The optical transmission method we use is the IrDA [143] standard infrared communication. This transfer method has only a limited bandwidth, but a constant latency if the sender and receiver are in a line of sight [144]. To realize the optical transmission we added a TIR1000 infrared transceiver [145] to the master module.

For the configuration of the tactile book via IrDA a simple protocol was developed, consisting of ASCII characters which identify the command and binary data bytes as payload. The commands used by the host to configure the tactile book are shown in appendix A in table A.3 and the answers of the tactile book are shown in table A.4.
To remove the problems of possible data corruption that can occur during transmission (the communication can get disturbed by other IR sources) a CRC8 check-sum is attached to each command. There are two configuration commands that are sent to the tactile book, the first one tells the tactile book for how many seconds it should record data, and the second specifies a delay until it should start to record. Each configuration step is acknowledged by the tactile book.

Using this limited wireless interface the MILAB PC software, which is responsible for the synchronization of all devices in the MILAB, can instruct the tactile book to record for a specified duration after a specified start delay. When this delay has elapsed (the tactile book uses an highly accurate 8 Mhz oscillator to track its time) the book starts recording the tactile and movement data together with a time stamp onto the microSD card. After the experiment the timestamps of the tactile book can be synchronized with the timestamps of other MILAB devices by adding the constant delay caused by the IR transmissions and the starting delay as transmitted by the MILAB software.

4.4 Summary

In this chapter we have presented the tactile book, a tactile sensitive object created from the *Myrmex* system. We motivated the design of the book, and discussed the planning and implementation steps taken.

The resulting tactile book can be attached to the *Myrmex* central unit with a cable, or used in a cable free recording mode. In both modes it provides very high frames rates (680 Hz and 175 Hz) that allow the capture of fast changes in human finger forces and contact positions. In the cable free mode it offers full

free degrees of movement, working with a battery and saving the tactile data onto a microSD card. We have optimized the data storage for low latency and achieve a very constant frame rate - something which would not be possible with wireless communication as the signals could easily get disturbed.

Apart from its tactile sensing capabilities the tactile book features motion sensors to enrich the tactile view on the human interaction, a 3 axis accelerometer provides data about the acceleration of the tactile book and a 3 axis gyroscope provides data about the rotational movements. We have also designed and implemented a low latency synchronization and configuration protocol, which allows for integrating of the tactile book into complex human motion research setups.

Chapter

5

Evaluation of sensor response

5.1 Introduction

In this chapter we investigate the properties of the tactile sensor cells in relation to physical stimulation.
As described previously, the sensor is based on the single sided piezoresistive architecture as introduced in section 2.2. With this method the resistance between a sensor electrode and the common ground electrode is measured.
This resistance changes with the compression of the cover material. It is measured through a voltage divider, which converts the resistance into a voltage. This voltage is sampled by a 12 Bit ADC on the *Myrmex* module to acquire a digital value.
The electrical properties of the sensor circuit itself can be described by the behavior of the voltage divider. The output of the voltage divider circuit can be calculated as already done in section 3.3.1 for selecting an appropriate fixed resistor using formula 3.1.

The relationship between the resistance of the cover material (R_2) and the sensor output voltage U_{out} using the same parameters as in the *Myrmex* modules ($U_{in} = 5V$, $R_1 = 470kOhm$) and formula 3.1 is depicted in figure 5.1.

However the other important factor that determines the sensor respone is the behavior of the elastomer that is used as cover material. To investigate this, we tested the sensor response of a *Myrmex* module with three different elastomers that we will present in the next section. We not only investigated the output of the sensor to force/pressure, but also how stable and repeatable this output is over time and location.

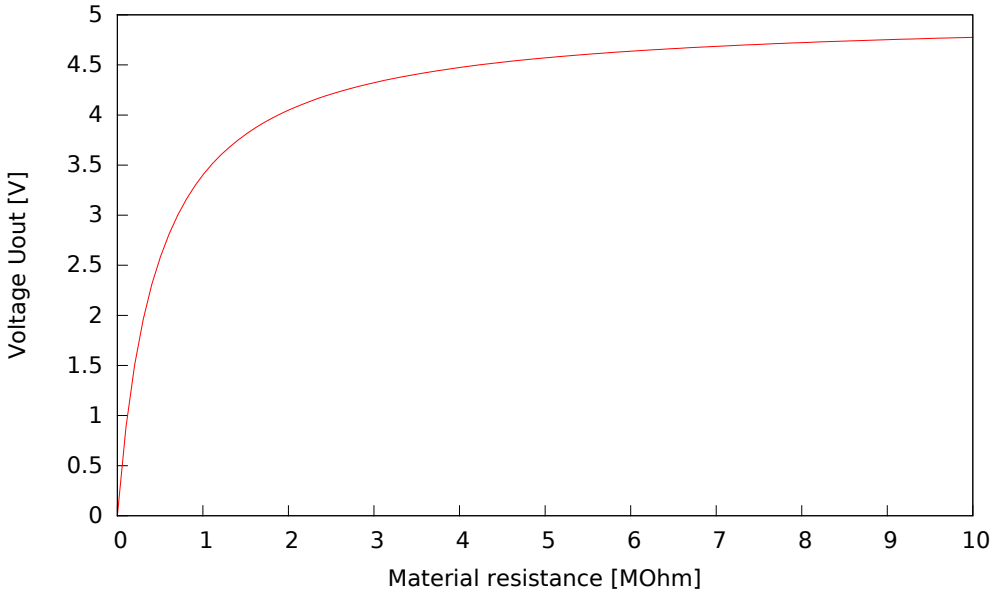

Figure 5.1: Output of the voltage divider circuit in relation to cover material resistance.

5.1.1 Sensor Materials

The sensor cells of the system were designed to provide a high sensitivity output when using an open cell polyurethane (PU) foam, the initial experiments and results for this were shown in section 3.3.4.
Additionally we tested two more materials: a conductive foam made by Weiss Robotics [146] and a conductive fabric by Eeonyx called EeonTex [147]. All three materials are depicted in figure 5.2.

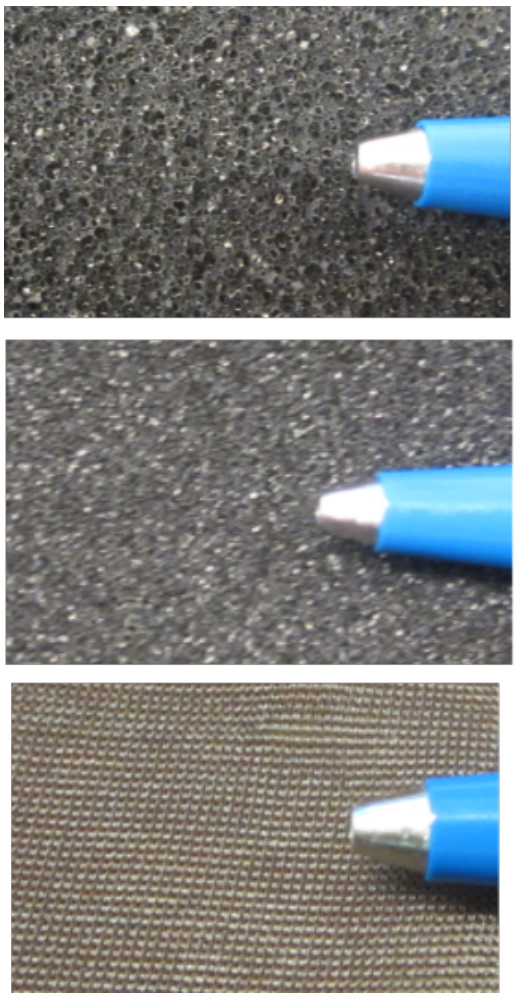

Figure 5.2: Materials that were tested as cover material for the sensor, from top to bottom: Polyurethane foam, Weiss foam and EeonTex fabric. The PU foam has open cells that have about double the size of the ones in the Weiss foam. The EeonTex fabric is tightly woven. A pen is shown for size reference.

5.1.2 Measurement setup

To test the materials, a measurement rig was available which was improved compared to the one used in section 3.3.4 by having a more accurate and faster measurement of force.
The measurement setup is depicted in figure 5.3. It consists of a 3 DOF positioning unit, which is controlled by PC using a National Instruments (NI) card.

At the end effector an industrial strain-gauge sensor is mounted. The strain-gauge can be read out by the PC using the NI card.
Attached to this strain-gauge is a spring damped rod, which can be equipped with different probes. When the probe is pressed on a surface, the applied force can be measured by the strain-gauge.

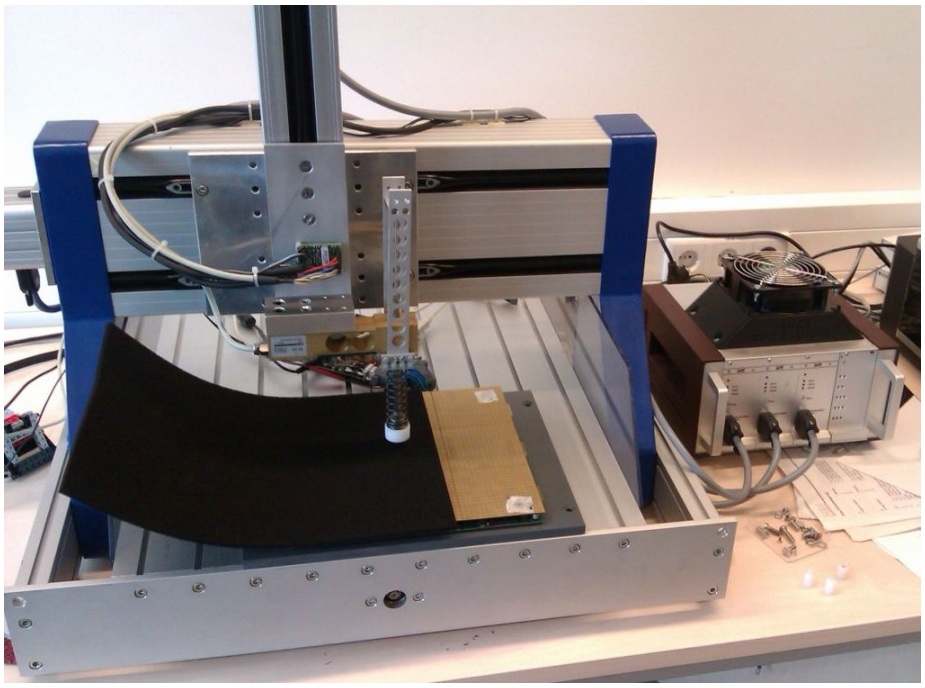

Figure 5.3: A photo of the measurement setup. The probe head (white) is driving into the foam cover (black) of an array of 3x3 *Myrmex* modules.

5.2 Properties of the sensor

5.2.1 Type of sensing

The first property we want to investigate is if the materials / the sensor form a force or a pressure dependent sensor. For this we use a constant force and change the area that is used to apply this force.
If the sensor output does not change while the area changes, it is a force sensor, otherwise it is a pressure sensor.
The result of this test can be seen in figure 5.4. For all materials, the change in area produces a change in sensor output, so the sensor is reacting to the pressure.

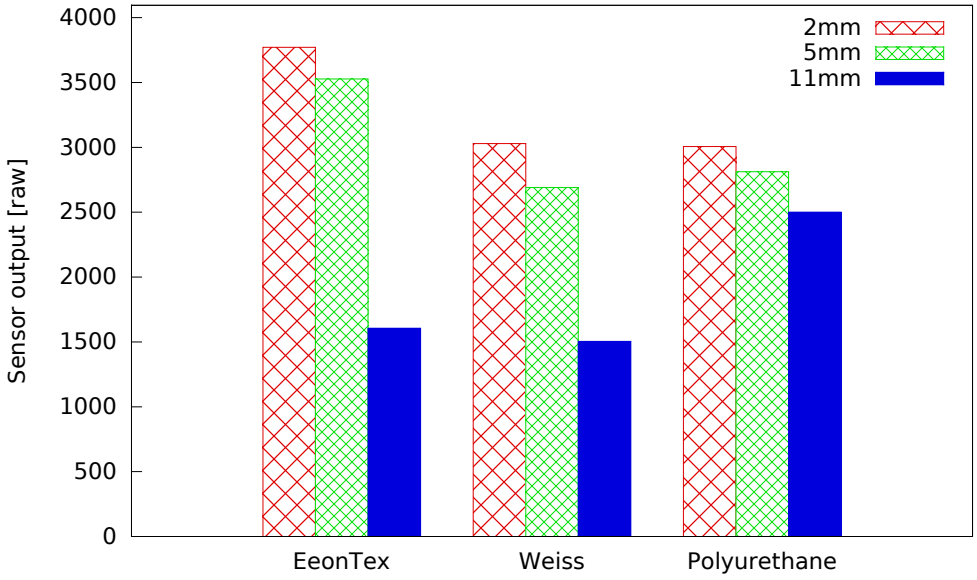

Figure 5.4: Sensor output for a single cell. The three different cover materials were tested with three different probe sizes and a constant force of 1N.

5.2.2 Pressure deflection

The foams and rubbers that are used as cover materials for piezoresistive sensors (see section 2.2) are elastic. This has the side-effect that the pressure exerted by the measuring probe is not fully transferred in normal direction but also partially deflected in other directions.

This is illustrated by figure 5.5, where a 2mm diameter probe was positioned above the center of a sensor cell and pressed with a pressure of 80kPa into the PU foam.
The resulting tactile image shows that not only the cell directly beneath the probe was activated, but also surrounding cells due to the bending of the foam.

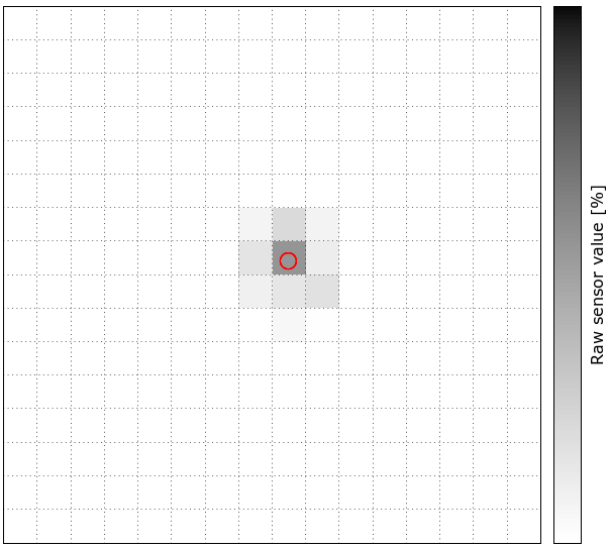

Figure 5.5: Sensor cell activation for a 2mm tip (red) pressed with 80kPa. The 16x16 matrix corresponds to the sensor cells of a single module. The sensor output is shown from white (no output) to black (maximum output)

To examine the influence of this effect on all materials, a test was done with the 2mm probe and the three materials. The results for different pressure levels is shown in table 5.1.

One can see that even when using a probe that is considerably smaller then a sensor cell (2mm probe tip vs. 5mm sensor cell) that nearby sensor cells get activated.
An interesting result is also that the foam materials show a considerable pres-

Table 5.1: Sensor cell activation for a 2mm probe. Shown is the number of sensor cells that are activated when pressing the probe on the sensor material with the given pressure.

Pressure [kPa]	80	160	320	480	640
Polyurethane foam	9	13	14	15	16
Weiss foam	6	7	8	9	9
EeonTex fabric	1	1	1	1	1

sure deflection, while the fabric does not. As the fabric is by itself elastic (it can be stretched up to 100% [148]) we attribute this to the small thickness of the fabric.

5.2.3 Sensor output

The most defining characteristic for a tactile sensor is the basic relationship between force/pressure and the corresponding sensor output.
To evaluate this, we probed 256 tactels of a module with a 5mm probe and recorded the output of the tactel directly below the probe. Each tactel was probed 10 times. We then averaged the output from the tactels of all trials. The resulting curves for the different materials are shown in Fig. 5.6.

We see that all materials show an exponential behavior, similar to the output of the voltage divider when assuming a linear increase in resistivity (Fig. 5.1).
All materials show a high sensitivy to low pressure, there is a rapid increase in sensor output until about 100kPa, then the output continues to grow but at a much slower rate.
We can see that the Weiss foam gives the strongest output for high pressure, followed by the EeonTex fabric and the polyurethane foam.
To investigate the initial material response, we take a more detailed look at the region between 0 and 100 kPa in Fig. 5.7.

In this figure we see that the materials show variations in response to low pressure. The Weiss foam has the lowest initial sensitivity, but then exhibits the steepest slope and reaches the highest output. The EeonTex fabric has the fastest initial response. The polyurethane foam has the second fastest response, and then the lowest output of the three materials at higher pressure levels.

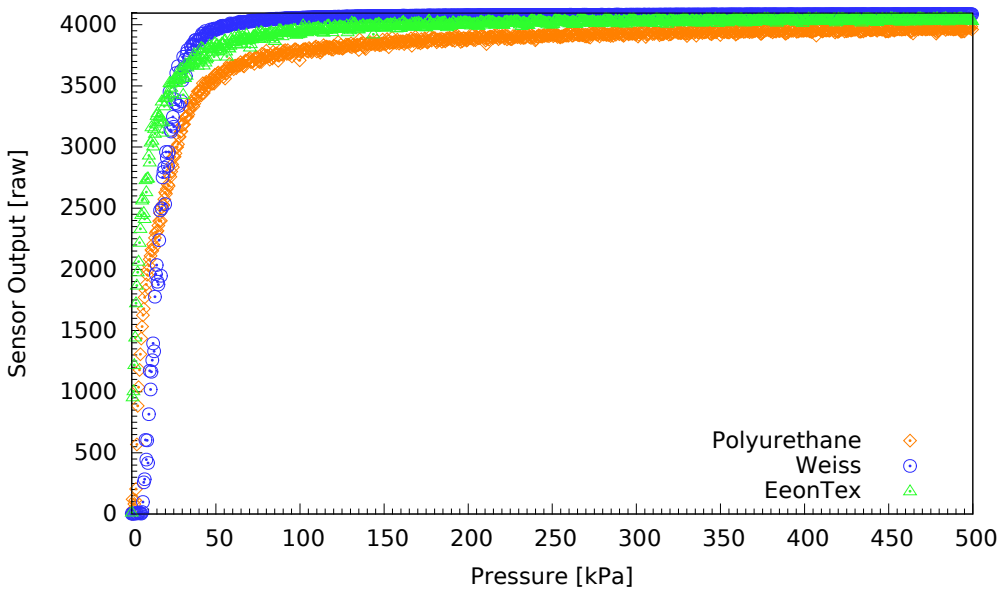

Figure 5.6: Sensor response to pressure in the range of 0 to 500 kpA.

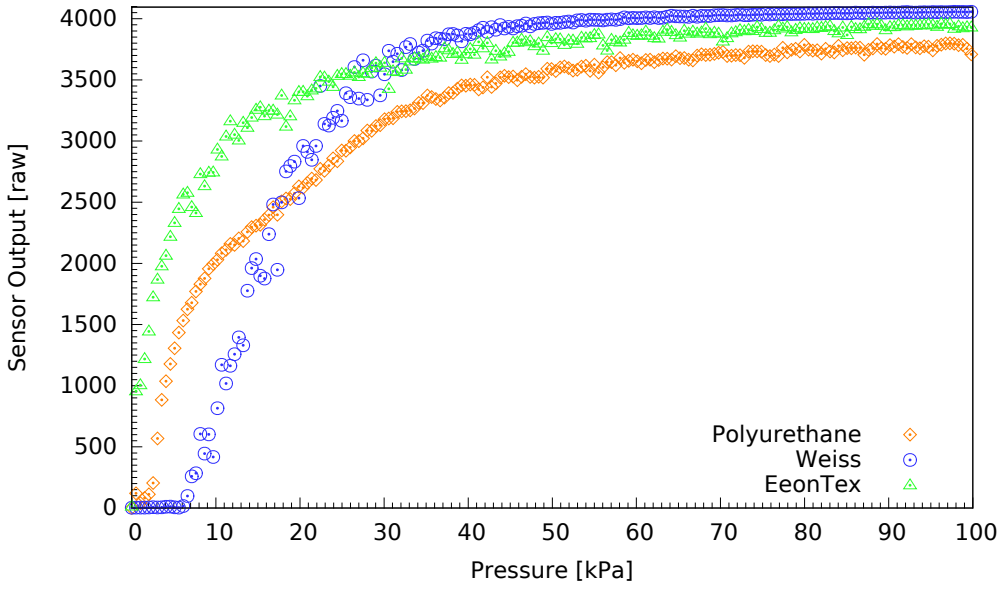

Figure 5.7: Sensor response for pressure in the range of 0 to 100 kpA.

5.2.4 Spatial homogeneity

An interesting observation that was made during the experiments is that there is quite a large deviation between the output of sensor cells.
Figure 5.8 shows a comparison of the sensor output of the tactels from a *Myrmex* module. Thereby the same pressure acts on all sensor cells. We assume that the differences in tactel output are the result of inhomogenity in the elastomers.

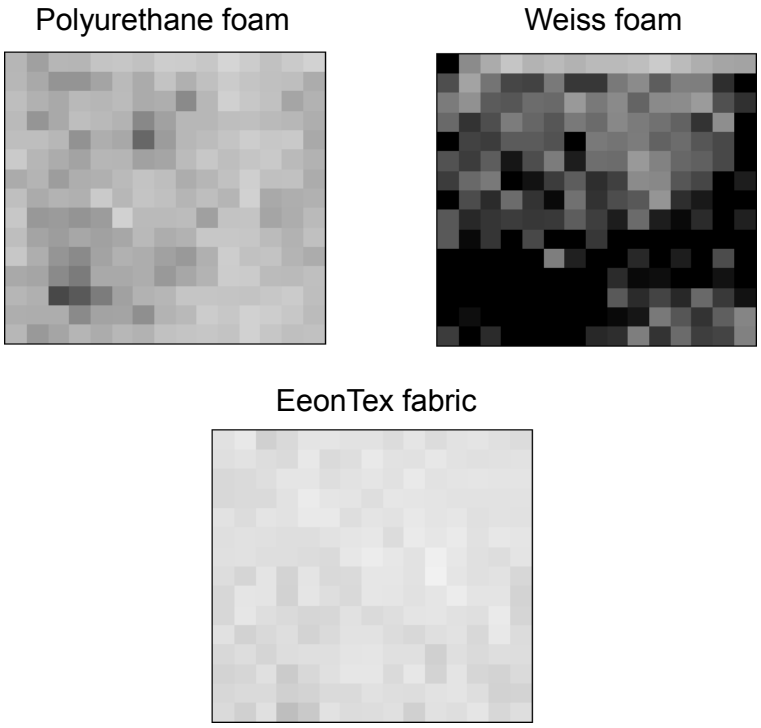

Figure 5.8: Sensor output of a *Myrmex* module with 16x16 tactels for the three materials. The same input pressure was used, the outputs have a different brightness because the materials have a different sensitivity. What is visible for all materials is that the individual sensor cells also have different sensitivities.

In figure 5.9 we show the standard deviation of the sensors cells that were probed for the previous figure 5.6. We see that the deviation is different between materials, and also that is varies with applied pressure. The deviation seems to highest when the pressure to output curve of a material has its steepest slope.

5.2.5 Temporal homogeneity

Another interesting property is the behavior of the sensor over time. As the materials are elastic, it is possible be that they continue to deform when pressure is applied over a longer time-period, and this would influence the sensor output.

For this we conducted an experiment where we used a cylindrical steel rod with 6mm diameter and a weight of 70g as probe.
The rod was placed over a sensor cell and stabilized in the horizontal.
In the vertical plane however it was free and thus able to sink into the material.
We recorded the sensor output over a time-span of 40 minutes. The results are shown in figure 5.10.

It can be seen that the foams exhibit a larger drift over time then the fabric. The polyurethane foam shows the the largest increase of the sensor value with about 5% during the time-span, and is still rising after this.
The fastest increase for the foams occurs during the first two minutes. There the Weiss foam shows a fast increase of about 2%. After this, it shows slight growth. The EeonTex fabric remains relatively stable.

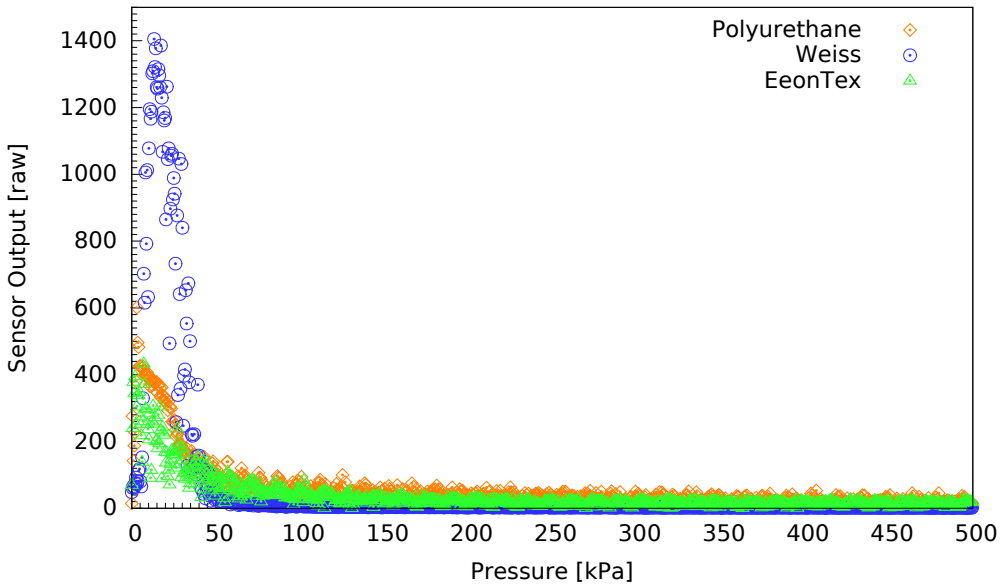

Figure 5.9: Standard deviation of the sensor response to increasing pressure. The data was generated from the same experiment as Fig. 5.6.

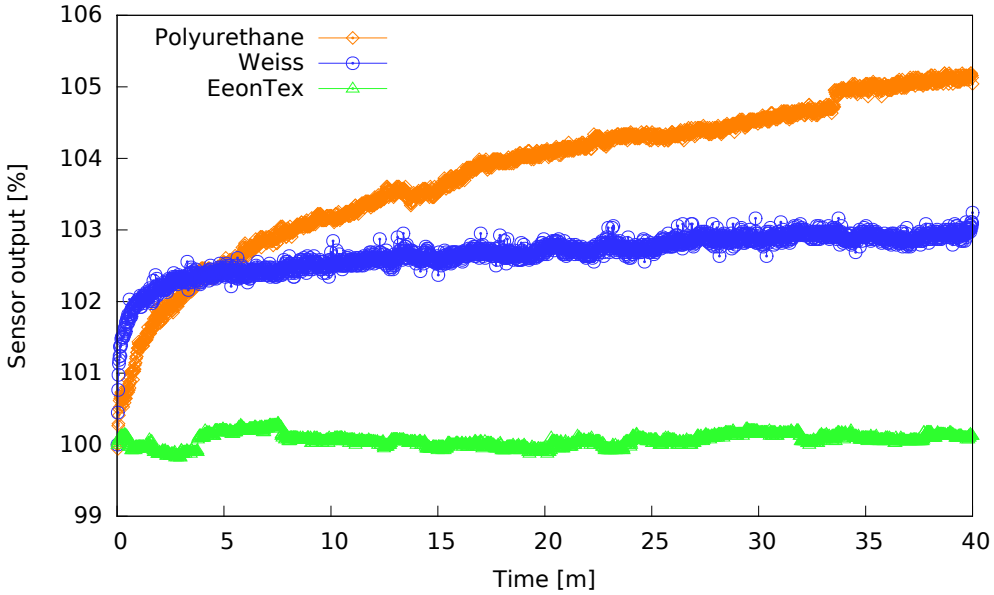

Figure 5.10: Sensor output for the three materials over a time-span of 40 minutes.

5.2.6 Repeatability

Another important aspect of the sensor is the repeatability: when applying pressure to one sensor cell over and over again, does it experience hysteresis?

This was tested by probing a sensor cell with a 5mm probe for 100 times, with a constant pressure of 25kPa. After this we left the material untouched for 24hrs and then did another run of 100 times pressing the probe into the material. Our motivation was that the materials may experience some deformation in the process and their form could recover when given enough time to rest. The results of the experiment are depicted in figure 5.11.

We interpret the results in a way that the only material that shows a recovery of material structure / sensor output is the foam by Weiss robotics. The Weiss foam shows a change in output over all trials, but mostly during the first 15 trials.
After given 24hrs rest, the starting output value of the second phase of the experiment and the following change in output is similar to the first phase. The polyurethane foam shows a strong change during the first 15 trials smiliar to the Weiss foam, but after that a clear trend in change of output can not be determined. The EeonTex fabric does not show much change at all.

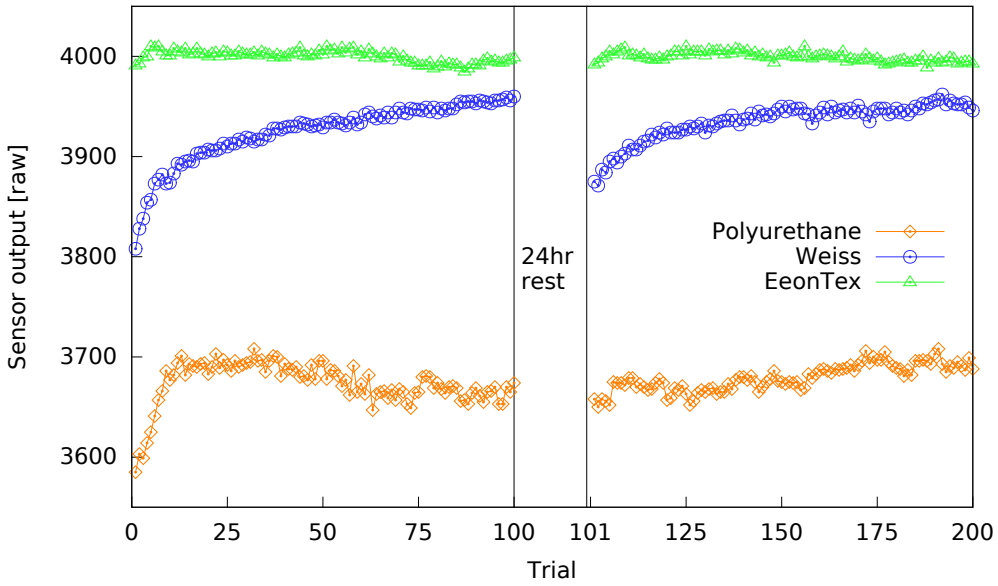

Figure 5.11: Sensor output for 200 trials of probing the same location with the same pressure, with a 24hr rest after the first 100 trials.

5.3 Continuous autoequilibration

In the previous sections we have seen that the sensor response suffers from inhomogeneity, especially in the spatial domain.

In addition to this the output of a sensor cell can change during usage, as with some materials the sensor exhibits hysteresis. As we have seen in our repeatability tests, this change can be permanent due to wear of the cover material.

From this also follows that when the usage is concentrated to one area of the sensor, the spatial inhomogeneity across the whole sensor matrix will increase further. Repeated recalibration of each sensor cell can counter this, but is time-consuming and to a certain degree even counter-productive as the multiple probing of the tactels leads to more wear and hysteresis.

However in many applications an exact calibration to output a pressure value in physical units is not required. For applications that e.g. use vision algorithms for object detection or investigate the relative distribution of pressure, uniformity of the sensor output is more important.

Achieving a uniform sensor output is not a novel problem and a method to achieve this is called equilibration which is employed by the Tekscan company for its piezoresistive sensor arrays [149].

The equilibration as done by Tekscan is a process that creates a mapping between the output values of the tactels and an ideal value [150]. The ideal value for a certain pressure is chosen to be the averaged sensor output of all tactels that experience this pressure. The mapping is done by using factors that are stored for each sensor cell and pressure level. So when a uniform pressure is applied onto a sensor matrix, all sensors will show uniform output after being multiplied with their equilibration factors [151].

This mapping is realized in software. As the sensor response is nonlinear, there are multiple measurements of actual pressure and average sensor value used as reference points. The factors for the sensor values between the reference points are interpolated. The measurements for the reference points are obtained by using a special equilibration unit that is placed on the sensor array. This equilibration unit is a pneumatic or hydraulic device that applies a uniform pressure on the surface [152].

One drawback of this method is however that the equilibration process requires manual effort and a 'downtime' of the sensor. And as the sensor continues to be used, the equilibration effect will be reduced due to nonuniform usage of the sensor matrix, so this process has to be repeated sooner or later. This is disadvantageous when a long continuous operation of the sensor surface is required, or the sensor is embedded into a robot system and needs to be removed in order to use the equilibration device. Also curved sensor surfaces as found in tactile fingertips or robot skins would likely require a specially adapted equilibration unit.

From this motivation we propose a method for the continuous autoequilibration of sensor arrays. This method works without a special equilibration device or a sensor downtime. We argue that during usage, there are occasionally areas on the sensor matrix were homogeneous pressure exists and these can be used to update the sensor equilibration factors.

In our method, we strive to find these these homogenous areas by statistical analysis of the sensor data. As we have seen in the evaluations of section 5, the sensor array shows a spatial inhomogeneity, which leads to a gaussian distribution of the sensor values that experience the same pressure. In Fig.

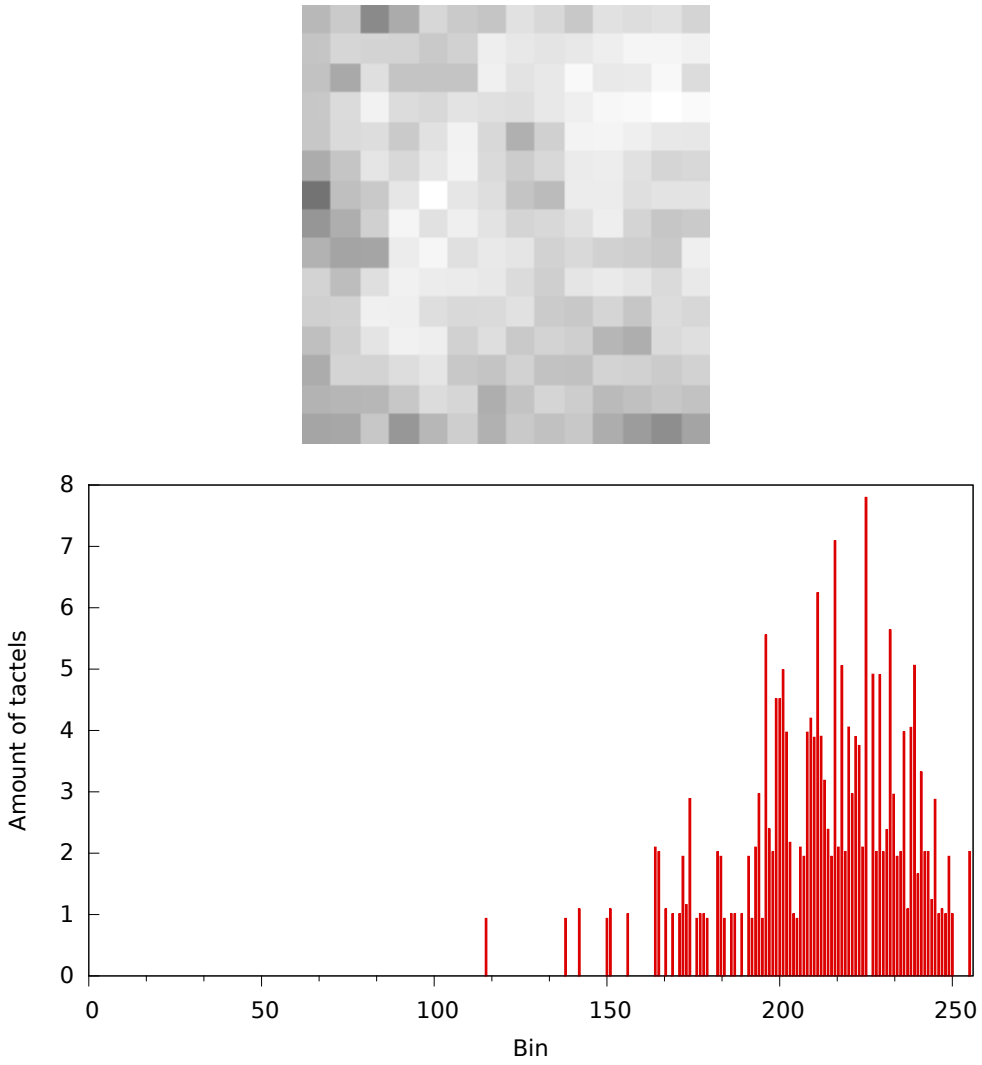

Figure 5.12: Top: Sensorimage for a module under uniform load. Bottom: A histogram of the sensor data, the sensor values have been grouped into 256 bins.

5.12 one can see the distribution for a *Myrmex* sensor module under uniform pressure. On the other side, if the pressure on the sensor matrix is nonhomogenous, the distribution is different. In Fig. 5.13 we can see the distribution when a pressure gradient is applied.

We use the sensor value distribution as a homogeneity criterion to detect a region that has a uniform load. We get the ground truth data from the ini-

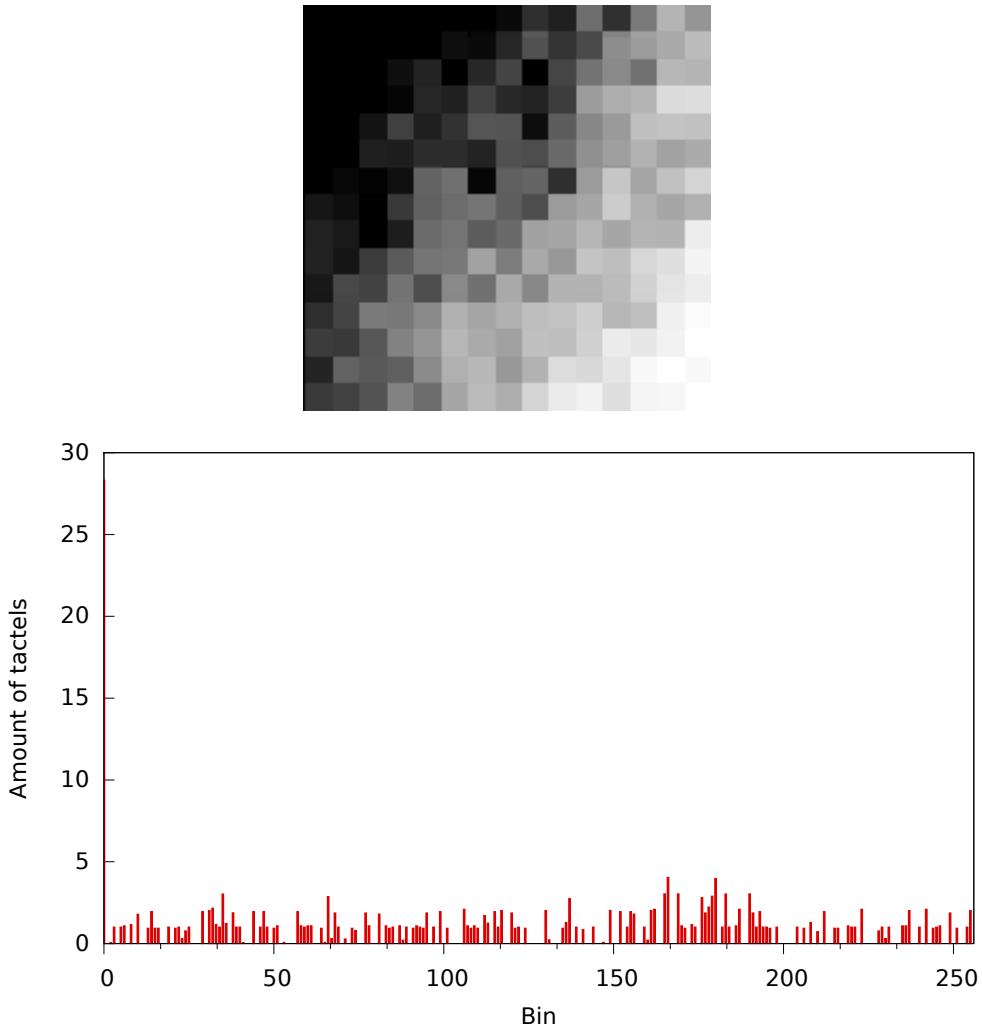

Figure 5.13: Top: Sensorimage for a module under a non uniform (tilted) load. Bottom: A histogram of the sensor data, the sensor values have been grouped into 256 bins.

tial calibration data of a sensor module, where we can calculate the mean and standard deviation for uniform loads at different pressure levels.

The algorithm for our autoequilibration continually scans the sensor matrix for regions that fulfill our homogeneity criteria. It does so by sliding a 4x4 window over the tactile data matrix and calculating the mean and standard deviation of the window. If the region has been found to be homogenous, a

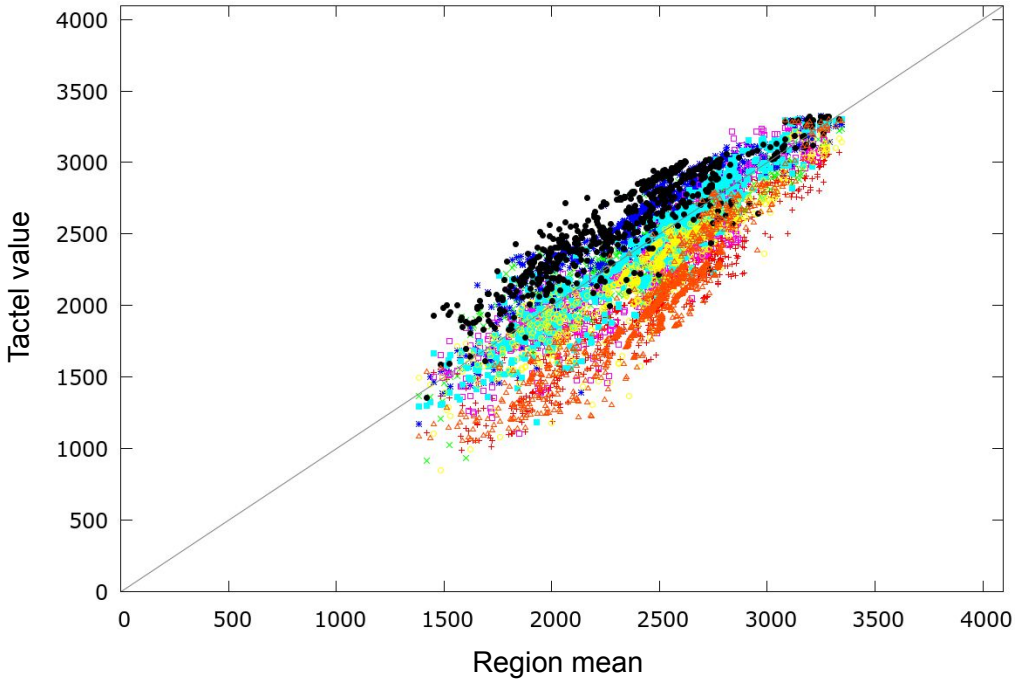

Figure 5.14: Measurement points of eight tactels that were collected during autoequilibration. As it can be seen, the sensor cell outputs are quite different. The diagonal line shows the theoretical ideal response, were each individual tactel output is equal to the mean of all tactels.

measurement point is created and stored for each tactel separately. The measurement point consists of the current sensor value of the tactel along with the mean of the region.

If enough measurement points for a tactel have been collected, we fit a linear function through the measurement points. The resulting parameters are used in our linear conversion function. This conversion function can then be used to output the tactel value in a equalized form - calibrated relatively to the rest of the tactels. This produces a much more uniform sensor output.

In Fig. 5.14 we can see the measurement points for 8 tactels recorded during autoequilibration. In Fig. 5.15 we see the measurement points after being processed with their respective conversion functions. One can see that the sensor output is more homogenous between the tactels. This effect is even visible in the graphical sensor output as shown in Fig. 5.16.

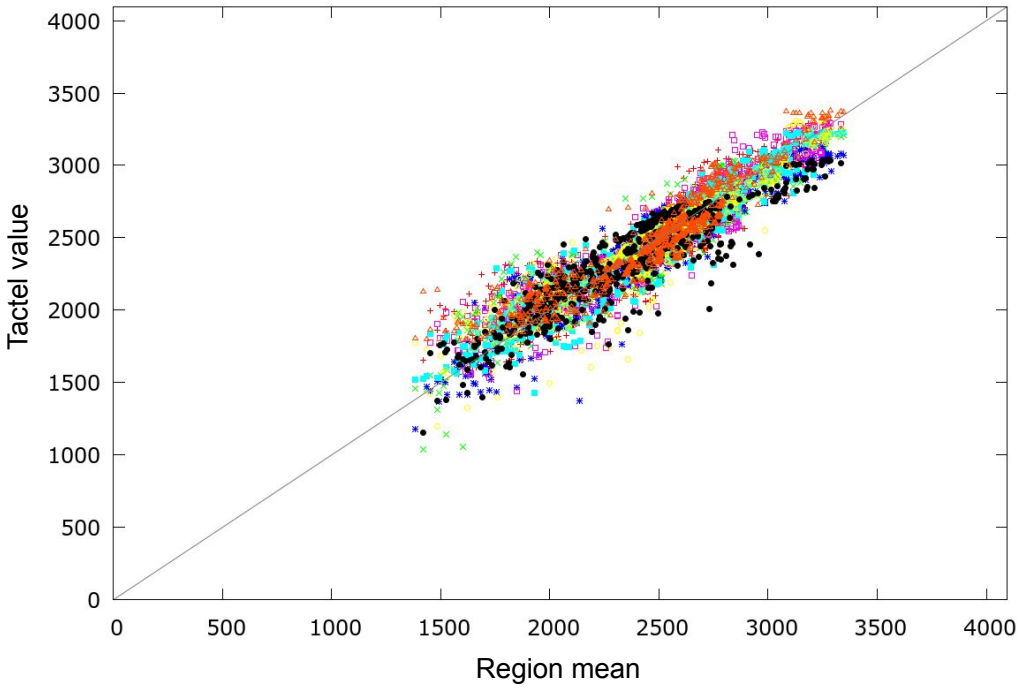

Figure 5.15: The measurement points of the eight tactels that were shown in Fig. 5.14 have now been processed with the conversion function. As it can be seen, the sensor cell outputs are much more homogenous and closer to the ideal line.

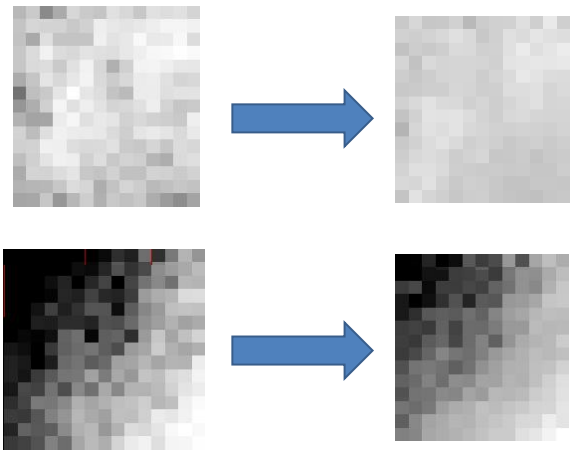

Figure 5.16: Sensorimages for uniform and gradient pressure shown with unprocessed (left) and converted/equilibrated output (right).

5.4 Summary

In this chapter we have investigated the sensor response in relation to physical stimulation. For this we tested three different cover materials. We have found that a proper calibration of the sensor is made difficult by the deflection of pressure inside the materials. Even when only one sensor cell is targeted, nearby cells get also activated as the elastomer deforms and a part of the pressure is deflected.

Nevertheless the sensor output in relation to increasing pressure shows a hyperbolic characteristic, a very steep increase on low pressure and a more flat response in higher pressure regions. This was found to be the case for all materials, although they all show slightly different response curves and working ranges. This is positive as we targeted a high sensitivity to low forces from the start and also optimized the sensor cell shape to increase the sensitivity.

We have found that the sensor shows quite a bit of spatial inhomogeneity, this means that sensor cells under the same pressure give different output values depending on their location. The reason for this is the surface structure and carbon distribution inside the cover materials. These two properties are inhomogeneous in the materials which is reflected in the corresponding inhomogeneous sensor output.

As a next step we have investigated the temporal homogeneity and repeatability. All materials are to some degree subject to changes over time or from wear. Because of this we have proposed an method for autoequilibration, which allows to provide a more consistent output of the sensor cells. This method extends the conventional equilibration method. It does so by statistical analysis of the sensor data. As this can happen continuously, a down time of the sensor and the attachment of special equilibration units is not needed anymore.

Chapter

6

Applications

6.1 Introduction

In this chapter we will present a range of applications that have been realized with the *Myrmex* system. Through this we will not only demonstrate the versatility, as the applications are quite different, but also the usability of the system: some of these applications have been realized by people who are not developers of the system.

Because of this we have divided the applications into two groups: the first one presents the applications that were realized by the author himself, the second shows applications realized by external users.

Both application groups cover multiple of the tactile sensor scenarios that we introduced in section 2.2. Figure 6.1 shows an overview of what scenarios have been realized with the *Myrmex* system. The applications include the scenarios outlined in the motivation, the tactile table surface, the tactile object for human grasping research and the tactile gripper for slip detection.

The first application will show how data for the study of manual interactions can be gathered by using a tactile object made out of *Myrmex* modules - the tactile book. We will present an experiment done with 15 people that investigates grasping behavior when lifting an object.

We will then introduce the concept of a tactile table, a tactile surface formed by multiple *Myrmex* modules. Due to the modularity of the system, a wide range of different sized tables can be created. We will show how one can use

image processing algorithms on the tactile data to determine the rotation of cups. This method together with a tactile table might be a feature that could be found in intelligent kitchens of the future.

The tactile table can be also be used as an input device for virtual reality scenarios. We will show how such a tactile surface could be used to help handicapped people to retrain some of their finger motor skills. For this we will present a range of training scenarios that couple the tactile data with a 3D scene. We will also show how a tactile sensitive surface made out of *Myrmex* modules can be used to develop better control algorithms for prostheses.

Using industrial robot arms, the *Myrmex* modules can be used as end-effectors to grasp objects. For this scenario we will first show a slip detection algorithm with subsequent grasp force adaption. This application was made possible by the very high speed of the *Myrmex* system.

Employing *Myrmex* modules as end-effectors also allows the realization of new control methods that are driven by tactile data. For this we present a tactile servoing framework which allows robot systems to track or search for surface features. This framework will be used to track an unknown cable and keep steady tactile contact, such a skill enables the autonomous exploration of objects by intelligent systems. This application was made possible through the good spatial resolution and high sensitivity of the *Myrmex* system.

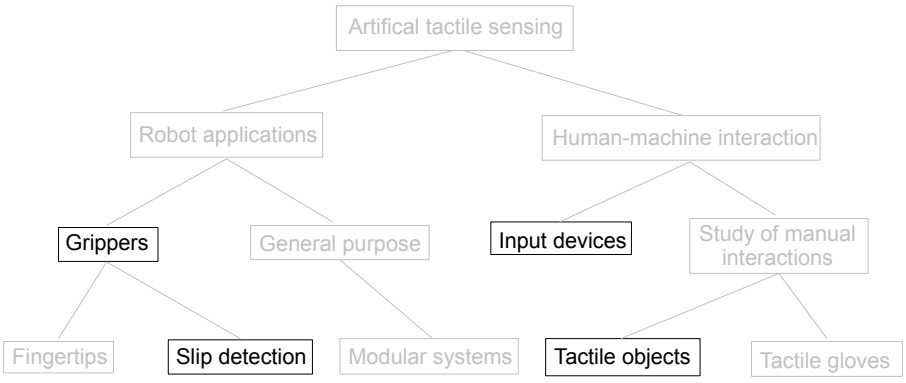

Figure 6.1: A modification of Fig. 6.1 that was shown in 2.2. Here we have highlighted the applications that will be presented in this section.

6.2 Applications by the author

6.2.1 Haptic action capture of a Pick and Place task

Multifinger hands for robots come in a variety of implementations, most have a range of three to five fingers. Prominent examples are the 3 finger SDH hand from Schunk [153], the 4 finger DLR hand and 5 finger hands like the Shadow (Fig. 6.2), the Gifu hand [154] Robonauts hand [155] and the Barrett-Hand [156].

Figure 6.2: Left: The Schunk SDH hand with three fingers is a robust hand that is also used in industrial applications. Right: The anthropomorphic Shadow hand with five fingers has a dexterity that is comparable to humans. [103]

Many of these hands have tactile sensors in their fingertips and can achieve a dexterity similar to that of humans. This allows for a large possible number of finger position configurations when handling objects. From this of course follows the problem of how to select a posture for an action. One way to do so is to look at the configurations humans use for grasping or manipulating objects.
The range of human grasps has already been already been analyzed and organized in a taxonomy [157]. Based on such prototypes, finger configurations

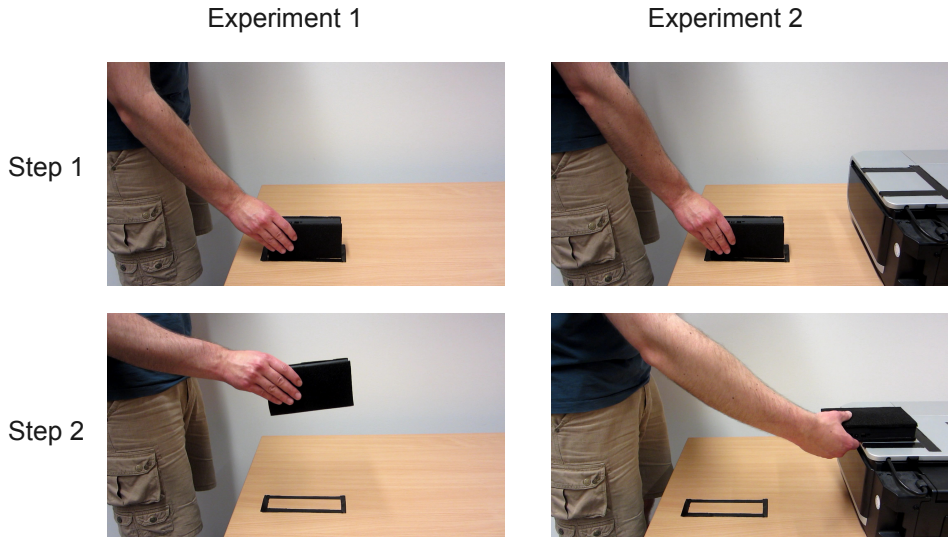

Figure 6.3: Description of the two experiments. The first step in both experiments was to grasp the book on the table. The next step was to just lift the book straight into the air for experiment one, while in experiment two the book had to be laid down onto a shelf in a marked position.

for robot hands can be derived, and parameterized for objects properties like size as was done in [158].

However the taxonomy of human hand postures does not take into account the actual force exerted by each finger. To acquire this information from humans, tactile gloves can be used, but these necessarily interfere with the contact of skin and object and thus change the sensory feedback during manipulation, in addition they do not allow for a monitoring of all contacts e.g. the sides of the fingers. To overcome this, objects can be used which are covered with tactile sensors. Our tactile book, presented in detail in section 4 offers the possibility for a haptic action capture during natural object handling.

We demonstrate the capabilities of the tactile book here with two experiments involving a pick-and-place task. Both experiments consist of a repetition of five identical, successive trials.
In each trial, the tactile book initially is in the same position (see Fig. 6.3, top row) in front of the subject. The task for the subject in experiment 1 (Fig. 6.3, left) was to pick up the book with his preferred hand and lift it up to a speci-

fied height of 30cm, and then return it to its original place as marked on the table. In experiment 2 (Fig. 6.3, right), the subject has to pick up the book, lift it to the 30cm height and then, instead of returning the book to its original position, the book is to be deposited onto an elevated shelf (arranged within direct reach, see Fig. 6.3, right). Here, depositing the book requires a rotation of the object by 90° about its longer axis.

With these experiments we try to get an additional view on what is called the "end state comfort" effect [159]. This is the anticipation of the planned outcome ("end state"') of a grasp, where one chooses a hand posture that makes the end-state "comfortable". This however may require that the initial grasp posture is uncomfortable (as in picking up a glass that is placed upside down on a table).

In an experiment that confronted children from preschool and kindergarten (<6 years old) with this task only 11 of 40 [160] exhibited the end-state comfort effect. In a more detailed study, with a slightly different task, a clear correlation between age and task performance was found : 57% of 5 year olds used an end-state comforting grasp, compared to 45% of the 4-year-olds and 18% of the 3-year-olds [161].

For adult humans the presence of the end-state effect has been widely documented [162–164]. The end-state comfort effect is also present in primates, as has been shown in a study with tamarin monkeys [165]. Even lemurs, which are the evolutionary most distant primate relatives of humans, exhibit the end state comfort effect in grasp planning. From this follow that this planning ability has evolved at least 65 million years ago [166].

For the reasons as to why the end state comfort is so of such importance, the precision hypothesis is very popular. This hypothesis says that a positioning movement at or near the middle of the range of motion is easier to execute that at or near the extremes [163].
The consequence is that precision increases while the subjects hand is in a comfortable posture and movements can be made more quickly [167]. For humans it has been shown that the end state comfort can also be influenced by a social component: when handing a tool to another person we present it in such a way that their beginning state is comfortable [168].

Our experiments were done with 15 subjects in the age of 24 to 34 years. The subjects included two females and two left handers. Each subject did five trials of experiment one and after that five trials of experiment two. The exper-

iments were also recorded on video to enable a better labeling of the fingers in the tactile data. During the task the tactile book recorded data from all tactile sensor cells and the internal acceleration sensors.

We will now look at how we processed the tactile data to extract information of the finger postures.

Data processing

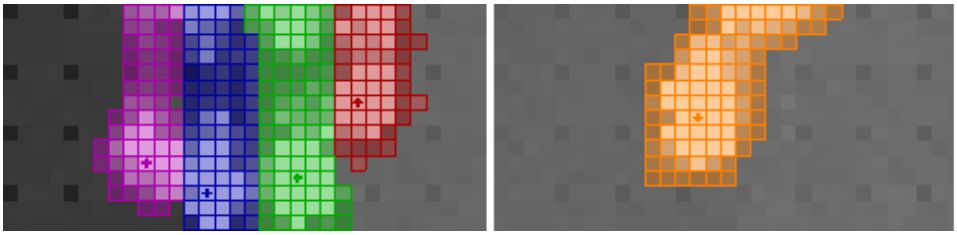

Figure 6.4: Example of the tactile image recorded by the tactile book (both sides combined) with all five fingers visible. They were manually labled with different colors: Red for the first finger, green for the ring finger, blue for the middle finger, purple for the small finger and orange for the thumb.

The tactile data is recorded as a sequence of frames with a spatial resolution of 64x16 tactels and a value range of 0-4095 for each tactel. Figure 6.4 shows an example of the tactile data recorded with the book. The tactile data is recorded every 5.6ms together with the acceleration data from the accelerometer and gyroscope in the tactile book. From the resulting spatio-temporal pressure profiles we aim to extract detailed information about both the geometry and the force parameters of the manual action sequences. As a consequence, we can compare the different force levels which each finger uses during the experiments.

Extraction of geometry parameters. We first removed sensor noise by thresholding all tactel responses. After that the finger shapes were manually labeled by associating each tactel with a specific finger ID, or as background. The digital video data recorded during each experiment was used to aid this process. The shape of a finger contains all tactels that are activated (above the noise threshold) during a trial. By measuring the outlines of the finger shapes it was possible to determine the overall rotation of the fingers as compared to the book.

Extraction of pressure/force parameters. Due to the sensor characteristics, the response value [0..4095] of a tactel cannot be taken as a simple linear mea-

sure of the net normal force applied at the tactel. As outlined in Sec. 4.3.2 the response value of a tactel is directly correlated with the part of the conductive elastomer used as sensor cover on the tactel. This normally requires a time consuming calibration process for each tactel together with the specific piece of elastomer. For this experiment we were not interested in the absolute forces exerted by the fingers, but in the relative change of forces that each finger undergoes during the experiment. As the fingers did not change their location on the book during a single trial, the relative change during each trial can be calculated by summing up the tactel values associated with each finger and normalizing it by dividing through the maximum value observed in a trial.

Results

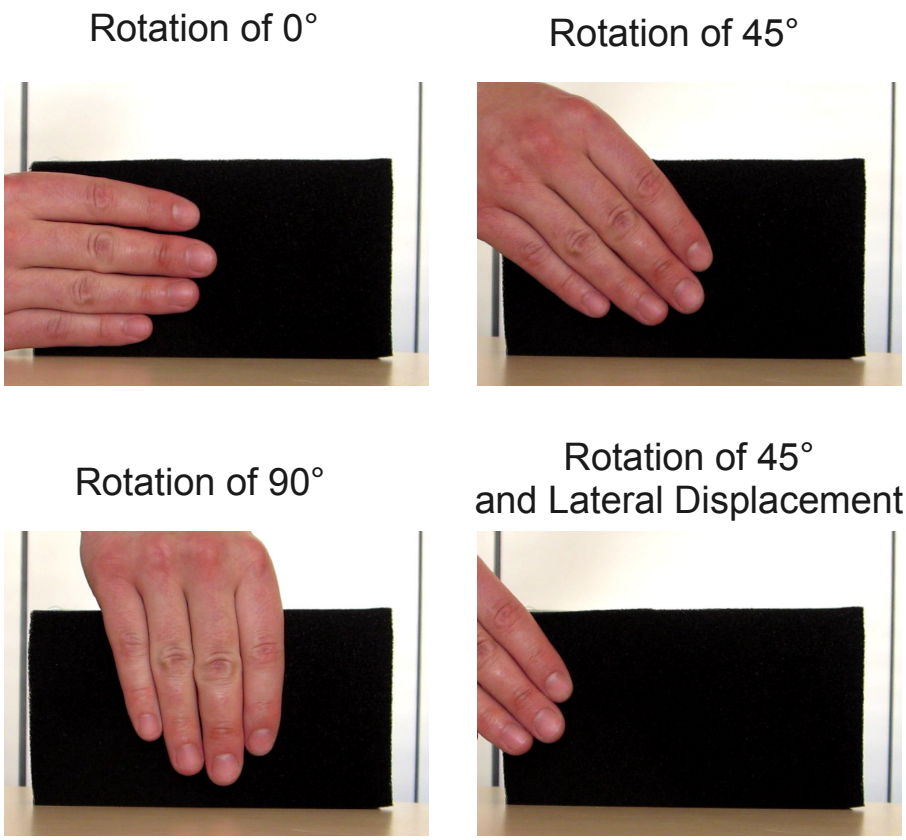

Figure 6.5: Examples for our notation of different rotations and (here positive) lateral displacement of the fingers. The rotation and lateral displacement is measured relative to the center of the book.

After data processing we obtained the geometry parameters and could assign pressure profiles for the five fingers during the task. We found that the experiments provide interesting insights about different aspects of the employed grasping strategies.

A first aspect is the impact of the anticipated task on the relative positioning of the fingers with respect to the object. To analyze this influence we evaluated both hand orientation, as the angle between hand axis and the longer side of the book, and the lateral displacement of the hand (see Fig. 6.5). The lateral displacement was calculated by using the position of the ring-finger, which was the best visible finger in the data, as reference position.

The hand orientation between experiments 1 and 2 is shown in Fig. 6.6. Despite significant variation in the individual orientations there is a clear tendency towards a stricter alignment of the hand axis with the direction of the longest extension of the book for the second experiment.
This is in line with the expectation that such an alignment facilitates the required rotation of the tactile book about this axis for this task. We also see wider range of orientations between subjects in experiment 2, together with a much higher coefficient of variation.

A second systematic trend is a more pronounced lateral displacement (Fig. 6.7), negative values in some trials indicate a ring finger placement towards the opposite side of the tactile book center. This is also in line with the expectation to better avoid contact between the fingers and the shelf when depositing the book.

We interpret the difference in the variations in the following way: For experiment 1 the favored grasp orientation was taken from the start, and similar for all subjects. What was adjusted during the course of the trials was the hand position, which shows a great variance between the trials and subjects.
In experiment 2, there was more testing of the most comfortable orientation, and apparently the most comfortable angle was different for the subjects. However the position of the hand thereby remained more consistent.

The variety in the lateral displacement has been also found in a different grasping experiment using the *Myrmex* system. This has been done by external authors in [169]. Thereby a tactile object ("TACO") is created similar to the tactile book by using 4 *Myrmex* modules in a 3D printed case. The TACO is used to investigate human grasping under force perpetuation. Because of this it is attached to a Phantom force feedback device.

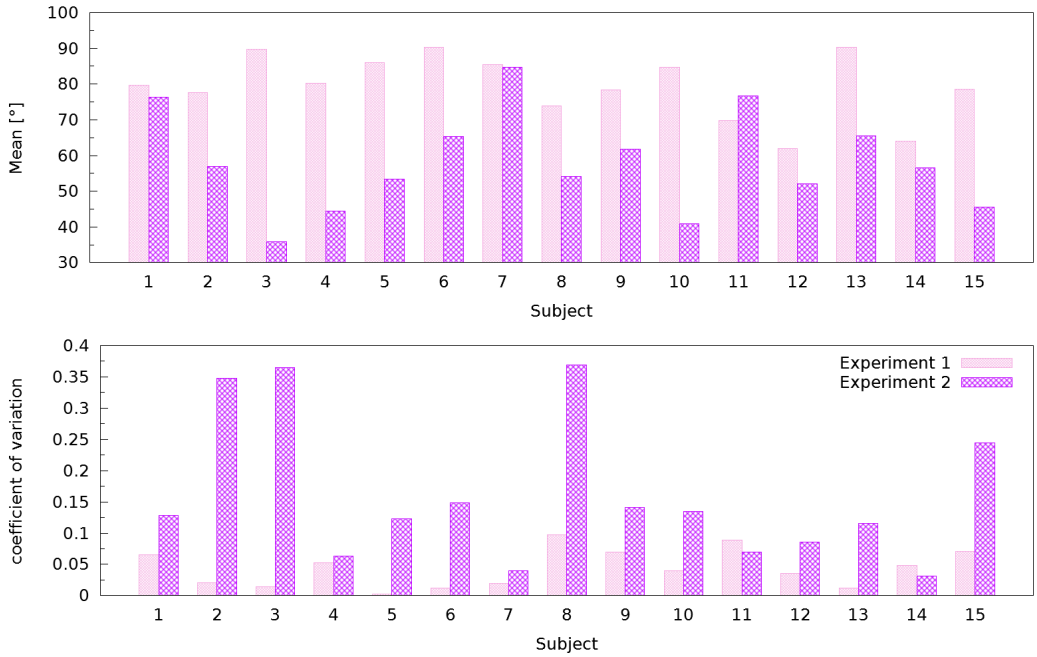

Figure 6.6: Comparison of the absolute finger rotation for the 15 subjects and both experiments.

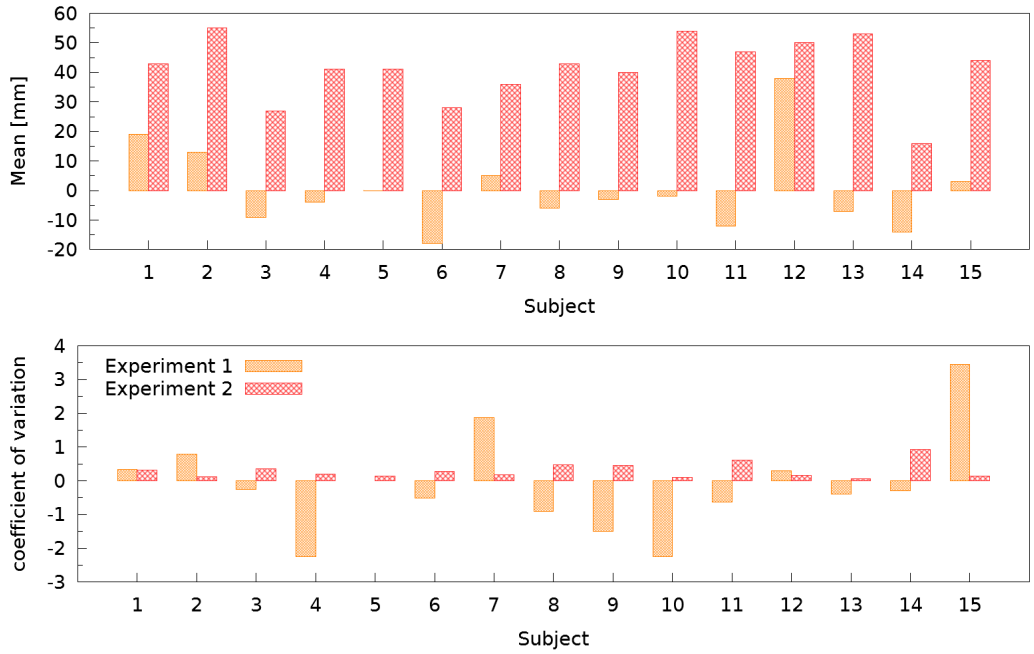

Figure 6.7: Comparison of the absolute lateral displacement for the 15 subjects and both experiments.

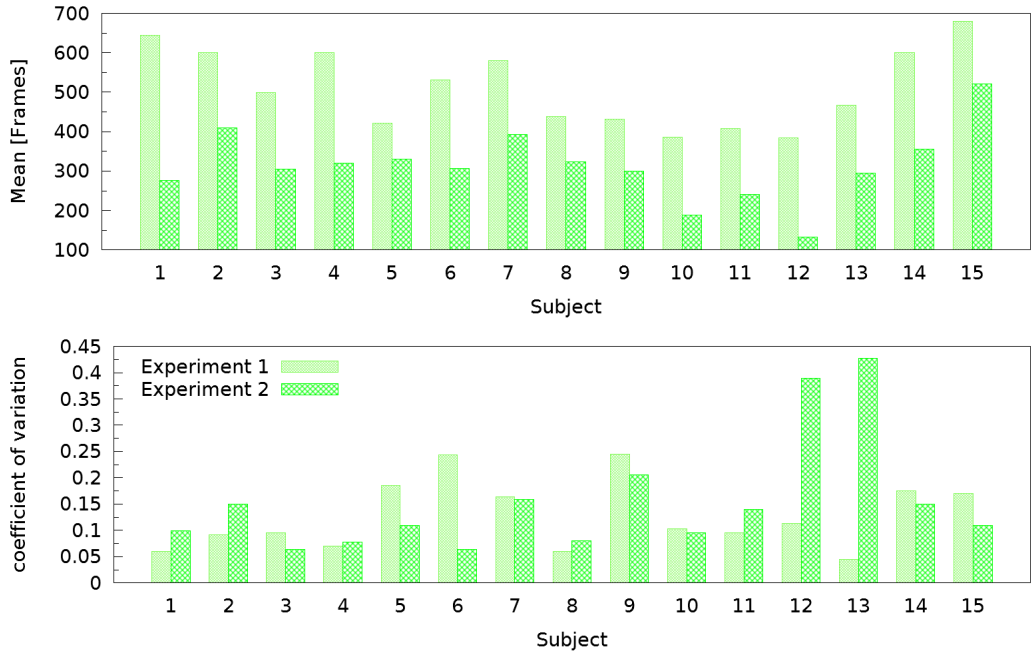

Figure 6.8: Comparison of the time needed to complete the experiments for the 15 subjects and both experiments.

As a next step we can look at the temporal dimension of our pick-and-place experiments. We can extract how long each person took for a trial using only the tactile data. For this we register the start of the trial through the activation of multiple tactels above a certain threshold. For the end time, we look for the tactile activation to fall below the minimum.
The mean times and the coefficient of variation for each subject is depicted in Fig. 6.8. A general trend for all subjects is that experiment 2 was faster then experiment 1. Also the relative speed of the subjects seems to be mostly consistent between both experiments. A person that took a longer time in experiment 1, also took a relative longer time in experiment 2.

The next point that we look at are the relative finger forces. As already stated we calculate the relative force for each finger during each trial by summing up the tactel values associated with this finger and normalizing it by dividing through the maximum value observed in a trial. Figure 6.9 shows the temporal profile of grip strength for three subjects during experiment 1.

In the graphs we can see three different grasp strategies. Type “A”, which exhibits a rapid rising curve, then stays constants and then rapidly decays.
The type “C” is also rapidly rising and then starts decay for the rest of the time.
The type “S” exhibits a rapid overshooting and then stabilizes.
While further profiles would be conceivable, it was a remarkable finding that all 15 subjects adopted a grasp strength profile that could be well characterized by one the depicted three types “A”,“C” and “S”.

To further investigate these profiles, we take advantage of the acceleration data that was stored along with the tactile data.
It can be found that type “A” corresponds to a rather constant velocity for lifting and return, type “S” was accompanied by rapid lifting, a pause and a slow return, while “C” appeared similar to “A”. The acceleration together with the force data is depicted in figure 6.10. The results show that the grasp force of the participants is matched to the object accelerations in order to ensure proper control through their grip. For the second experiment, the anticipated task, the same behavior is apparent.

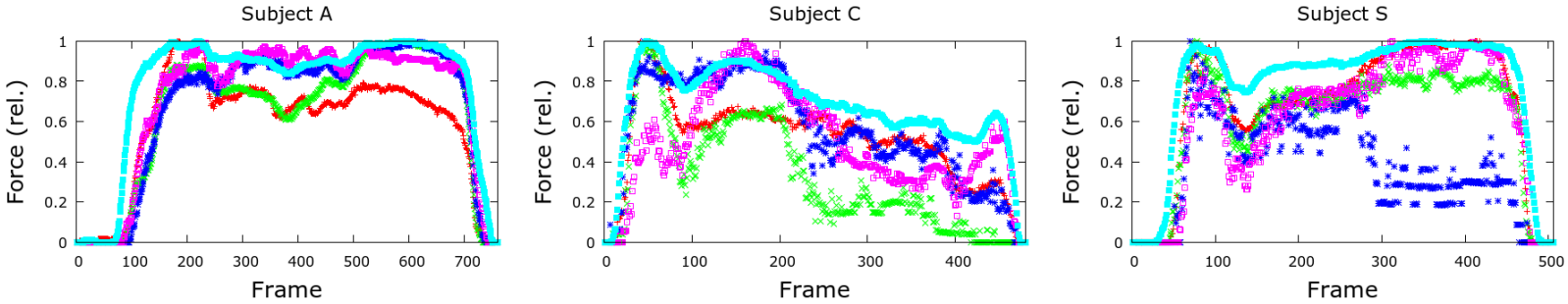

Figure 6.9: Force curves of three subjects with the normalized force given for each finger. The subject's curves are prototypical for the force profiles (therefore denoted by the letters "A","C", "S" of these subjects in the text). The cyan curve (thumb) is equivalent to the relative total grip force applied onto the book.

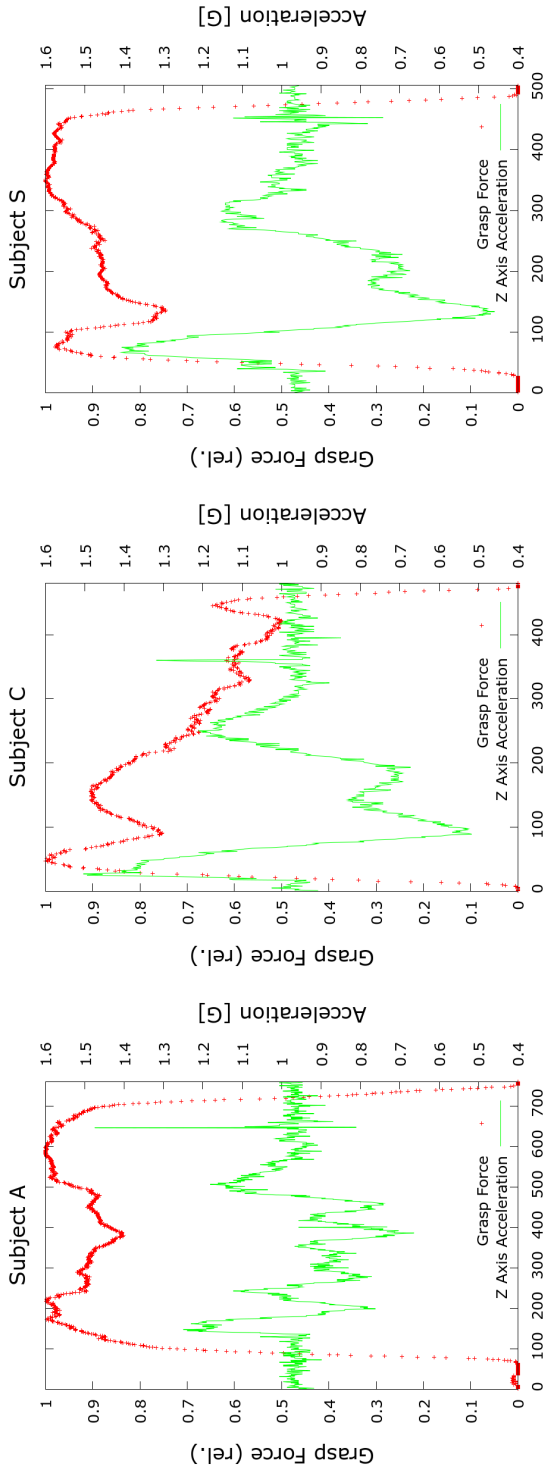

Figure 6.10: The grasp force data (red) together with the acceleration data (green) for each prototype subject.

6.2.2 A tactile table for an intelligent household

In this section we will show the usage of the *Myrmex* system as a tactile table / input device. This tactile table could be a part of an intelligent room or household with robotic devices.

The human home has gone through a constant improvement in terms of living quality, mainly due to electrification and automation. If we think of disabling our dishwasher, refrigerator or microwave for even a day - we suddenly become aware of their convenience factor. The current state of technology indicates that these are not the last improvements to our living space.

Visions of a future with highly automated and smart homes have been around for a long time. Key ideas have been formulated more than 75 years ago in a Popular Mechanics article [170] where the interconnection and the remote control of household machines is envisioned. After the appearance of computers systems they were integrated into this vision. In 1957 Frigidaire (a part of General Motors) presented the design study 'Kitchen of the Future' [171] which includes a IBM computer which processes recipes given in by punch cards. A 1969 Japanese vision of a future kitchen then also includes a mobile robot (Fig. 6.11), which serves food as well as doing the cleanup tasks.

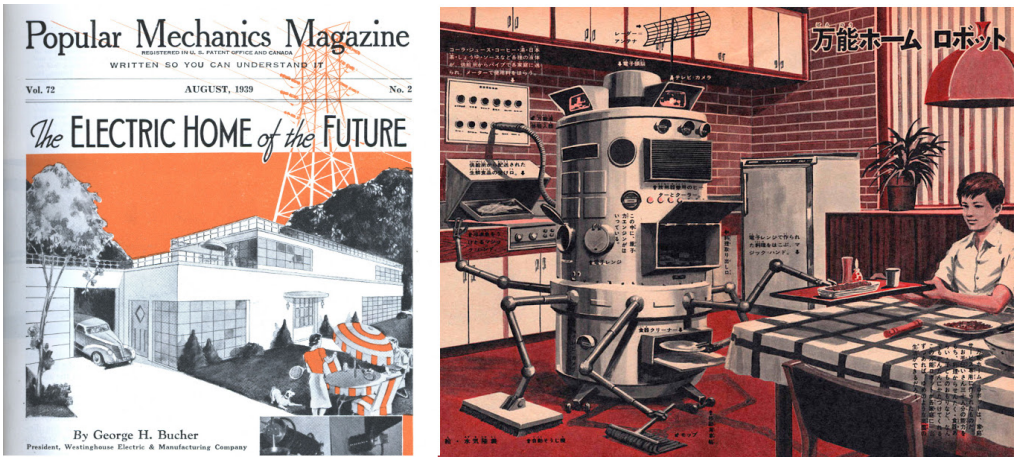

Figure 6.11: Left: The 1939 issue of the popular mechanics magazine envisioned advanced and intelligent home electronics. Right: A 1969 Japanese vision of a (very multitasking) kitchen assistance robot extends this. Image sources: [172, 173]

Some of these futuristic concepts have been realized with the technology available today in prototype environments, such as the Microsoft Home [174] which allows to control appliances via a smart phone and features a voice controlled home computer - which is even informed about the watering level of

plants. Today a whole research field called Ambient Intelligence is devoted to develop applications and stepping stones for the intelligent and all-round comfortable home. These intelligent environments are made be aware of people's needs, while being discret and unobtrusive [175, 176].

Estimation of Object Pose

In respect to such an intelligent environment scenario, we investigate the use of a tactile table composed from multiple *Myrmex* tactile modules. This is presented in detail in [177].
The tactile table could be used as a surface on which humans interact, as integrated into a normal living room or kitchen table. We investigate if it is possible to determine the rotation of a cup placed on the tactile table by only using the tactile data - without any markers or visual feedback.
Such a method could enable a smart environment to determine that there are cups on the table (and likely persons using them). As the cups must be rotated in a certain way to be accessible it can give a clue how the people are seated. Additional information could be drawn from the size (type of cup) or strength (cup filled or empty) of the tactile contact. It might also be possible to discriminate different individuals by the way they rotate their cup.

To implement the cup rotation estimation algorithm, we used a single *Myrmex* sensor module and range of different cups, as depicted in figure 6.12.

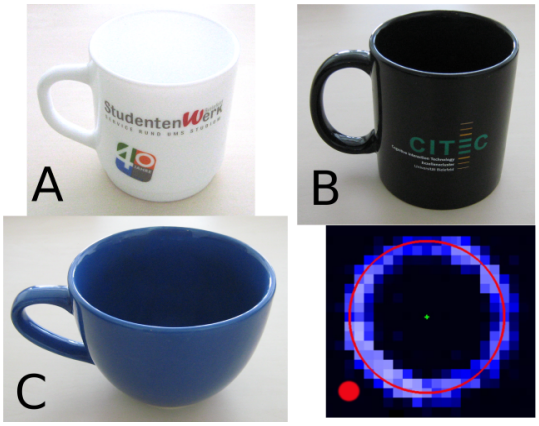

Figure 6.12: Photographs of the three cup types used to predict the handle orientation. The lower right image shows the tactile feedback obtained from cup B. The red dot indicates the orientation of the handle.

Table 6.1: Prediction results for the handle orientation of different cups

	diameter	weight	prediction error	std. deviation
Cup A	7cm	265g	16.8°	5.0°
Cup B	8cm	342g	13.5°	5.4°
Cup C	6cm	520g	10.2°	4.5°

Each cup produces a circular response pattern which is visible on the tactile image and can be processed using algorithms known from computer vision. For this we use a hough circle transformation [178] to detect the center and size of the circle. For the sensitive table scenario, this would give the intelligent environment the information where the cup is spatially located and also an estimate of the cups size from the diameter of the circle.

To determine the cups orientation, we use the fact that there is a slight weight gradient caused by the handle of the cup. This leads to a slightly stronger tactile response in the area where the handle is located.
To use this information, we take all tactels that are inside the detected circle and calculate the center of gravity. From the position of this center compared to the middle-point of the circle we then know the orientation of the handle, as the gravity center is 'pulled' outwards by the extra weight of the handle. The distance between this points can be used as a confidence measure.

To evaluate the performance of the proposed algorithm, for each cup the prediction error was averaged from five measurements obtained at eight orientations equally distributed around a circle. The results are shown in Table 6.1. The heaviest cup gives the best prediction results due to a better signal-to-noise ratio.
An extension of this application could also include other objects, such as a fork or a spoon placed along a dish and this could lead to a combined robot hand - dinner scenario as shown in figure 6.13. This scenario also nicely demonstrates the advantage of the systems modularity to scale its physical dimensions. It is easy to create a bigger surface for more objects by connecting more modules together. And the systems auto configuration and USB parameter transmission allows the detection software to function without user adjustments - it just gets a larger image as input.

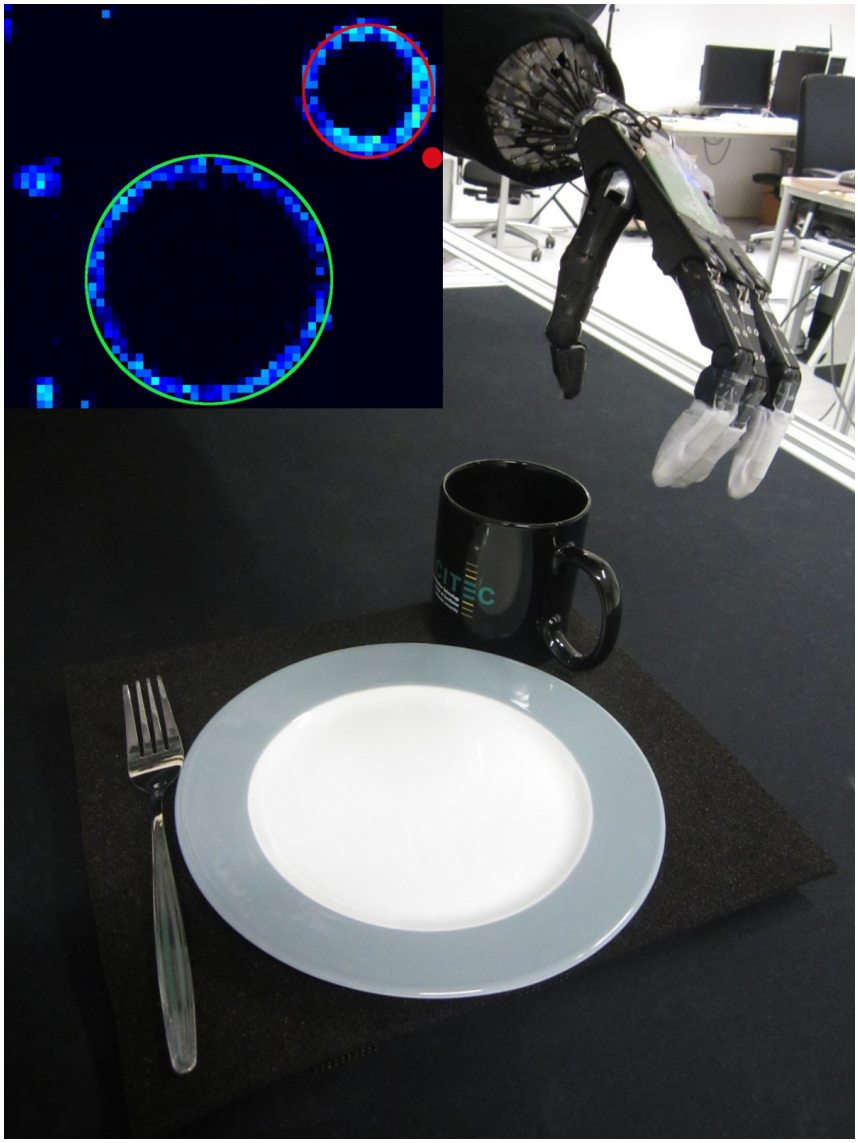

Figure 6.13: The tactile table could be integrated into a human-robot scenario, where a robot hand can assist the human and grasp or fill the cup. The sensorimage from the tactile table is shown in the upper left. The cup is recognized and its orientation calculated (red). The plate is too large to be registered as a cup (green). The fork on the left produces, due to its bended shape, two contacts at its top and bottom.

6.2.3 Manipulation of virtual clay

In the previous section we have seen how a sensitive surface composed from multiple *Myrmex* modules could be used as a helpful input device in an intelligent household. However this is not where the possibilities for a sensitive surface end. We think that combining such tactile sensors with virtual reality (VR) could be helpful in rehabilitation of patients with neurological damage.

Virtual reality is already used as a training tool in areas where the real training is dangerous or expensive [179]. Famous example are flight simulators for pilot training or for surgeons [180, 181]. Maybe less famous, but still prominent is the use of virtual reality to treat patients to overcome fears. This has be done successfully for patients with arachnophobia (fear of spiders) [182] and acrophobia (fear of heights) [183].

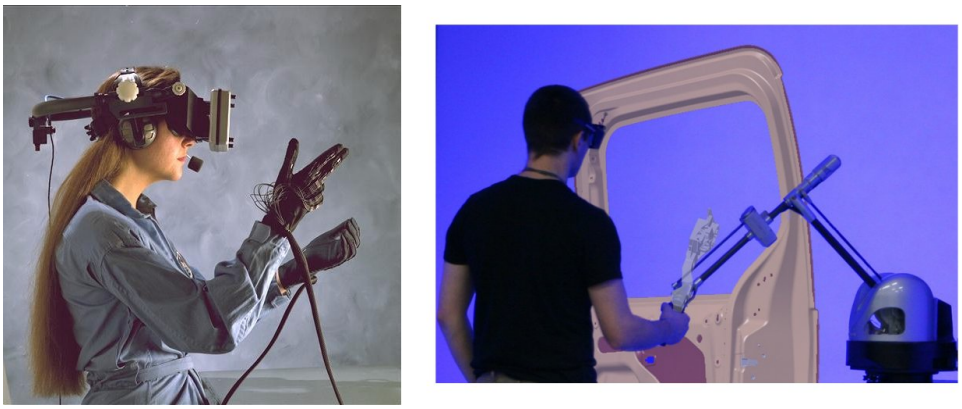

Figure 6.14: Left: A typical VR setup includes VR goggles to present a 3D scene and Datagloves to manipulate it. Right: Such a scenario can also be augmented by using force feedback devices like the Haption Virtuose 6DOF. Images sources: [184, 185]

But virtual reality therapy can also be helpful for the recovery of patients with neurological damage (neurorehabilitation). Victims of a stroke can often regain a considerable amount of motor skills with effective training such as constraint-induced movement therapy [186].
Also for patients who have received incomplete damage to the spinal cord it is possible to regain motor skills through training [187]. And the training of movements in virtual environments helps to reorganize neural connections involved in motor skills [188].

Virtual reality uses a set of in and output modalities to present an interac-

tive virtual scene to the user. A common set of devices that are is used to enter the virtual environment (see Fig. 6.14) includes datagloves and 3D goggles or surround-screens [189]. Also devices that create a 3D sound experience [190] and for force/haptic feedback [191] are often employed. The common goal of all VR setups is to make the user feel a connectedness (immersion) with the virtual scene [192].

For the task of neurorehabilitation a number of combined VR and robotic setups have been built. The GENTLE/s project created a training device which includes visual, haptic and auditory feedback [193].
For training the patients view a 3D scene on a screen, while their wrist is placed in the arm of a 3DOF Haptic interface called HapticMaster [194]. They can move objects in the virtual environment by moving the HapticMaster with their arm.
Different stages of the therapy command different action sequences or movement profiles. Because the arm of the HapticMaster can be actively controlled, it can act as a guide for the patient during the movements. On the lowest level of guidance, the endeffector can move the patients arm alone to 'learn' the movement. When the patient is moving his arm himself, the HapticMaster can be controlled by a spring and damper algorithm [195], which keeps the arm in a desired trajectory 'tunnel' by adding resistance to the movement on deviation.

A very similar setup is used in [196], which adds haptic rendering [197] into the setup. Thereby the patient feels a physical resistance when he touches virtual objects. In one of their scenarios the patient has to place a virtual cup onto a shelf which is also occupied by other objects. The collisions that occur during that task can be felt by the patient and help shaping the arm trajectories of the patient.
The more recent Rehabilitation Gaming System [198] uses data gloves like the Cyberglove [199] and a vision based motion capture system to the track the hand movements of the patients. The hand movements are used to control a virtual hand in a 3D scene displayed on a monitor.
The game concept motivates the user to grasp floating spheres in the 3D scene using the virtual hands, where each sphere is awarded with points. The difficulty of the game adapts to the performance of the patient.
A combined setup with a Cyberglove, a Cybergrasp [200] (for haptic single finger feedback) and a HapticMaster (giving force feedback for the whole hand) is used in [201]. It offers a range of different training games, including a virtual piano which trains the finger movements.

For the training of fine motor finger skills also the use of a 3DOF device like the

Phantom [202] or the Omega [203] is possible, which are similar to the HapticMaster but have smaller dimensions so their endeffector could be controlled by a single human finger. A combination of all three devices (Cyberglove + Cybergrasp + Phantom) for use in a virtual environment is shown in [204].

While such setups can provide information about the finger movements in air, they cannot collect information about multifinger forces when handling objects. For this tactile gloves as introduced in Section 2.2 could be used, but one has to keep in mind their drawbacks: the not 100% natural haptic experience, as the tactile sensors are between the skin and the handled object, and the limited number of tactile sensors (all current tactile gloves have regions on the hand where no tactile feedback is sensed).

With this motivation we investigate the use of a tactile sensitive surface as an alternative input device for such virtual reality applications. In the future this might be tactile surfaces as already implemented in common devices such as tablets or mobile phones. However we find that currently our *Myrmex* system is superior for this task in performance and haptic sensation. The foam used as cover on the modules provides a better haptic experience of deforming a virtual object due to its softness and possible indentation depth when compared to the glass or plastic screens that are used for other tactile interfaces. But the ideas and software developed here could be easily adapted for other tactile sensor arrays.
We will present the idea of a virtually deformable clay object, that can be deformed by the user through his real fingers by pressing onto a tactile sensitive surface such as an array of *Myrmex* modules.

To realize the tactile manipulation of 3D objects, we need a visualization component for the display of a 3D scene and a processing component to acquire and process the tactile image.
For the visualization we use the open-source 3D modeling program Blender [205] and for the data processing we employ the image processing library ICL [206].
The Blender software offers solutions for many 3D related tasks, like modeling of 3D objects, composition of 3D scenes, animation, rendering and interaction with the user by using an integrated game engine. In addition it is open-source, widely used and its continued maintenance seems very likely.
The ICL is an open-source computer vision library, which apart from fast image processing functions also has functions for image display, GUI design and user interaction. This in addition to the low overhead implementation and good documentation allowed a fast development of the application.

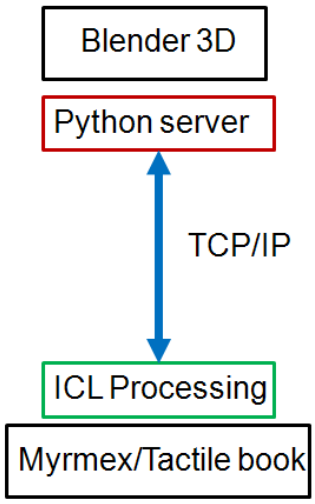

Figure 6.15: Overview of the programs involved. The visualization is done in 3D with Blender, the tactile data is acquired and processed by an ICL application. The communication between the programs happens via TCP/IP.

As the Blender software is highly complex and under constant development, the integration of our tactile sensor processing code directly into Blender would require a considerable amount of time to realize and consequently to maintain, so we use a release build of Blender and create a separate ICL based C++ program to acquire and process the tactile data. From this of course follows the problem of how to transfer data between the two applications. We solve this by using a TCP/IP connection, which also allows the two programs to run on different machines in a network. The overall application setup is shown in figure 6.15.

As Blender features an integrated Python API and interpreter, a minimal TCP server module for Blender was implemented in Python. This module is loaded when a prepared 3D scene is started using the Blender game engine.
The Blender game engine is a mode integrated in the Blender software that can be used to implement and run games which have been designed with the Blender 3D model and scene editor part.
In this mode the developer can make use of python scripts to modify the scene or objects, intercept keystroke and activate a physics simulation which is based on the Bullet Engine [207]. A use of the TCP server component with the 3D modeling part of Blender is also possible, but in the current versions of Blender not stable. The reason is that Blender in this mode does not allow for threading with python scripts.

This means that one could use the server component to edit 3D models, but at the same time it is not possible to use the GUI e.g. for viewing or editing the scene with keyboard or mouse input.

The ICL based program is used to obtain and process the tactile data from the *Myrmex* sensor system. As virtual clay object we use a 3D cube with 48x48 vertices at the top surface (Fig.6.16) and a 3x3 *Myrmex* sensor array. With this configuration each vertex in the surface of the cube can correlate to a tactel of the *Myrmex* sensor.
The ICL program sends the changes of the vertex positions to the Blender program via a TCP connection. The change of the vertex position is calculated by a formula which is specific to the application scenario, this is how different scenarios are realized. As in our interactive scenarios the delay between the actions of the patient and the reaction in the 3D scene is important for the immersion, we optimized our software for the best performance.
A small computational benchmark reveals that calculations within the integrated python interpreter are about 10-20x slower than when done in the C++ ICL program. Therefor we implement the necessary calculations of tactile and vertex data into the ICL program as far as possible and only send vertex data updates to Blender.
With this setup one can realize a multitude of scenarios which use tactile input to manipulate a virtual 3D setting. We have implemented four and will present them now.

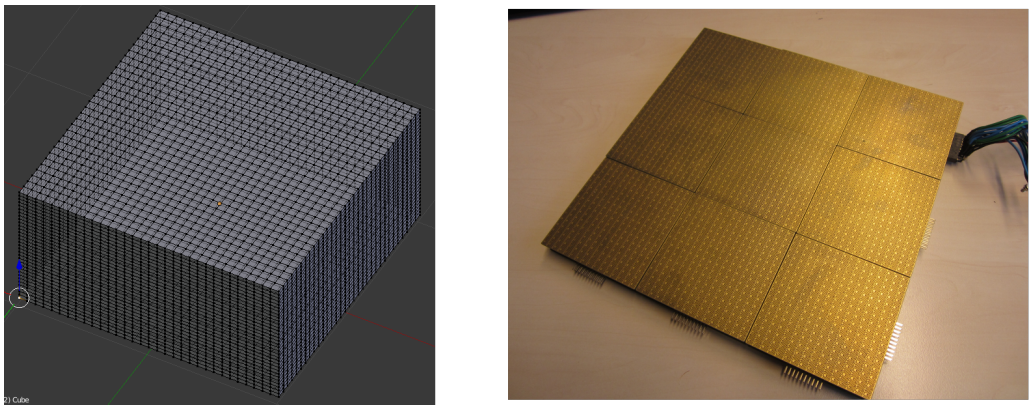

Figure 6.16: Left: The virtual cube which surface consists of vertices. Right: A *Myrmex* sensor array which has the same number of tactile sensor cells. The output of the sensor cells can be used to control the positions of the cube vertices, creating a deformable virtual object - our virtual clay.

Free form modeling

The most simple way to use the virtual clay is the free-form modeling.
In this mode the tactel value changes of the *Myrmex* surface directly correlate to vertex changes of the virtual clay in the Blender 3D scene. The Z value for each vertex is calculated by the formula:

$$v_z = u * m(x, y) \tag{6.1}$$

Where $m(x, y)$ is the tactel value at location (x,y) and u is a constant weight factor. The change of v_z is kept permanent, after pressing a finger on the sensor and removing it, the virtual fingerprint stays. This allows to manipulate the virtual clay in a similar fashion as real one.

As the *Myrmex* system uses a 12 Bit value range for its tactels, it is possible to generate indentations of many different depths. In contrast to many other tactile surfaces known from section 2.2.3, the *Myrmex* sensor surface allows for true multi-touch, that is the system can register contact at all tactels at the same time. Through this it is possible to use multiple fingers or even the whole hand to stimulate a larger area of the virtual clay at the same time.
In figure 6.17 one can see how a single finger was used to 'write' letters into the clay. The free form mode can also be extended by making use of Blender capabilities as a full featured 3D tool: One can also color the clay or attach a texture and it is possible to load other 3D models into the scene as shown in Fig. 6.18.

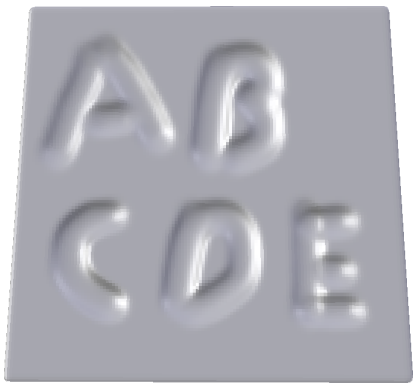

Figure 6.17: An example of free form modeling. A finger was used to draw characters into the virtual clay.

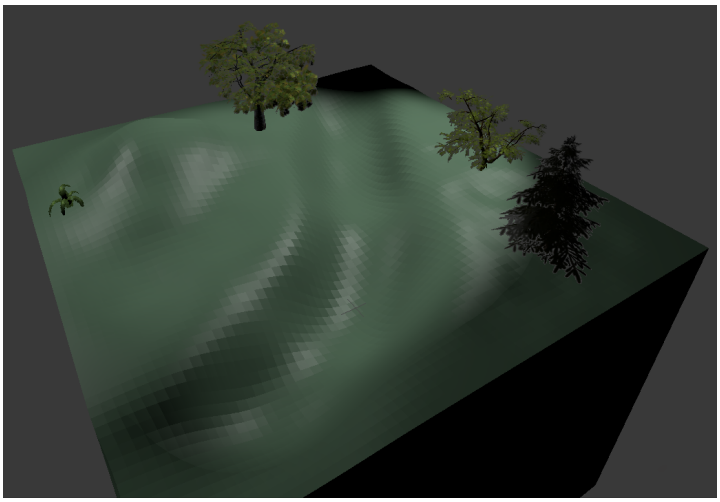

Figure 6.18: Another example of free form modeling. A landscape created by changing the clay texture and adding additional 3D models.

Physics interaction

A next step to make the scenario more exciting is to add physical feedback. For this we use the Bullet physics engine that is integrated into Blender. Through this a wide range of game-like applications become possible. The physics engine can enable gravity and collision checks on objects, through this we can easily realize rolling or bouncing objects. In figure 6.19 we show two example scenarios that use virtual balls with physics enabled.

The first one uses the 3D shaped clay and lets a single ball interact with it. The shaped clay could be the result of the free form modeling, making this a two stage interaction scenario. In the first stage the clay could be shaped by the fingers, and in the second stage the clay is tilted and the physics will cause the ball to roll inside the ridges carved by the finger.
It is also possible to manipulate the clay while the physics engine is enabled, through this the ball could roll in real time into ridges carved by the fingers.

A different scenario is to abstract from the direct mapping of tactels to vertices and to group multiple tactels which in turn control bigger objects inside the scene. Through this one would leave the domain of virtual clay and use the *Myrmex* surface as a freely programmable tactile input device, acting more like a tactile keyboard. An example application of this concept is shown in the lower part of figure 6.19.

In this scenario the mean value of a group of tactels corresponds to the height position of a block in the virtual scene. Because physics are activated, the ball rolls, can be lifted and fall down from a block. A game scenario could be to use the blocks to move the ball in a certain position or height.

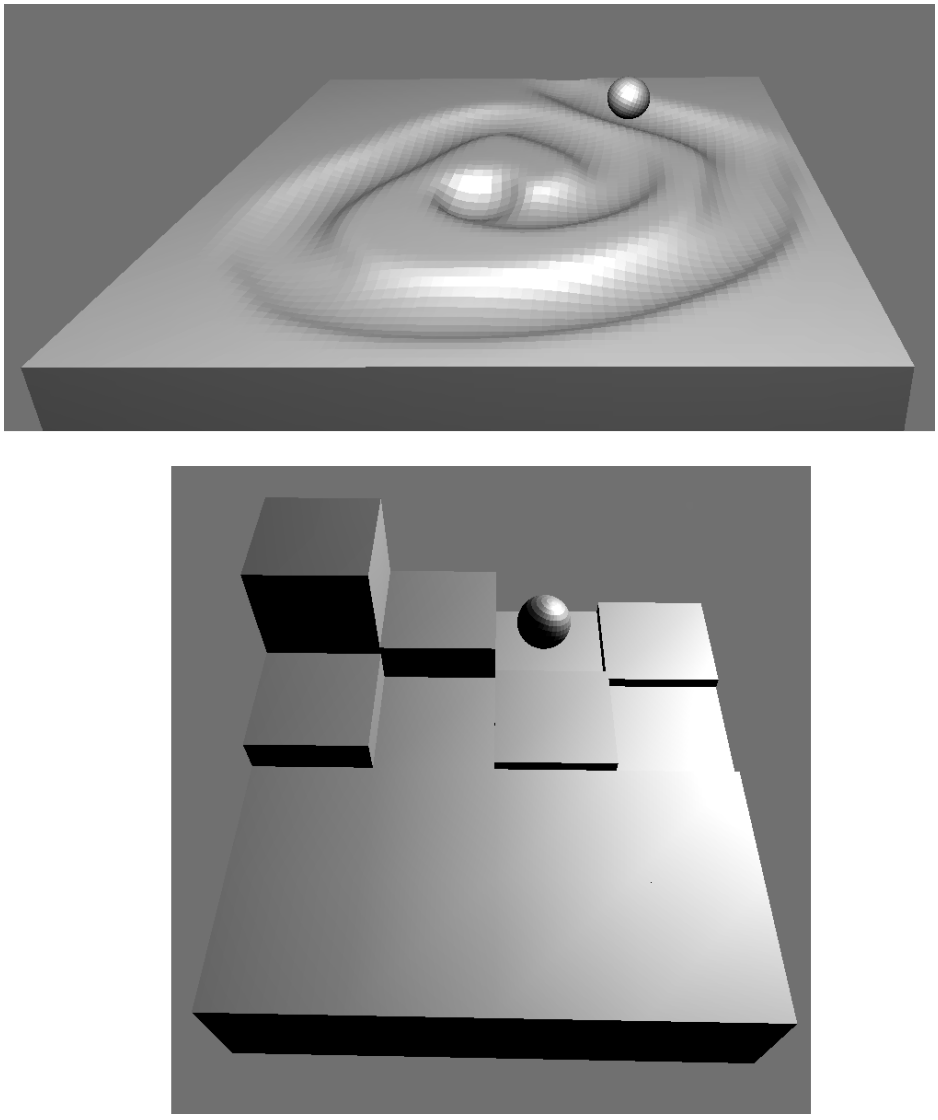

Figure 6.19: Examples of physics interaction with the tactile *Myrmex* surface and a 3D scene. Top: A ball rolls down a maze that was created with a finger in the virtual clay. Bottom: Groups of tactels are used to control the Z position of blocks, which can be used to maneuver the ball.

Virtual exploration of hidden objects

So far we have used a direct 1:1 mapping of tactel to vertex (except in the previous ball game scenario). However we can increase the possible scenarios and degree of complexity if we use an inhomogeneous mapping.

For this we define a different stiffness level in separate areas of the virtual clay. We do so by assigning a weight factor to each vertex (=tactel), which increases or decreases the distance that the vertex is moved.
The Z value for each vertex is calculated by the formula:

$$v_z = u(x, y) * m(x, y) \tag{6.2}$$

Where $m(x, y)$ is the tactel value and $u(x, y)$ is a weight factor for each tactel at location (x,y). If we take the weight as 1.0 for a normal vertex, a weight of 0.5 for example will be a stiff or slowly responding vertex while a weight of 1.5 will be a fast responding vertex.
With this we can realize the scenario of having hidden virtual objects in the virtual clay, that the subject has to explore through proper application of finger / hand force.

Consider figure 6.20, where the weight factors are shown as an 8 Bit gray level map.
They are used to define various areas with different weights, resulting in a different response strength of the virtual clay in these areas. In this case we have used geometrical objects: two circles and a square can be seen in the gray level weight map and are now 'hidden' in the virtual clay.
The square and one of the circles also have a gradient inside them. When pressing the foam on the tactile sensor, the differences between background and objects will become visible in the 3D scene through the different response strength of the vertices.

With this technique one can design a multitude of different weight maps to realize different training scenarios. One can use a small hidden object to train the movement / force application of a single finger. Also bigger or multiple hidden objects could be used to the train the movement / force application of the whole hand.

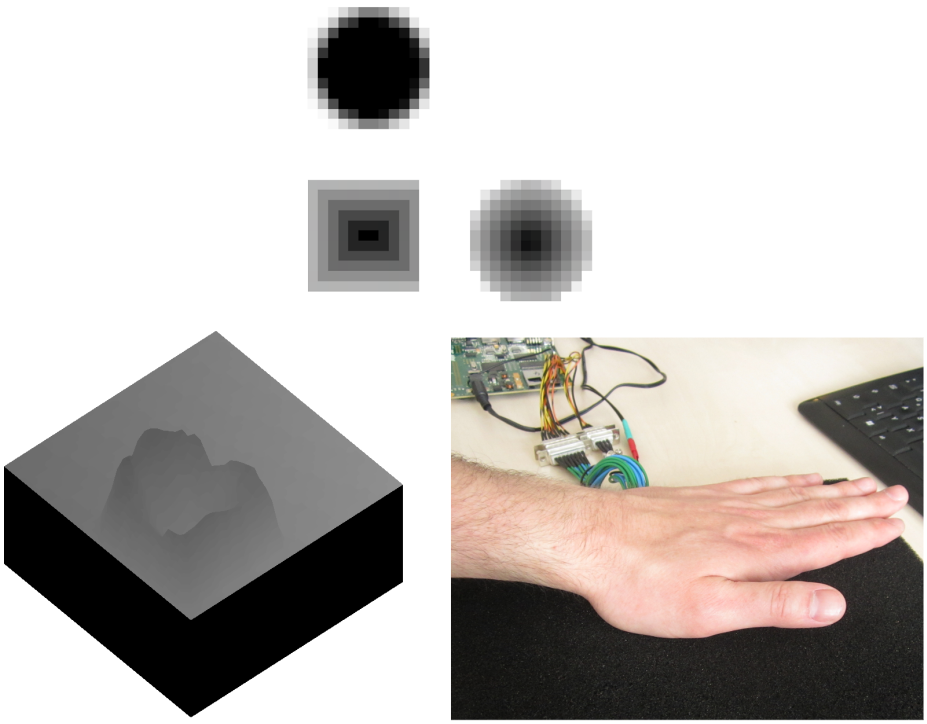

Figure 6.20: Virtual exploration of hidden objects. A weight map (top) is used to determine the mapping between tactels and vertices. White means a strong response and black means no response. To locate and identify the different shapes in this case the palm of the hand is used. In the current scene the palm is pressing on the area where the square is located in the weight map. To be able to properly discriminate the different shapes using the visual feedback, force has to be applied in various amounts and angles by the palm.

Mimicking the shape of virtual objects

Another scenario is to make the objects visible in the 3D scene from the start, and instruct the subject to modify the clay so that the shape of the object gets approximated. For this we use a mapping from sensor value to vertex position with a constant weight as in the free form scenario. However we add one or multiple 3D objects to the scene in Blender.

The goal of the patient is first to find out which spatial location on the tactile surface corresponds to the location of the 3D object. This can be done by sweeping the fingers around and noticing the position of the virtual clay deformation. When the location is found the finger should be pressed down with just enough force to rise the clay slightly above the virtual object so it is covered. In figure 6.21 we see how this looks with the human thumb and a sphere.

An additional challenge is created by trying to match the 3D shape, which requires the finger to be positioned at specific angles and rotations for the most accurate match. An example for two fingers is shown in figure 6.22.

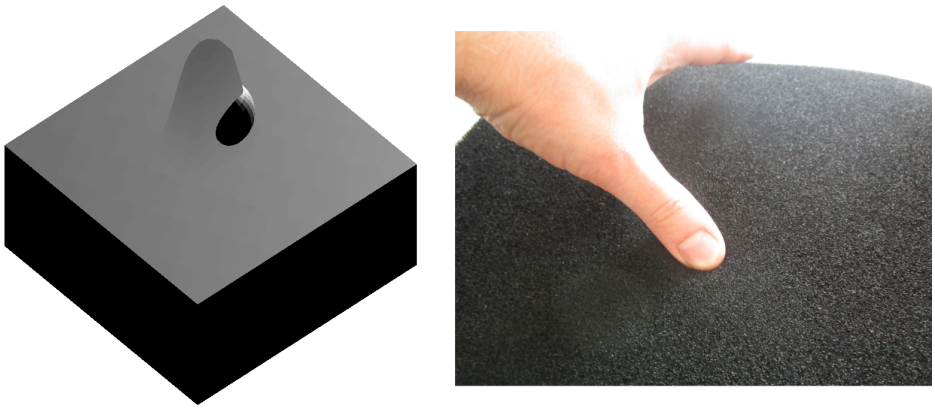

Figure 6.21: Using a thumb to cover a ball shape, here the ball is half covered. For a good match of the shapes there is a lot of fine-tuning of thumb rotation and pressure necessary.

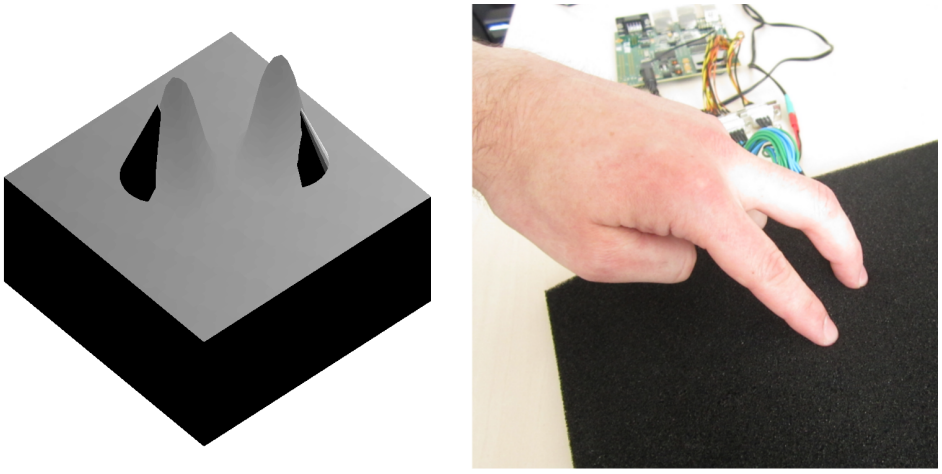

Figure 6.22: Using multiple fingers to mimick multiple shapes, here two cones, is an additional challenge for proper hand positiong and posture.

6.3 External Applications

In the previous section we have presented multiple scenarios that were realized with the *Myrmex* system by the present author. In this section we will show a selection of scenarios that have been realized by external users. Due to this, we keep the presentations compact and focus on the role of the *Myrmex* system in the applications. For complete descriptions of the applications we reference to the respective publications.

6.3.1 Prosthesis control

Apart from the retraining of patients with neurological damage, the *Myrmex* system can also be used to improve hand prostheses for handicapped people. This has been done by recording ground truth data for the development of advanced control algorithms for hand prostheses. This work by Castellini and Kõiva is presented in [208], their motivation is that current state of the art hand prostheses do not allow the force control of single fingers because no sensible control system is available.

Prosthetic devices have a long history. Written reference to prostheses is given even from ancient times: Herodotus describes the story of a prisoner cutting his leg off and replacing it with a wooden one to escape [209] and Pliny the elder tells of the roman general Marcus Sergius, who lost his hand in battle and had it replaced with an iron one to hold his shield [210].
For a long time prostheses only consisted of wooden or metal imitations of the missing body part. Around 1500, functional prostheses began to appear. A famous example is the iron hand of Götz von Berlichingen (Fig. 6.23) which is considered to be ahead of its time.

Today the domain of hand prostheses can be categorized into passive, body powered and myoelectric prostheses.
Passive prostheses are mainly worn for cosmetic aspects, while today having a very natural appearance and flexible skin their functionality is very limited.
Body powered hand prostheses allow the wearer to actively grasp and hold objects. They consist of a terminal device which is usually a two finger metal hook or a hand which has three three or five active fingers and has a silicon cover to look human-like.

A myoelectric prosthesis uses electromyography signals to acquire potentials from voluntarily contracted muscles from the limb of the person. The signals are evaluated by control electronic inside the prosthesis and used to

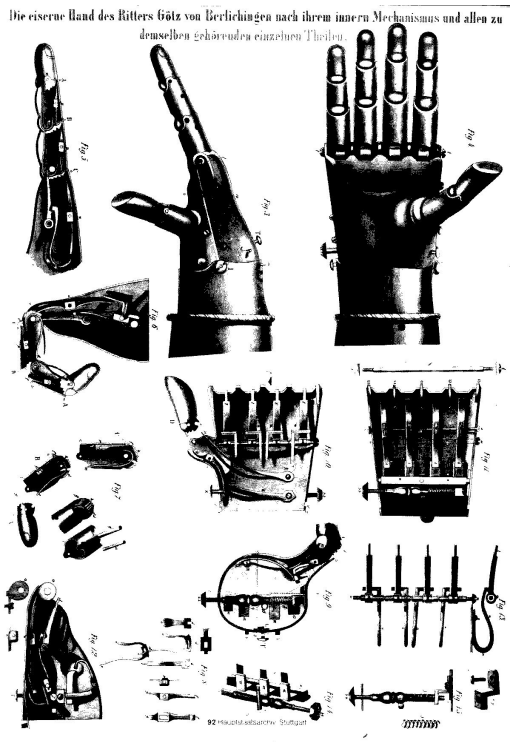

Figure 6.23: The iron hand of Götz von Berlichingen. The knight lost his right hand in the battle of Landshut in 1504. His replacement hand had, unusual for his time, individually bendable fingers with three joints, as well as a thumb with two joints and a bendable wrist. The fingers can be bended by the other hand and keep their position by a chain of springs and ratchets. It is equipped with multiple buttons which reset the finger positions. Image adapted from: [211]

control the movements of the prosthesis, which is equipped with electrical motors that actuate the joints. To execute a movement, the patient activates a certain muscle. To close or open the fingers, the patient uses pulsing on the muscles, repeatedly flexing the same muscle with a short time delay. Current state of the art myoelectric hands are the Michelangelo hand from Otto Bock [212] and the I-Limb ultra revolution from TouchBionics (Fig. 6.24).

Apart from the price (up to 30000$ for a myoelectric hand), an ongoing problem of hand prostheses is that of patient acceptance. An extensive survey conducted in 2007 reviews the prostheses acceptance studies done in the last 25 years [214]. Despite technological advances, the rejection rate is still high with mean rejection rates of up to 45% in pediatric and 26% in adults.

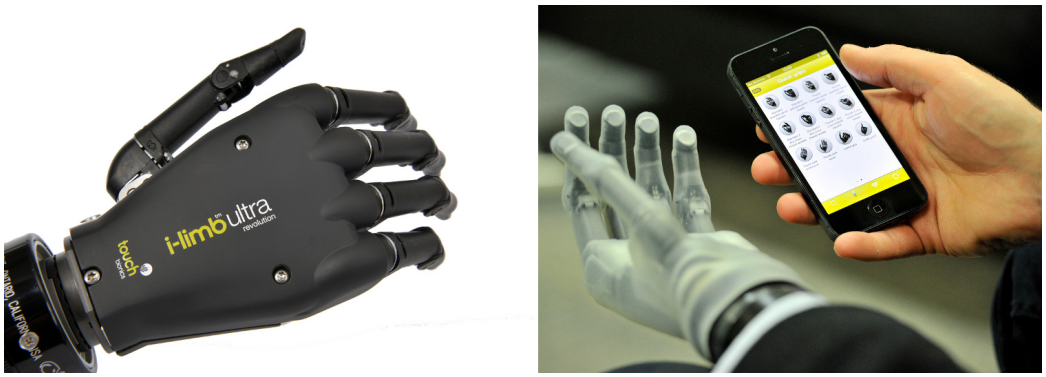

Figure 6.24: The I-Limb prosthesis hand from TouchBionics. It features 24 different postures, which can also be selected via a smartphone application (right). Image source: [213]

Rejection thereby means the patients choosing to wear their prosthesis very seldom or not at all.

For this there are many reasons cited, the main ones are lack of functionality, lack of control and wearing discomfort.

With this motivation, the more accurate control of finger forces for myoelectric devices was investigated using an experimental setup with *Myrmex* modules. The goal of Castellini and Kõiva is to predict the targeted finger force from the surface electromyography (sEMG) data.

As the traditional approach for myoelectric hand control is based on static hand posture classification, the number of predefined grip patterns is limited. If one could predict the flexion or force for each finger from the muscle data, a much more natural control would be possible.

To do so, an experiment was designed to collect sEMG data from the arm muscles and force data from the fingers. Twelve able bodied subjects took part in this experiment. To acquire the sEMG data, nine sEMG electrodes where attached to the subjects forearm. To acquire the force data, a 3x3 *Myrmex* sensor matrix (see Fig. 6.25) was employed.
The *Myrmex* setup was modified by adding a 3D printed attachment structure for a single iObject strip. This strip was added to record the thumb abduction, as the hand should be placed flat on the *Myrmex* sensors.

With this setup, both the finger flexion and thumb rotational force can be measured. For this the tactile sensors was calibrated with a 3 axis measurement table and equipped with the sensitive Polyurethan foam.

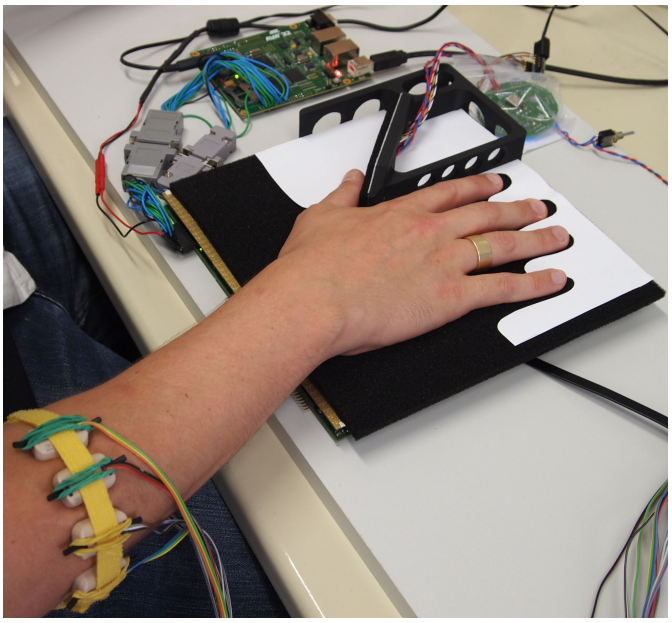

Figure 6.25: The experiment to acquire sEMG and finger force data. Subjects had electrodes attached to their muscles and placed their hand on a tactile table made with *Myrmex* modules. On a screen a training program is displayed which provides target force levels and also shows the sensor response of the *Myrmex* array. Image source: [208], ©2012 IEEE.

To develop a proper prediction of forces, multiple measurements of finger pressure and sEMG data are necessary. A training program was implemented to instruct the subjects to match a range of different target forces as indicated by the program.
This stimulus was presented in form of different bars for the fingers, where each bar denotes the target force level. The target force was indicated by both the height and color of the bar. The output of the *Myrmex* sensor was also shown on the screen, with the output color scheme matching that of the bars.

The sEMG data and the force values acquired from the tactile sensors were used to train multiple support vector machines (SVMs [215]). This technique has already been proved as effective in literature [216].

The results are encouraging: For single subjects, the prediction error can be lower then 2% for all fingers. In the multi subject analysis, that is using the combined data sets of all subjects, the results are nearly the same. When comparing the single finger to multi finger sets, the prediction error on the

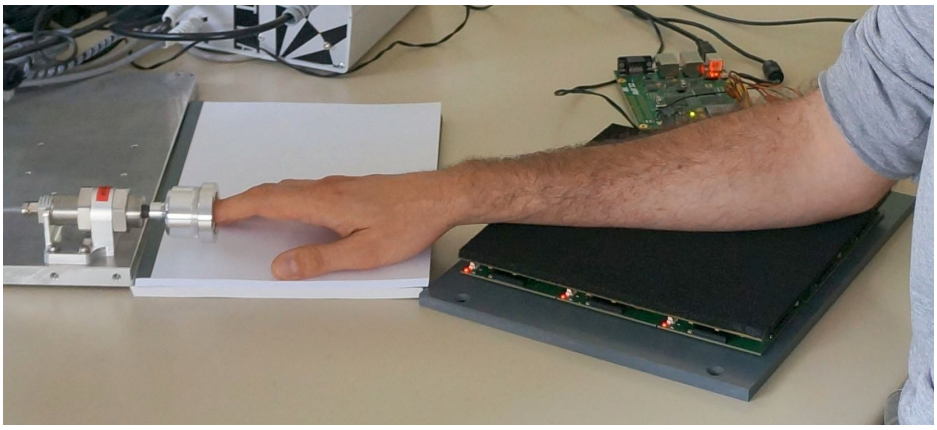

Figure 6.26: The experiment to develop a tactile based prosthesis control. This time the forearm is placed on the *Myrmex* table and the fingers are placed in a force sensing device. The tactile profile of the forearm (visible on the screen) is then correlated to the exerted finger force.

multi finger sets is about 3% higher.

Direct control using tactile data

In a closely related experiment, using the *Myrmex* sensor itself as input device for prosthesis control has been tested and published in [217,218]. In this work Castellini and Kõiva again used a 3x3 *Myrmex* sensor array to capture tactile images for the intention gathering of finger movements. The motivation is similar to the sEMG experiments, to find a good input method for the convenient control of hand prostheses.

Their hypothesis is that the physical contractions of the remaining muscles in the forearm can be sensed by a tactile sensor attached to the arm and correlated to the force that the fingers exert.
To test this, they designed an experiment where the tactile profile of the muscle acivity is recorded together with finger force data. For this they placed the arm of subjects on a 3x3 *Myrmex* array (see Fig. 6.26) and instructed them to apply various forces with their index finger.

The actual force exerted by the finger was recorded with the finger-force linear sensor (FFLS) presented in [125], which uses a radial dual strain gauge sensor. The finger had to press in four different directions (up,down,right,left) on the strain gauge sensor with four different force (1-4N) levels. Each combination was repeated five times. For each subject 80 tactile images were taken

with the *Myrmex* system (four directions, four magnitudes, five repetitions). Each image consists of 2304 tactels (48x48). As this is a very high dimensionality, a principal component analysis (PCA) was performed on the collected data, which showed that five principal components would account for 88% of the signal variance.

Their conclusion is that a simple classification system could use tactile data from the *Myrmex* system and determine the correct target direction and force.

6.3.2 Slip Detection

For artificial systems like robots, the manipulation of objects is an extraordinary difficult task, as the process is highly dynamic and there are many physical parameters influencing both the object and the manipulator. One very important part in manipulation is finding a stable grasp, so the object does not fall or slip out of hand.

Figure 6.27: Featuring slip detection and automatic grasp force adaption, humans are able to firmly hold objects even in very dynamic scenarios.

Along with the posture, the applied force is a very important parameter for proper grasping. Humans are very skilled at (automatically) adjusting their grasp force (Fig. 6.27). But this is not always the case: for humans it has

been shown that the control of grip force is very unstable until the age of two [219] and a large margin of safety against slippage is employed until the age of five [220]. Analog to this it has been found that older (>70 years) people make use of a strong grasp force [221]. This has been as explained as compensation for age-related changes in skin properties and the central nervous system that lead to a decline in tactile sensitivity.

But usually it is not advisable to grasp objects with the maximum possible force as it causes muscle fatigue and consumes more energy then necessary, which might may have been an influential factor during the biological evolution of hand and grasp control.
For our robot systems a slightly higher power consumption can be neglected in most cases, more important, however, is that a strong force can damage the object - as most robotic devices are typically able to exert high forces.
In humans the suitable balance of grip force is achieved through measurement of the frictional condition between the surface structure and the fingers [1]. Slippage of an object is detected through micro-vibrations, which occur when the object slides at microscopic distances and the contact alternates between stick and slip [6]. These vibrations are sensed by the various mechanoreceptors in the skin (as known from section 2.1).

This detection of slippage can occur consciously [222], but it also triggers an automatic adaption of grasp force [223] which ensures the object does not slip out of hand. Such an automatic response would also be very desirable for robot hands. As it is so desirable, there have already been multiple approaches to create artificial slip detection for robot fingers as we have shown in section 2.2.2.

However many of these sensors are only designed to record dynamic events. So for an more complete tactile sensation they would need to be combined with another static tactile sensor. In addition, for dextrous manipulation it is advantageous to not have only a single static force sensor, but an array of sensors (like the human finger which is equipped with a multitude of mechanoreceptors) so some spatial information about the contact situation can be evaluated. Currently most robot hands have densely integrated electronics, and including multiple tactile sensors is not possible in all designs.

With this motivation a slip detection method was realized using the *Myrmex* tactile sensor system. This slip detection method uses only the static force data from the sensor matrix and does not require any additional sensors. The method was developed by Schöpfer et. al in [224] and presented with additional results in [225], here we will present the most prominent points.

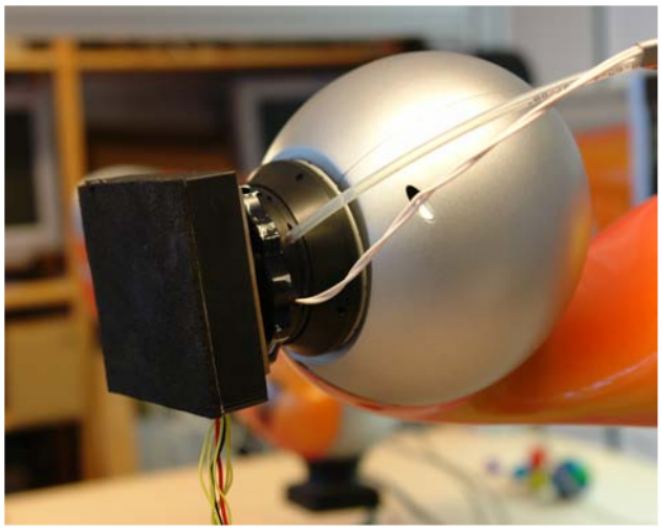

Figure 6.28: A *Myrmex* module mounted on the endeffector of a Kuka LWR arm. The module is enclosed in a 3D printed plastic case. The case contains small neodym magnets which stick to a metal mount attached to the Kuka arm.

To provide the hardware for the artificial slippage detection, a single *Myrmex* sensor module was mounted as end effector onto a Kuka robot arm to create a (big) tactile sensitive "finger" (Fig. 6.28).
To acquire ground truth data for slip / no slip conditions, different object surfaces were scrubbed with this finger and the sensor output was recorded during the process. Each object was sampled five times, at three different locations with two different forces. The resulting stream of tactile data was then processed with an one dimensional fast fourier transformation (FFT) to gain information about the frequency spectrum [226]. For the application of the FFT, the sensor output of each frame was averaged over all tactels.

This method highlighted significant differences in the frequency energies between slip and stick condition as shown in figure 6.29.
To realize an automatic method for detecting slip conditions, methods from machine learning, in particular a neural network were employed. Neural networks consist of computational elements (called nodes or neurons) that are connected via weights that typically are adapted during operation to improve performance [227].

The recorded data was arbitrarily divided into a training and a test set. For each set of parameters, five randomly initialized neural nets were trained and then tested.

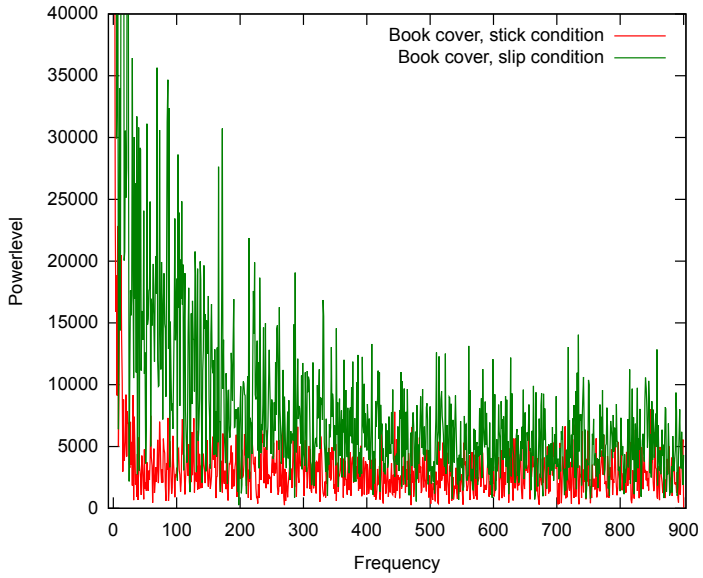

Figure 6.29: Comparison of power spectra for a book that is in slip or stick condition. The slip condition produces a spectrum that is visibly different from the stick condition. The data was recorded using a *Myrmex* module.

During the training it was found that more then 20 input neurons lead to over-fitting and that a larger window size improves the classification rate.

With the results from the slip detection network, an algorithm for automatic grasp force adaption was developed [225], which increases the grasp force on detection of slippage.

The functionality of this algorithm was demonstrated by a real world experiment: To let robot fingers grasp an object with minimum force and then dynamically increase its weight, which will result in slippage.
However if the grasp force adaption is functional, the contact force should be increased based on the output of the neural network and no slippage will be visible.

For this experiment two Kuka arms with two *Myrmex* modules were used. The object to be filled is a plastic cup as used for liquids, which is very lightweight (ca. 2g) and fragile thus it is not possible to use a strong starting grasp force.

The cup is filled rapidly with ca. 250g of small pebble stones, which is a multitude of the initial weight.
Without any grasp force adaption the increased weight would cause it to slip out of the fingers immediately.
But because of the developed grasp force adaption the cup is firmly held in place. The experiment was recorded on video [228], a typical scene is shown in figure 6.30.

Figure 6.30: Using the slip detection and grasp force adaption, two robot fingers equipped with *Myrmex* modules can master dynamic scenarios. They hold a plastic cup (2g weight) while it gets filled with 250g of small stones.

6.3.3 Tactile servoing control framework

In the previous section we have learned that the detection of slip and the subsequent grasp force adaptation is an important skill for humans, and we have presented a similar mechanism for robots using the *Myrmex* tactile sensors. This skill however is only one of many that can be realized using tactile feedback. Tactile feedback also has a prominent role in the manual exploration of objects by humans, as for finding and tracking characteristic surface structures. Cognitive psychology has investigated our abilities to haptically recognize objects. Passive perception was found to be inferior to active perception, where our hand acts as a freely moving effector that can capitalize on the resulting variation in sensory input.
Particular object features are determined by specific motion patterns that are called exploratory procedures (EP). An overview of different EPs is shown in Table 6.2.

Figure 6.31: Searching for the light switch in a dark room: The wall is scanned with slight tactile contact until the fingers detect the outline of the switch. Then the hand is positioned to align the fingers with the center of the switch to operate it.

Many of the exploratory procedures require a constant contact with the object while moving the hand. Such a scanning movement across the surface has also been proposed as a strategy to determine adequate grasp points for unknown objects using a robot hand [229], given that no object model or 3D vision information is available or accurate enough.
Consider the real life scenario depicted in figure 6.31. On entering a dark

room, we can navigate our hand towards the light switch. This is done by maintaining a slight tactile contact with the wall and scanning the surface for the appearance of the light switch. Done without visual feedback, this is an example of tactile servoing.

Table 6.2: Object knowledge and corresponding exploratory procedures (adapted from [230]).

Object knowledge	Exploratory procedure
Texture	Lateral motion
Hardness	Pressure
Temperature	Static contact
Weight	Unsupported holding
Volume	Enclosure, contour following
Global shape	Enclosure
Exact shape	Contour following

Tactile servoing is also partly involved in all other kinds of manipulation tasks, as the actual area of physical contact is often obstructed to vision.
This control strategy however is typically not implemented in the frameworks which are responsible for generating the movement of robots.
The earliest works that address the development of a tactile servoing framework are found in [231] and [232].
However they do not integrate classical end-effector servoing and lack a flexible set of controller primitives which can be used to realize multiple tasks with the same framework. To overcome this, a tactile servoing framework was developed with the *Myrmex* modules by Li et al. and presented in [233].

For this control framework, the goal is to control the contact position, contact force and the orientation of an object edge relative to the sensor array. The first challenge thereby is to extract the relevant features from the tactile images which generalize to this set of control tasks.

To extract these features from the tactile data, multiple methods were implemented. To acquire the contact position, a connected component analysis as known from image processing is used. This takes as input the binarized tactile image and outputs a list of regions, were the largest one is taken as the main contact position. For this region the overall contact force is computed by the sum of the forces within the contact region.

For the extraction of the orientation of a line-shaped contact two methods were compared, classic line detection using the hough transform [178] and image moment analysis [234], both methods are known well from computer vision.
The methods were tested with real world data acquired from a *Myrmex* module. The module was stimulated by a pen-like object in various angles and the data fed into the algorithms. It was found that the image moment method produced a lower error for the estimation of line angle then the hough method.

To control the robot end-effector, the control basis framework (CBF) [235, 236] is employed, a CBF implementation is responsible for the inverse kinematic calculations for the Kuka arms [237].
In the tactile servoing framework the error between the actual and desired tactile feature parameters is calculated. From this a sensor (end-effector) motion which aims to reduce this error is calculated which is fed to the CBF.

With the tactile features and the combined framework one can realize sliding and rolling motions along the contact point while maintaining a specified normal contact force.
This was demonstrated by using the *Myrmex* modules as fingertips mounted onto the Kuka lightweight robot arms.
With this setup tactile servoing tasks such as tracking point contacts, tracking object edges or exploring the shape of an unknown object were successfully executed.

The tactile servoing framework allows to combine motion targets (e.g. move the end effector on the X axis) and tactile targets (e.g. maintain a specific contact force, keep angle of contact constant). The experiment of successfully tracking an unknown cable was recorded on video [238], a typical scene is shown in figure 6.32, with the changes in contact force and position depicted in figure 6.33.
To track the cable, the Kuka is performing the task of moving the endeffector in the Y Axis, while the target for the line contact is to be at a 0° angle.
With this method the finger follows the cable along its curvature, figure 6.34 shows the resulting trajectory.

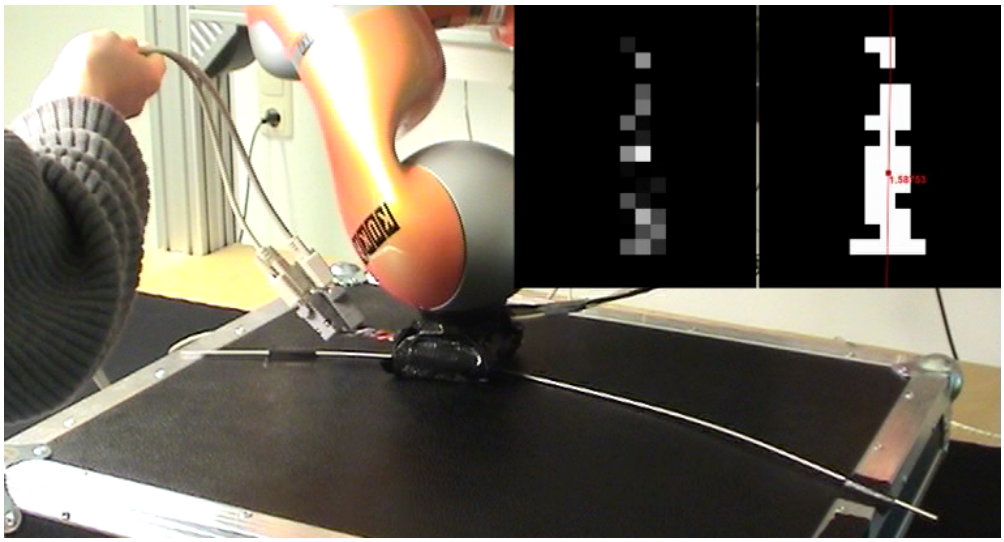

Figure 6.32: The Kuka robot can track an unknown cable using a *Myrmex* module and the tactile servoing framework. In the upper right one can see the original sensor output (left) and the processed one (right). The red line in the processed image shows the calculated angle of the line contact.

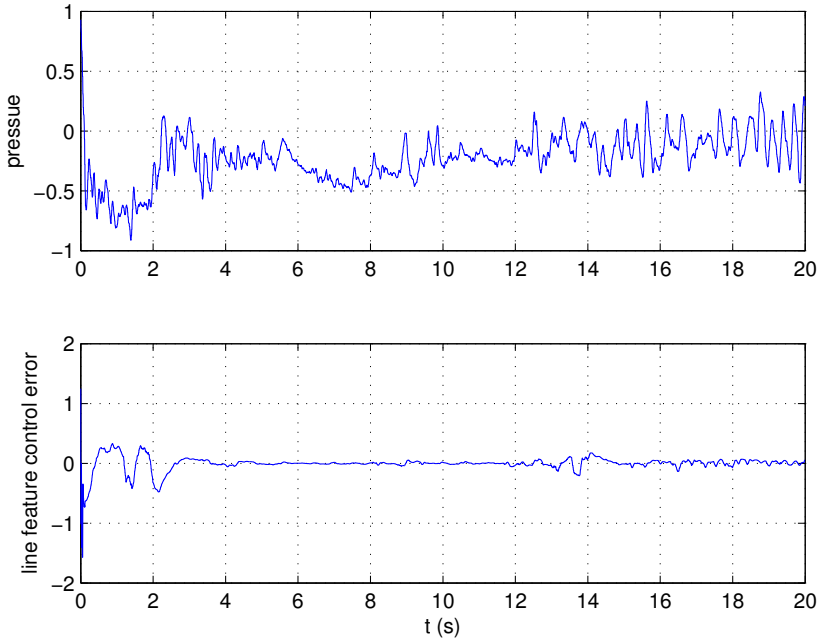

Figure 6.33: Data recorded during the line tracking experiment with the *Myrmex* gripper. Shown is the evolution of the contact pressure and the error in orientation angle. After some initial oscillations, the robot manages to align the tactile contact of the cable with its y-axis.

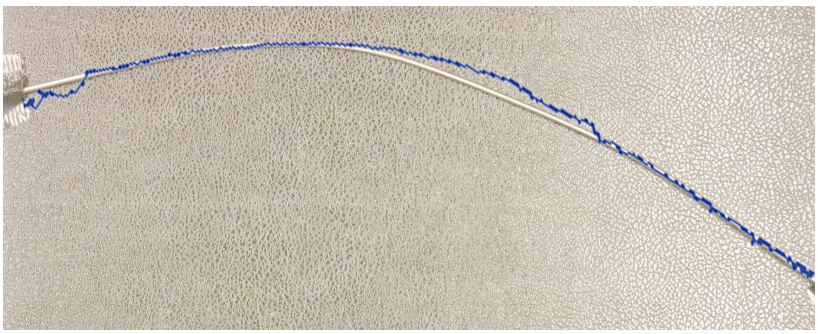

Figure 6.34: The tracking result (blue) superimposed on the actual cable. Despite a slight overshooting, the cable is tracked very accurately.

6.4 Summary

In this chapter we have presented a wide range of applications that have been realized with the *Myrmex* system, both by the present author and external users.
We have presented a first experiment to employ our tactile sensitive object, the tactile book which was used in a pick-and-place experiment. We have demonstrated how the tactile data can be processed to gain information about finger position, rotation and forces. We have highlighted differences and similarities between subjects and have also shown how the data from the integrated movement sensor can be used to augment the tactile data.

We have seen how the extraordinary high speed of the *Myrmex* system enabled the development of a slip detection algorithm. Using a *Myrmex* module as a gripper, this could be demonstrated by using automatic grasp force adaption to hold a cup that gets filled with pebbles.
The *Myrmex* sensor as end effector has been further utilized in the development of a tactile servoing framework, which allows the tracking of surface features and object exploration. This was demonstrated in an experiment where a cable is tracked with constant contact only using information from the *Myrmex* sensor. This was made possible by the high sensitivity and good spatial resolution of the *Myrmex* system.

Tactile tables in different dimensions made out of *Myrmex* modules have been proven to be useful for various applications. One is to integrate the tactile table into an intelligent home, where it can provide feedback about the table usage of users. In future scenarios the information from our algorithm for cup rotation detection may be used in an interactive scenario between human and robot.

A different field was explored with the introduction of virtual clay which can be manipulated through a *Myrmex* sensor array by the fingers of the user. We have presented different scenarios involving the virtual clay, with the motivation that these could be helpful in the retraining of finger skills by patients with neurological damage. The idea of using a virtual object in therapy blends in with existing projects that train arm movements using virtual scenes.

A tactile sensitive surface made out of *Myrmex* modules has also been used to acquire ground truth data for prosthesis control. Along this application we also presented first and promising experiments to directly use tactile data for the control of prostheses.

Chapter

7

Conclusion

Conclusion

In this work we have presented a high speed sensor system for tactile interaction research - the *Myrmex* system. In the beginning we motivated our work with three different tactile interaction scenarios that could not be realized with a single sensor system. We have also listed the requirements that our new system should have to fulfill them. We have now seen that our system matches these criteria and also surpasses them in many points, as in the high frame rate or sensitivity to low forces that we achieve.

We have presented our design decisions and implementation strategies that made a sensor system possible which combines features previously only found in separate specialized tactile sensors. Our sensor system is fast enough to be used as a tactile gripper for slip detection, and the granularity of the system allows for a module to get mounted onto a robot arm and conveniently grasp everyday objects.

We realized the high speed through the development of a high speed data acquisition and transmission scheme. We have shown in detail how this is achieved by parallelization of tasks where ever possible.

Due to its modularity our system can also be used to create large tactile surfaces, like a tactile table. We have shown that it is possible to connect multiple modules to create large areas with thousands of tactels, and at the same our system is capable to deliver frame rates which are more then sufficient for real time operation.

The modularity of our system does not increase its complexity for the user, as we have developed an intelligent auto-configuration mechanism that presents a 'ready-to-use' system to the user. This was achieved by developing a new master slave bus, which allows for the localization of the participants through an auto discovery algorithm.

A novel tactile sensitive object for the study of human finger forces was constructed by us using the *Myrmex* sensor modules. While previous tactile objects come in round shapes, we have realized a rectangular 'tactile book' that is inspired by every day objects. The tactile sensing capabilities of this book are augmented by additional motion sensors. The tactile book offers a cable-less operation mode which allows for free movements in all directions during an experiment. Normally this is done with a wireless connection to transfer the data, but such a connection is subject to environmental influences that negatively impact the rate of data transmission. We have overcome this problem by developing a low latency on board storage that allows to capture data at a constant rate. As in some experiments a synchronization to external devices is necessary we also implemented a low latency method for synchronization.

The high sensitivity of the sensor design was achieved by advancing the state of the art of resistive tactile sensor design by investigating different sensor shapes in regard to sensitivity. With the results of these experiments we created a sensor cell design that is optimized for the usage with conductive foams. The results could also be transferred to the design of a tactile fingertip [102] which is based on similar technology.

The response of our sensor system to force/pressure was thoroughly characterized with regard to hysteresis, sensitivity and drift/stability with different materials. We found that the sensor experiences hysteresis as well as spatial and temporal drift depending on the material used as conductive elastomer. To weaken these effects, we have proposed an algorithm for the continuous auto-equibrilation of tactile sensor arrays that can be used with the *Myrmex* system.

Finally we employed the *Myrmex* system successfully in multiple scenarios of tactile interaction research. We have presented the scenarios designed and realized by the author of this work. These scenarios include the investigating of human grasp force control during a pick and place task, a tactile table for integration into an intelligent household and a tactile table for the manipulation of virtual clay as a form of finger training.

We have also presented a selection of scenarios where the *Myrmex* system was used by other researchers. The positive results from all the scenarios support our conclusion that the developed *Myrmex* system is a valuable and reliable tool for the research of tactile interaction.

Outlook

The *Myrmex* system with its many features also offers potential for future enhancements.
Through the high speed of our system it was possible for researchers to develop a slip detection algorithm based on frequency analysis. And as the high sampling rate applies for every individual sensor cell, it might be even possible to extend the slip detection algorithm to detect slippage in separate areas of the same sensor module.

Our sensor system is limited to cover planar surfaces only by the current hardware implementation, our modular high speed design and the *Myrmex* bus which allows the discovery of module structures could also be transferred to designs which use non rigid sensors.
The sensor response was tested in this work with several different cover materials which more or less suffered from spatial or temporal inconsistencies. If a material would be found that is more reliable in this regard, the calibration of the *Myrmex* sensor output would be easier and the data that the *Myrmex* system delivers to researchers would be even more valuable.

We developed an autoequilibration algorithm which might be interesting for further investigation. The strategies used to find homogenous regions and to create the conversion functions might leave room for optimization in regard to the sensor behavior with different materials or over longer time periods.
The hardware used in the *Myrmex* system is currently state of the art, but in the future it is likely that better components are available. A reimplementation of the system with future components like faster micro-controllers or ADCs could increase the system speed even more.

And finally the point where we see the most potential is that of actual usage scenarios. We have presented multiple scenarios from different directions, but we believe that there are still a lot of untouched and exciting tactile interaction scenarios that a creative researcher can realize with the *Myrmex*

system.

We think that our *Myrmex* system and the applications that can be realized with it will advance the state of the art of tactile interaction research and can ultimately improve the lives of many people.
We have already shown the application scenario of the prosthesis control using tactile data. In the future it might be possible to develop a prosthesis that is controlled through tactile sensors. This can improve the level of control for prostheses and allow for more complex multi-finger movements. Such a more intuitive and responsive control could also increase the rate of acceptance for prostheses.

The *Myrmex* system might also prove to be a good training tool for rehabilitation patients, we have shown that virtual scenes are already successfully used for the training of arm movements, and we propose that similar results could be achieved with our virtual clay scenario for finger training.
Also in the everyday live in our (hopefully not so distant) future we may encounter tactile kitchen tables as part of an intelligent household.
We might also live with household robots that can safely handle a slippy glass or perform complex manual interactions, relying on insights that were gained with help of our *Myrmex* system.

Appendix

A

Data structures

Table A.1: Commands used in the configuration mode by the central unit

Name	Byte	Description
COM_DISCOVER	0xFB	Discover command
SET_RANK	0x0C	Set module ID
GET_CONN	0x0E	Request active connection direction
SET_CONN	0x0F	Set active connection for full transmit mode
SWITCH_FULL	0x0D	Switch to full transmit mode
SET_COMPRESSION	0x10	Set compression level
SET_SPEED	0x11	Set speed divider
ENABLE_GATE	0xC0	Enable connection at given direction
DISABLE_GATE	0x80	Disable connection at given direction

Table A.2: Answers used in the configuration mode by the module

Name	Byte	Description
COM_DISCOVER_ANSWER	0x0B	Discover answer
CONNECTION_WEST	0x00	Connection found west
CONNECTION_EAST	0x01	Connection found east
CONNECTION_SOUTH	0x02	Connection found south
CONNECTION_NORTH	0x03	Connection found north

Table A.3: IR configuration packets sent by the host to the tactile book

Index:	0	1	2	3	4	5	6	7	Description
Byte:	S	T	A	R	B	B	B	X	Set start time
	S	T	O	P	B	B	B	X	Set stop time

All bytes are ASCII characters except B=Raw Byte, X=CRC8

Table A.4: IR configuration answers sent by the tactile book to the host

Index:	0	1	2	3	Description
Byte:	O	K	A	Y	Acknowledge of start time
	D	O	N	E	Acknowledge of record duration

All bytes are ASCII characters.

Bibliography

[1] G. Westling and R. S. Johansson, "Factors influencing the force control during precision grip." *Experimental brain research. Experimentelle Hirnforschung. Expérimentation cérébrale*, vol. 53, no. 2, pp. 277–84, Jan. 1984.

[2] J. Monzée, Y. Lamarre, and A. M. Smith, "The effects of digital anesthesia on force control using a precision grip." *Journal of neurophysiology*, vol. 89, no. 2, pp. 672–83, Feb. 2003.

[3] H. R. Nicholls and M. H. Lee, "A Survey of Robot Tactile Sensing Technology," *International Journal of Robotics Research*, vol. 8, no. 3, pp. 3–30, 1989.

[4] M. Lee and H. Nicholls, "Review Article Tactile sensing for mechatronics—a state of the art survey," *Mechatronics - The Science of Intelligent Machines*, vol. 9, no. 1, pp. 1–31, Feb. 1999.

[5] M. R. Cutkosky, R. D. Howe, and W. R. Provancher, "Force and Tactile Sensors," in *Handbook of Robotics*. Springer Berlin Heidelberg, 2008, ch. 20, pp. 455–476.

[6] R. S. Johansson, U. Landstrom, and R. Lundstrom, "Responses of Mechanoreceptive Afferent Units in the Glabrous Skin of the Human Hand to Sinusoidal Skin Displacements," *Brain Research*, vol. 244, pp. 17–25, 1982.

[7] M. R. Cutkosky and J. M. Hyde, "Manipulation Control with Dynamic Tactile Sensing," in *International Symposium on Robotics Research*, Hidden Valley, Pennsylvania, 1993.

[8] J. Dargahi and S. Najarian, "Human tactile perception as a standard for artificial tactile sensing - a review," *International Journal of Medical Robotics and Computer Assisted Surgery*, vol. 01, no. 01, pp. 23–35, 2004.

[9] C. Schürmann, "Entwicklung eines modularen und intelligenten Taktilsensorsystems mit Standard Imaging Interface zur Hochgeschwindigkeitsbild ubermittlung," Bielefeld, 2008.

[10] Wikipedia, "Schematic: Ion channel stretch model," 2013. [Online]. Available: http://en.wikipedia.org/wiki/File:Stretch_model,.jpg

[11] Rocky Mountain Laboratories NIAID NIH, "Photo: Escherichia Coli," 2013. [Online]. Available: http://de.wikipedia.org/w/index.php?title=Datei:EscherichiaColi_NIAID.jpg

[12] A. Kloda and B. Martinac, "Common evolutionary origins of mechanosensitive ion channels in Archaea, Bacteria and cell-walled Eukarya." *Archaea (Vancouver, B.C.)*, vol. 1, no. 1, pp. 35–44, Mar. 2002.

[13] A. Anishkin and C. Kung, "Microbial mechanosensation." *Current opinion in neurobiology*, vol. 15, no. 4, pp. 397–405, Aug. 2005.

[14] C. Kung, "A possible unifying principle for mechanosensation." *Nature*, vol. 436, no. 7051, pp. 647–54, Aug. 2005.

[15] P. G. Gillespie and R. G. Walker, "Molecular basis of mechanosensory transduction." *Nature*, vol. 413, no. 6852, pp. 194–202, Sep. 2001.

[16] M. B. Goodman and E. M. Schwarz, "Transducing touch in Caenorhabditis elegans." *Annual review of physiology*, vol. 65, pp. 429–52, Jan. 2003.

[17] J. Braam, "In touch: plant responses to mechanical stimuli." *The New phytologist*, vol. 165, no. 2, pp. 373–89, Feb. 2005.

[18] R. D. Allen, "Mechanism of the Seismonastic Reaction in Mimosa pudica." *Plant physiology*, vol. 44, no. 8, pp. 1101–7, Aug. 1969.

[19] Wikipedia, "Photo: Mimosa Pudica," 2013. [Online]. Available: http://en.wikipedia.org/wiki/File:Mimosa_Pudica.gif

[20] T. Visnovitz, I. Világi, P. Varró, and Z. Kristóf, "Mechanoreceptor Cells on the Tertiary Pulvini of Mimosa pudica L." *Plant signaling & behavior*, vol. 2, no. 6, pp. 462–6, Nov. 2007.

[21] C. Darwin, *The power of movement in plants.*, 1880, Ed. London: William Clowes and Sons.

[22] G. D. Massa and S. Gilroy, "Touch modulates gravity sensing to regulate the growth of primary roots of Arabidopsis thaliana." *The Plant journal : for cell and molecular biology*, vol. 33, no. 3, pp. 435–45, Feb. 2003.

[23] A. Duggan, J. García-Añoveros, and D. P. Corey, "Insect mechanoreception: what a long, strange TRP it's been." *Current biology : CB*, vol. 10, no. 10, pp. R384–7, May 2000.

[24] C. S. Sherrington, "Reflexes elicitable in the cat from pinna vibrissae and jaws," *Journal of Physiology*, vol. 51, no. 6, pp. 404–431, 1917.

[25] A. S. Ahl, "The role of vibrissae in behavior: a status review." *Veterinary research communications*, vol. 10, no. 4, pp. 245–68, Jul. 1986.

[26] Emelie Schäfer, "Photo: Cat whiskers," 2013. [Online]. Available: http://en.wikipedia.org/wiki/File:Cats_whiskers.jpg

[27] M. J. Z. Hartmann, "A night in the life of a rat: vibrissal mechanics and tactile exploration." *Annals of the New York Academy of Sciences*, vol. 1225, pp. 110–8, Apr. 2011.

[28] C. Y. McLean, P. L. Reno, A. A. Pollen, A. I. Bassan, T. D. Capellini, C. Guenther, V. B. Indjeian, X. Lim, D. B. Menke, B. T. Schaar, A. M. Wenger, G. Bejerano, and D. M. Kingsley, "Human-specific loss of regulatory DNA and the evolution of human-specific traits." *Nature*, vol. 471, no. 7337, pp. 216–9, Mar. 2011.

[29] Z. Halata, "Sensory innervation of the hairy skin (light- and electron-microscopic study." *The Journal of investigative dermatology*, vol. 101, no. 1 Suppl, pp. 75S–81S, Jul. 1993.

[30] W. Montagna, "The Evolution of Human Skin," pp. 3–22, 1985.

[31] P. E. Wheeler, "The influence of the loss of functional body hair on the water budgets of early hominids thermal," *Journal of Human Evolution*, vol. 23, pp. 379–388, 1992.

[32] K. O. Johnson, "The roles and functions of cutaneous mechanoreceptors." *Current opinion in neurobiology*, vol. 11, no. 4, pp. 455–61, Aug. 2001.

[33] W. Hamann, "Mammalian cutaneous mechanoreceptors." *Progress in biophysics and molecular biology*, vol. 64, no. 1, pp. 81–104, Jan. 1995.

[34] R. S. Johansson and A. Vallbo, "Tactile sensibility in the human hand: relative and absolute densities of four types of mechanoreceptive units in glabrous skin," *Journal of Physiology*, vol. 286, pp. 283–300, 1979.

[35] S. Bensmaia and L. Manfredi, "The Sense of Touch," in *Encyclopedia of Human Behavior*, 2nd ed. Elsevier Inc., 2012, vol. 1, pp. 379–386.

[36] R. J. Nelson, Ed., *The Somatosensory System*. CRC Press, 2002.

[37] J. H. Kaas, "Evolution of somatosensory and motor cortex in primates." *The anatomical record. Part A, Discoveries in molecular, cellular, and evolutionary biology*, vol. 281, no. 1, pp. 1148–56, Nov. 2004.

[38] P. B. Brown, H. R. Koerber, and R. Millecchia, "From innervation density to tactile acuity: 1. Spatial representation." *Brain research*, vol. 1011, no. 1, pp. 14–32, Jun. 2004.

[39] R. O. Duncan and G. M. Boynton, "Tactile hyperacuity thresholds correlate with finger maps in primary somatosensory cortex (S1)." *Cerebral cortex (New York, N.Y. : 1991)*, vol. 17, no. 12, pp. 2878–91, Dec. 2007.

[40] J. R. Ponsford, "Tactile spatial resolution in blind braille readers." *Neurology*, vol. 55, no. 10, p. 1597, Nov. 2000.

[41] K. Sathian, "Practice makes perfect: Sharper tactile perception in the blind," *Journal of Neurology*, vol. 54, no. 12, pp. 2203–2204, 2000.

[42] H. Manning and F. Tremblay, "Age differences in tactile pattern recognition at the fingertip." *Somatosensory & motor research*, vol. 23, no. 3-4, pp. 147–55, 2006.

[43] F. Vega-Bermudez and K. O. Johnson, "Fingertip skin conformance accounts, in part, for differences in tactile spatial acuity in young subjects, but not for the decline in spatial acuity with aging." *Perception & psychophysics*, vol. 66, no. 1, pp. 60–7, Jan. 2004.

[44] B. G. Green, S. J. Lederman, and J. C. Stevens, "The Effect of Skin Temperature on the Perception of Roughness," *Sensory Processes1*, vol. 3, pp. 327–333, 1979.

[45] J. C. Stevens, "Temperature can sharpen tactile acuity." *Perception & psychophysics*, vol. 31, no. 6, pp. 577–80, Jun. 1982.

[46] A. Serino, S. Padiglioni, P. Haggard, and E. Làdavas, "Seeing the hand boosts feeling on the cheek." *Cortex; a journal devoted to the study of the nervous system and behavior*, vol. 45, no. 5, pp. 602–9, May 2009.

[47] B. G. Green, "Localization of thermal sensation: An illusion and synthetic heat," *Perception & Psychophysics*, vol. 22, no. 4, pp. 331–337, Jul. 1977.

[48] S. J. Lederman, "Skin and touch," in *Encyclopedia of human biology*, 2nd ed. Academic Press, 1997.

[49] F. Lacruz, J. Artieda, M. A. Pastor, and J. A. Obeso, "The anatomical basis of somaesthetic temporal discrimination in humans," *Journal of Neurology, Neurosurgery and Psychiarty*, vol. 54, pp. 1077–1081, 1991.

[50] S. Axelrod, L. W. Thompson, and L. D. Cohen, "Effects of senescence on the temporal resolution of somesthetic stimuli presented to one hand or both." *Journal of gerontology*, vol. 23, no. 2, pp. 191–5, Apr. 1968.

[51] D. Fucci and L. Petrosino, "Cuntaneous temporal resolution values for sophisicated and naive subjects," *Perceptual and Motor Skills*, vol. 58, pp. 831–834, 1984.

[52] M. Hoshiyama, R. Kakigi, and Y. Tamura, "Temporal discrimination threshold on various parts of the body." *Muscle & nerve*, vol. 29, no. 2, pp. 243–7, Feb. 2004.

[53] D. I. Shore, E. Spry, and C. Spence, "Confusing the mind by crossing the hands." *Brain research. Cognitive brain research*, vol. 14, no. 1, pp. 153–63, Jun. 2002.

[54] K. Inui, X. Wang, Y. Tamura, Y. Kaneoke, and R. Kakigi, "Serial processing in the human somatosensory system." *Cerebral cortex (New York, N.Y. : 1991)*, vol. 14, no. 8, pp. 851–7, Aug. 2004.

[55] D. Jung and A. Zelinsky, "Whisker based mobile robot navigation," *Proceedings of IEEE/RSJ International Conference on Intelligent Robots and Systems. IROS '96*, vol. 2, pp. 497–504, 1996.

[56] M. Lungarella, V. Hafner, R. Pfeifer, and H. Yokoi, "An artificial whisker sensor for robotics," in *IEEE/RSJ International Conference on Intelligent Robots and System*, no. October. IEEE, 2002, pp. 2931–2936.

[57] R. Russell, "Using tactile whiskers to measure surface contours," in *Proceedings 1992 IEEE International Conference on Robotics and Automation*. IEEE Comput. Soc. Press, pp. 1295–1299.

[58] M. Fend, S. Bovet, and R. Pfeifer, "On the influence of morphology of tactile sensors for behavior and control," *Robotics and Autonomous Systems*, vol. 54, no. 8, pp. 686–695, Aug. 2006.

[59] D. Kim and R. Möller, "Biomimetic whiskers for shape recognition," *Robotics and Autonomous Systems*, vol. 55, no. 3, pp. 229–243, Mar. 2007.

[60] A. E. Schultz, J. H. Solomon, M. A. Peshkin, and M. J. Hartmann, "Multifunctional Whisker Arrays for Distance Detection , Terrain Mapping , and Object Feature Extraction," in *Proceedings of the 2005 IEEE International Conference on Robotics and Automation*, no. April, 2005, pp. 2588–2593.

[61] S. Wang and P. Will, "Sensors for computer controlled mechanical assembly," *Industrial Robot: An International Journal*, vol. 5, no. 1, pp. 9–18, 1978.

[62] Wikipedia, "Schematic: Strain gauge," 2013. [Online]. Available: http://en.wikipedia.org/wiki/File:StrainGaugeVisualization.svg

[63] Interlink Technologies, "FSR 402 Data Sheet," Tech. Rep., 2013. [Online]. Available: http://www.interlinkelectronics.com/FSR402short.php

[64] Tekscan, "Tekscan Product Page." [Online]. Available: http://www.tekscan.com/products

[65] ——, "Sensor with a plurality of sensor elements arranged with respect to a substrate Patent," 2005.

[66] ——, "Tekscan Sensor Technology Website." [Online]. Available: http://www.tekscan.com/sensor-technology

[67] ——, "Control circuit for sensor array and related methods Patent," 2006. [Online]. Available: http://patents.justia.com/patent/20070235231

[68] N. Elkmann, M. Fritzsche, and E. Schulenburg, "Tactile Sensing for Safe Physical Human-Robot Interaction."

[69] M. Fritzsche and N. Elkmann, "A tactile sensor for collision detection and human robot interaction on complexly-shaped industrial robots."

[70] H. Alirezaei, A. Nagakubo, and Y. Kuniyoshi, "A highly stretchable tactile distribution sensor for smooth surfaced humanoids," *2007 7th IEEE-RAS International Conference on Humanoid Robots*, pp. 167–173, Nov. 2007.

[71] E. Somersalo, M. Cheney, and D. Isaacson, "Existence and Uniqueness for Electrode Models for Electric Current Computed Tomography," *SIAM Journal on Applied Mathematics*, vol. 52, no. 4, pp. 1023–1040, Aug. 1992.

[72] Y. Ohmura, Y. Kuniyoshi, and A. Nagakubo, "Conformable and scalable tactile sensor skin for curved surfaces," *Proceedings 2006 IEEE International Conference on Robotics and Automation, 2006. ICRA 2006.*, no. May, pp. 1348–1353, 2006.

[73] J. Rebman and K. A. Morris, "A Tactile Sensor With Electrooptical Transduction," D. P. Casasent and E. L. Hall, Eds., Feb. 1984, pp. 210–216.

[74] G. Hellard and R. A. Russell, "A Tactile Sensor Array that also Grasps Objects," in *Australasian Conference on Robotics and Automation*. Intelligent Robotics Research Centre Monash University, 2006, pp. 1–6.

[75] NXP Semiconductors, "UM10204 I2C-bus specification and user manual," 2012.

[76] OSRAM, "SFH 7221 Datasheet," pp. 1–16, 2012.

[77] P. Mittendorfer and G. Cheng, "Humanoid Multimodal Tactile-Sensing Modules," *IEEE Transactions on Robotics*, vol. 27, no. 3, pp. 401–410, Jun. 2011.

[78] JUMO, "JUMO PCS Temperature sensitive resistors," pp. 13–15, 2003. [Online]. Available: www.jumo.net

[79] Bosch, "Bosch BMA150 Acceleration Sensor Datasheet," 2008.

[80] Sharp, "Sharp GP2S60 Distance Sensor Datasheet," pp. 1–15.

[81] G. Cannata, M. Maggiali, G. Metta, and G. Sandini, "An embedded artificial skin for humanoid robots," *2008 IEEE International Conference on Multisensor Fusion and Integration for Intelligent Systems*, pp. 434–438, Aug. 2008.

[82] M. Maggiali, G. Cannata, P. Maiolino, G. Metta, M. Randazzo, and G. Sandini, "Embedded Distributed Capacitive Tactile Sensor," in *Mechantronics*, no. 039, 2008, pp. 1–5.

[83] Analog Devices, "AD7147 AN925 application note," Tech. Rep., 2011.

[84] Microchip, "Overview and Use of the PICmicro Serial Peripheral Interface (SPI)," Tech. Rep., 2013.

[85] iCub Project, "iCub Artifical skin flyer," 2013.

[86] J. C. Sullivan, B. Mitchinson, M. J. Pearson, M. Evans, N. F. Lepora, C. W. Fox, C. Melhuish, and T. J. Prescott, "Tactile Discrimination Using Active Whisker Sensors," *IEEE Sensors Journal*, vol. 12, no. 2, pp. 350–362, Feb. 2012.

[87] G. Carvell and D. Simons, "Biometric analyses of vibrissal tactile discrimination in the rat," *Journal of neurosciene*, vol. 10, no. August, 1990.

[88] K. Weiss, "Weiss Robotics DSAMOD-6," 2013. [Online]. Available: http://www.weiss-robotics.de/en/tactile-sensing/tactile-sensors/tactile-sensor-dsamod-6.html

[89] D. Göger, K. Weiß, C. Burghart, and H. Wörn, "Sensitive skin for a humanoid robot," Karlsruhe, 2009.

[90] O. Kerpa, K. Weiss, and H. Worn, "Development of a flexible tactile sensor system for a humanoid robot," *Proceedings 2003 IEEE/RSJ International Conference on Intelligent Robots and Systems (IROS 2003) (Cat. No.03CH37453)*, vol. 1, pp. 1–6.

[91] Atmel, "Atmel NGW100." [Online]. Available: http://www.atmel.com/tools/MATURENGW100NETWORKGATEWAYKIT.aspx

[92] K. Weiss, "Weiss Robotics DSA100 Datasheet." [Online]. Available: www.weiss-robotics.de

[93] Paolo Dario and D. D. Rossi, "Tactile sensors and the gripping challenge," *IEEE Spectrum Advanced Technology & Automation*, pp. 46–53, 1985.

[94] A. Barnea, C. Oprisan, and D. Olaru, "Force sensitive resistors calibration for use in gripping devices," *Mechanical Testing and Diagnosis*, vol. 3, no. Ii, pp. 18–27, 2012.

[95] F. Fuma and J. Bradley, "A Procedure for Characterizing Tactile Sensors," University of Pennsylvania, Tech. Rep., 1988.

[96] A. Koutsou, "Object Exploration Using a Parallel Jaw Gripper," University of Pennsylvania, Tech. Rep., 1988.

[97] D. Castro, L. Marques, U. Nunes, and A. de Almeida, "Tactile force control feedback in a parallel jaw gripper," in *ISIE '97 Proceeding of the IEEE International Symposium on Industrial Electronics*. IEEE, pp. 884–888.

[98] N. Wettels, D. Popovic, V. J. Santos, R. S. Johansson, and G. E. Loeb, "Biomimetic Tactile Sensor for Control of Grip," in *International Conference on Rehabilitation Robotics*, no. c, Jun. 2007, pp. 923–932.

[99] Syntouch, "BioTac Homepage." [Online]. Available: http://www.syntouchllc.com

[100] J. Fishel, G. Lin, G. Loeb, and Syntouch, "BioTac ® Product Manual," Tech. Rep., 2013.

[101] A. Schmitz, U. Pattacini, F. Nori, L. Natale, G. Metta, and G. Sandini, "Design, realization and sensorization of the dexterous iCub hand," in *2010 10th IEEE-RAS International Conference on Humanoid Robots*. IEEE, Dec. 2010, pp. 186–191.

[102] R. Kõiva, M. Zenker, C. Schürmann, R. Haschke, and H. Ritter, "A highly sensitive 3D-shaped tactile sensor," in *IEEE/ASME International Conference on Advanced Intelligent Mechatronics*, Wollongong, Australia, 2013.

[103] Shadow Robot Company, "Shadow Dexterous Hand." [Online]. Available: http://www.shadowrobot.com/products/dexterous-hand/

[104] LPKF, "LPKF LDS Webpage," 2013. [Online]. Available: http://www.lpkf.de/anwendungen/mid/index.htm

[105] M. T. Francomano, D. Accoto, and E. Guglielmelli, "Experimental characterization of a flexible thermal slip sensor." *Sensors (Basel, Switzerland)*, vol. 12, no. 11, pp. 15 267–80, Jan. 2012.

[106] R. Howe and M. Cutkosky, "Sensing skin acceleration for slip and texture perception," *Proceedings, 1989 International Conference on Robotics and Automation*, pp. 145–150, 1989.

[107] I. Fujimoto, Y. Yamada, T. Morizono, Y. Umetani, and T. Maeno, "Development of artificial finger skin to detect incipient slip for realization of static friction sensation," in *Proceedings of IEEE International Conference on Multisensor Fusion and Integration for Intelligent Systems, MFI2003.* IEEE, 2003, pp. 15–20.

[108] C.-H. Chuang, C.-T. Lu, and T.-H. Fang, "Slippage and direction sensing based on a flexible tactile sensor with structural electrodes," *2009 IEEE Sensors*, pp. 958–962, Oct. 2009.

[109] M.R.Davis and T. Ellis, "The Rand tablet: a man-machine graphical communication device," RAND corporation, Santa Monica, Tech. Rep., 1964.

[110] Yamanami, Funahashi, and Senda, "Wacom Tablet Patent," 1989.

[111] A. Sniderman, "Pressure-sensitive writing stylus Patent," 1978.

[112] M. Padula and H. Matthews, "Digitizer Stylus with pressure transducer Patent," 1988.

[113] E. Johnson, "Touch Display a novel input/output device for computers," *Electronics Letters*, vol. 1, no. 8, pp. 219–220, 1965.

[114] S. G. Smith and B. A. Sherwood, "Educational Uses of the PLATO Computer System," *Science*, vol. 192, pp. 344–352, 1974.

[115] J. Stifle, "The Plato IV Architecture," University of illinois, Tech. Rep., 1972.

[116] J. Schöning, P. Brandl, F. Daiber, F. Echtler, O. Hilliges, J. Hook, M. Löchtefeld, N. Motamedi, L. Muller, P. Olivier, T. Roth, and U. V. Zadow, "Multi-Touch Surfaces : A Technical Guide," Tech. Rep., 2008.

[117] R. Downs, "Using resistive touch screens for human / machine interface," Texas Instruments, Tech. Rep., 2005.

[118] J. Y. Han, "Low-cost multi-touch sensing through frustrated total internal reflection," in *Proceedings of the 18th annual ACM symposium on User interface software and technology - UIST '05.* New York, New York, USA: ACM Press, 2005, p. 115.

[119] R. Chang, F. Wang, and P. You, "A Survey on the Development of Multi-touch Technology," *2010 Asia-Pacific Conference on Wearable Computing Systems*, pp. 363–366, 2010.

[120] Microsoft, "PixelSense Homepage." [Online]. Available: http://www.microsoft.com/en-us/pixelsense/whatissurface.aspx

[121] Circle Twelve, "Diamondtouch homepage." [Online]. Available: http://circletwelve.com/

[122] G. Gerpheide, "Methods and apparatus for data input Patent," 1994.

[123] M. D. Layton and D. J. Lee, "Expanded electrode grid of a capacitance sensistive touchpad by using demultiplexing of signals and the grid as controlled by binary patterns from a touch sensor circuit Patent," 2006.

[124] V. M. Zatsiorsky, Z. M. Li, and M. L. Latash, "Enslaving effects in multi-finger force production." *Experimental brain research. Experimentelle Hirnforschung. Expérimentation cérébrale*, vol. 131, no. 2, pp. 187–95, Mar. 2000.

[125] R. Kõiva, B. Hilsenbeck, and C. Castellini, "FFLS: an accurate linear device for measuring synergistic finger contractions." in *Annual International Conference of the IEEE Engineering in Medicine and Biology Society.*, Jan. 2012, pp. 531–4.

[126] S. Sato, M. Shimojo, Y. Seki, A. Takahashi, and S. Shimizu, "Measuring system for grasping," in *Proceedings 5th IEEE International Workshop on Robot and Human Communication. RO-MAN'96 TSUKUBA.* IEEE, 1996, pp. 292–297.

[127] T. Sagisaka, Y. Ohmura, Y. Kuniyoshi, A. Nagakubo, and K. Ozaki, "High-density conformable tactile sensing glove," *2011 11th IEEE-RAS International Conference on Humanoid Robots*, pp. 537–542, Oct. 2011.

[128] G. Büscher, R. Kõiva, C. Schürmann, R. Haschke, and H. J. Ritter, "Tactile dataglove with fabric-based sensors," in *IEEE-RAS International Conference on Humanoid Robots*, 2012.

[129] J. Hermsdörfer, C. Marquardt, J. Philipp, A. Zierdt, D. Nowak, S. Glasauer, and N. Mai, "Grip forces exerted against stationary held objects during gravity changes." *Experimental brain research. Experimentelle Hirnforschung. Expérimentation cérébrale*, vol. 126, no. 2, pp. 205–14, May 1999.

[130] N. Nakazawa, Y. Uekita, H. Inooka, and R. Ikeura, "Experimental study on human's grasping force," *Proceedings 5th IEEE International Workshop on Robot and Human Communication. RO-MAN'96 TSUKUBA*, vol. 4, no. 3, pp. 280–285.

[131] M. Kondo, J. Ueda, and T. Ogasawara, "Recognition of in-hand manipulation using contact state transition for multifingered robot hand control," *Robotics and Autonomous Systems*, vol. 56, no. 1, pp. 66–81, Jan. 2008.

[132] R. Kõiva, R. Haschke, and H. Ritter, "Development of an intelligent object for grasp and manipulation research," *2011 15th International Conference on Advanced Robotics (ICAR)*, pp. 204–210, Jun. 2011.

[133] Analog Devices, "AD7490 16-Channel, 1 MSPS, 12-Bit ADC with Sequencer in 28-Lead TSSOP Data Sheet (Rev. D)," pp. 1–28, 2012.

[134] Xsens, "MTx-28A53G25 Datasheet," Tech. Rep., 2013. [Online]. Available: http://www.xsens.com/en/general/mtx

[135] K. Weiss and H. Worn, "The working principle of resistive tactile sensor cells," in *IEEE International Conference Mechatronics and Automation, 2005*, Institute for Process Control and Robotics. Karlsruhe: IEEE, pp. 471–476.

[136] USB Implementers Forum, "Universal Serial Bus Device Class Definition for Video Devices 1.1," 2005.

[137] Fourcc.org, "YUV2 Video Format Website." [Online]. Available: http://www.fourcc.org/yuv.php#YUY2

[138] J. Maycock, D. Dornbusch, C. Elbrechter, R. Haschke, T. Schack, and H. Ritter, "Approaching Manual Intelligence," *KI - Künstliche Intelligenz*, vol. 24, no. 4, pp. 287–294, Aug. 2010.

[139] Vicon Motion Systems, "Vicon MX Hardware System Reference," *2012*.

[140] Analog Devices, "ADXL330 Datasheet," 2012.

[141] InvenSense, "ITG-3200 Product Specification Revision 1.4," vol. 1, no. 408, pp. 1–39, 2010.

[142] SD GROUP, "SD Specifications Part 1 Physical Layer Simplified Specification," vol. 4.10, 2013.

[143] Infrared Data Association, "IrDA Homepage." [Online]. Available: http://www.irda.org/

[144] D. K. Borah, A. Boucouvalas, C. C. Davis, S. Hranilovic, and Y. Konstantinos, "A review of communication-oriented optical wireless systems," *EURASIP Journal for Wireless Communication and Networking*, vol. 91, pp. 1–28, 2012.

[145] Texas Instruments, "TIR1000, TIR1000I Standalone IrDA™ encoder and decoder," 1999. [Online]. Available: http://www.ti.com/product/tir1000

[146] K. Weiss, "Weiss Robotics Homepage." [Online]. Available: http://www.weiss-robotics.de/

[147] Eeonyx, "Eeontex Product Page," 2013. [Online]. Available: http://www.eeonyx.com/datasheets.php?type=eeontex

[148] G. Büscher, R. Kõiva, C. Schürmann, R. Haschke, and H. Ritter, "Flexible and stretchable fabric-based tactile sensor," in *IEEE/RSJ International Conference on Intelligent Robots and Systems (IROS 2012) Workshop on Advances in Tactile Sensing and Touch based Human-Robot Interaction*, 2012.

[149] Tekscan, "Grip System Homepage." [Online]. Available: http://www.tekscan.com/grip-pressure-measurement

[150] ——, "Tekscan equilibration description." [Online]. Available: http://www.tekscan.com/what-equilibration

[151] G. Papaioannou, V. Protopappas, T. Panagiotis, C. Mitrogiannis, G. Nianios, and S. Tashman, "A new method for pressure sensor equillibration and conditioning," *Brazilian Journal of Biomotricity*, pp. 176–195, 2008.

[152] Tekscan, "Tekscan Equilibration Device." [Online]. Available: http://www.tekscan.com/pb100t

[153] Schunk, "Schunk Robot SDH Robot Hand," 2013. [Online]. Available: http://mobile.schunk-microsite.com/de/produkte/produkte/servoelektrische-3-finger-greifhand-sdh.html

[154] H. Kawasaki, T. Komatsu, and K. Uchiyama, "Dexterous anthropomorphic robot hand with distributed tactile sensor: Gifu hand II," *IEEE/ASME Transactions on Mechatronics*, vol. 7, no. 3, pp. 296–303, Sep. 2002.

[155] L. B. Bridgwater, C. A. Ihrke, M. A. Diftler, M. E. Abdallah, N. A. Radford, J. M. Rogers, S. Yayathi, R. S. Askew, and D. M. Linn, "The Robonaut 2 hand - designed to do work with tools," in *2012 IEEE International Conference on Robotics and Automation*. IEEE, May 2012, pp. 3425–3430.

[156] Barrett Technology, "BarrettHand." [Online]. Available: http://www.barrett.com/robot/products-hand.htm

[157] M. Cutkosky, "On grasp choice, grasp models, and the design of hands for manufacturing tasks," *IEEE Transactions on Robotics and Automation*, vol. 5, no. 3, pp. 269–279, Jun. 1989.

[158] J. Steffen, R. Haschke, and H. Ritter, "Using Manifolds for Dextrous Hand Control," *RSS Workshop on Robot Manipulation: Intelligence in Human Environments*, 2008.

[159] D. A. Rosenbaum and M. J. Jorgensen, "Planning macroscopic aspects of manual control," *Human Movement Science*, vol. 11, no. 1-2, pp. 61–69, Feb. 1992.

[160] C. F. Adalbjornsson, M. G. Fischman, and M. E. Rudisill, "The end-state comfort effect in young children." *Research quarterly for exercise and sport*, vol. 79, no. 1, pp. 36–41, Mar. 2008.

[161] M. Weigelt and T. Schack, "The development of end-state comfort planning in preschool children." *Experimental psychology*, vol. 57, no. 6, pp. 476–782, Jan. 2010.

[162] M. G. Fischman, D. F. Stodden, and D. M. Lehman, "The end-state comfort effect in bimanual grip selection." *Research quarterly for exercise and sport*, vol. 74, no. 1, pp. 17–24, Mar. 2003.

[163] M. W. Short and J. H. Cauraugh, "Precision hypothesis and the end-state comfort effect." *Acta psychologica*, vol. 100, no. 3, pp. 243–52, Jan. 1999.

[164] ——, "Planning macroscopic aspects of manual control: end-state comfort and point-of-change effects." *Acta psychologica*, vol. 96, no. 1-2, pp. 133–47, Jun. 1997.

[165] D. J. Weiss, J. D. Wark, and D. A. Rosenbaum, "Monkey see, monkey plan, monkey do: the end-state comfort effect in cotton-top tamarins (Saguinus oedipus)." *Psychological science*, vol. 18, no. 12, pp. 1063–8, Dec. 2007.

[166] K. M. Chapman, D. J. Weiss, and D. A. Rosenbaum, "Evolutionary roots of motor planning: the end-state comfort effect in lemurs." *Journal of comparative psychology (Washington, D.C. : 1983)*, vol. 124, no. 2, pp. 229–32, May 2010.

[167] D. A. Rosenbaum, C. M. van Heugten, and G. E. Caldwell, "From cognition to biomechanics and back: The end-state comfort effect and the middle-is-faster effect," *Acta Psychologica*, vol. 94, no. 1, pp. 59–85, Oct. 1996.

[168] D. Gonzalez, B. E. Studenka, C. M. Glazebrook, and J. L. Lyons, "Extending end-state comfort effect: do we consider the beginning state comfort of another?" *Acta psychologica*, vol. 136, no. 3, pp. 347–53, Mar. 2011.

[169] A. Naceri, A. Moscatelli, and M. O. Ernst, "Modulation of Digit Normal Forces and Locations During Unconstrained Grasping," in *International Conference on Robotics and Automation*, 2013.

[170] G. H. Bucher, "The electric home of the future," *Popular Mechanics Magazine*, vol. 72, no. 2, pp. 161–167, 1939.

[171] A. O'Connor, "Kitchens of the future." [Online]. Available: http://www.moma.org/explore/inside_out/2010/09/22/kitchens-of-the-future/

[172] Popular Mechanics Magazine, "The electric home of the future," vol. 72, no. 2, 1939.

[173] Shonen Sunday magazine, "Computopia," 1969.

[174] Microsoft, "Microsoft Home," 2011. [Online]. Available: http://www.microsoft.com/en-us/news/features/2011/aug11/08-08MicrosoftHome.aspx

[175] E. Aarts and R. Wichert, "Ambient intelligence," in *Technology Guide*, 2009, pp. 244–249.

[176] C. Ramos, J. C. Augusto, and D. Shapiro, "Ambient Intelligence—the Next Step for Artificial Intelligence," *IEEE Intelligent Systems*, vol. 23, no. 2, pp. 15–18, Mar. 2008.

[177] C. Schürmann, R. Kõiva, R. Haschke, and H. Ritter, "A modular high-speed tactile sensor for human manipulation research," *2011 IEEE World Haptics Conference*, pp. 339–344, Jun. 2011.

[178] J. Illingworth and J. Kittler, "A Survey of the Hough Transform," *Computer vision, Graphics and image processing*, vol. 47, pp. 87–116, 1988.

[179] J. Psotka, "Immersive training systems: Virtual reality and education and training," *Instructional Science*, vol. 23, no. 5-6, pp. 405–431, Nov. 1995.

[180] R. M. Satava, "Virtual reality surgical simulator," *Surgical Endoscopy*, vol. 7, no. 3, pp. 203–205, 1993.

[181] T. P. Grantcharov, V. B. Kristiansen, J. Bendix, L. Bardram, J. Rosenberg, and P. Funch-Jensen, "Randomized clinical trial of virtual reality simulation for laparoscopic skills training." *The British journal of surgery*, vol. 91, no. 2, pp. 146–50, Feb. 2004.

[182] A. S. Carlin, H. G. Hoffman, and S. Weghorst, "Virtual reality and tactile augmentation in the treatment of spider phobia: a case report," *Behaviour Research and Therapy*, vol. 35, no. 2, pp. 153–158, Feb. 1997.

[183] B. O. Rothbaum, L. F. Hodges, R. Kooper, D. Opdyke, J. S. Williford, and M. North, "Virtual reality graded exposure in the treatment of acrophobia: A case report," *Behavior Therapy*, vol. 26, no. 3, pp. 547–554, Jun. 1995.

[184] NASA, "VR Goggles / Dataglove Photo." [Online]. Available: https://commons.wikimedia.org/wiki/File:AC89-0437-20_a.jpeg

[185] Gottfried Roosen and HAPTION Deutschland, "Photo: Haption Virtuose 6Dof Force-Feedback Montage." [Online]. Available: http://commons.wikimedia.org/wiki/File:Haption_Virtuose_6Dof_Force-Feedback_Montage.jpg

[186] P. Langhorne, F. Coupar, and A. Pollock, "Motor recovery after stroke: a systematic review." *Lancet neurology*, vol. 8, no. 8, pp. 741–54, Aug. 2009.

[187] M. Hubli and V. Dietz, "The physiological basis of neurorehabilitation - locomotor training after spinal cord injury." *Journal of neuroengineering and rehabilitation*, vol. 10, p. 5, Jan. 2013.

[188] M. K. Holden, "Virtual environments for motor rehabilitation: review." *Cyberpsychology & behavior : the impact of the Internet, multimedia and virtual reality on behavior and society*, vol. 8, no. 3, pp. 187–211; discussion 212–9, Jun. 2005.

[189] C. Cruz-Neira, D. J. Sandin, and T. A. DeFanti, "Surround-screen projection-based virtual reality," in *Proceedings of the 20th annual conference on Computer graphics and interactive techniques - SIGGRAPH '93*. New York, New York, USA: ACM Press, 1993, pp. 135–142.

[190] T. Lentz, D. Schröder, M. Vorländer, and I. Assenmacher, "Virtual Reality System with Integrated Sound Field Simulation and Reproduction," *EURASIP Journal on Advances in Signal Processing*, vol. 2007, no. 1, p. 070540, 2007.

[191] G. C. Burdea, "Haptic Feedback for Virtual Reality," *Virtual Reality and Prototyping Workshop*, no. June, 1999.

[192] J. Steuer, "Defining Virtual Reality: Dimensions Determining Telepresence," *Journal of Communication*, vol. 42, no. 4, pp. 73–93, Dec. 1992.

[193] R. U. I. Loureiro, F. Amirabdollahian, M. Topping, B. Driessen, and W. Harwin, "Upper Limb Robot Mediated Stroke Therapy—GENTLE/s Approach," *Autonomous Robots*, vol. 15, no. 1, pp. 35–51, 2003.

[194] Moog, "Haptic Master," 2013. [Online]. Available: http://www.moog.com/products/haptics-robotics/

[195] F. Amirabdollahian, R. Loureiro, and W. Harwin, "Minimum jerk trajectory control for rehabilitation and haptic applications," *Proceedings 2002 IEEE International Conference on Robotics and Automation (Cat. No.02CH37292)*, vol. 4, no. May, pp. 3380–3385, 2002.

[196] S. V. Adamovich, G. G. Fluet, A. S. Merians, A. Mathai, and Q. Qiu, "Incorporating haptic effects into three-dimensional virtual environments to train the hemiparetic upper extremity." *IEEE transactions on neural systems and rehabilitation engineering : a publication of the IEEE Engineering in Medicine and Biology Society*, vol. 17, no. 5, pp. 512–20, Oct. 2009.

[197] K. Salisbury, F. Conti, and F. Barbagli, "Haptic rendering: introductory concepts." *IEEE computer graphics and applications*, vol. 24, no. 2, pp. 24–32.

[198] M. S. Cameirão, S. B. I. Badia, E. D. Oller, and P. F. M. J. Verschure, "Neurorehabilitation using the virtual reality based Rehabilitation Gaming System: methodology, design, psychometrics, usability and validation." *Journal of neuroengineering and rehabilitation*, vol. 7, p. 48, Jan. 2010.

[199] Cybergloves Systems, "CyberGlove ® II," 2012. [Online]. Available: http://www.cyberglovesystems.com

[200] ——, "Cybergrasp," 2013.

[201] A. S. Merians, G. G. Fluet, Q. Qiu, S. Saleh, I. Lafond, A. Davidow, and S. V. Adamovich, "Robotically facilitated virtual rehabilitation of arm transport integrated with finger movement in persons with hemiparesis." *Journal of neuroengineering and rehabilitation*, vol. 8, no. 1, p. 27, Jan. 2011.

[202] T. H. Massie and T. Systems, "The PHANTOM Haptic Interface: A Device for Probing Virtual Objects," *Proceedings of the ASME Winter Annual Meeting*, 1994.

[203] Force Dimension, "Omega Haptic Device." [Online]. Available: http://www.forcedimension.com/products

[204] G. Nikolakis, D. Tzovaras, S. Moustakidis, and M. G. Strintzis, "CyberGrasp and PHANTOM Integration: Enhanced Haptic Access for Visually Impaired Users," in *Speech and Computer*, 2004.

[205] Blender Foundation, "Blender," 2013. [Online]. Available: http://www.blender.org/

[206] C. Elbrechter, M. Götting, and R. Haschke, "Image Component Library." [Online]. Available: http://www.iclcv.org/

[207] Real-Time Physics Simulation, "Bullet Engine Homepage." [Online]. Available: http://bulletphysics.org/wordpress/

[208] C. Castellini and R. Kõiva, "Using surface electromyography to predict single finger forces," *2012 4th IEEE RAS & EMBS International Conference on Biomedical Robotics and Biomechatronics (BioRob)*, pp. 1266–1272, Jun. 2012.

[209] Herodotus, *Histories*, 440 B.C.

[210] Pliny the Elder, *Natural History*, 77 A.D.

[211] Wikipedia, "Schematic: Berlichingen Hand," 2013. [Online]. Available: http://commons.wikimedia.org/wiki/File:Götz-eiserne-hand2.jpg

[212] Otto Bock, "Michelangelo Hand." [Online]. Available: http://www.ottobock.de/cps/rde/xchg/ob_com_en/hs.xsl/49464.html

[213] TouchBionics, "TouchBionics Homepage." [Online]. Available: http://www.touchbionics.com/

[214] E. Biddiss and T. T. Chau, "Upper limb prosthesis use and abandonment: a survey of the last 25 years." *Prosthetics and orthotics international*, vol. 31, no. 3, pp. 236–57, Sep. 2007.

[215] C. Cortes and V. Vapnik, "Support-vector networks," *Machine Learning*, vol. 20, no. 3, pp. 273–297, Sep. 1995.

[216] S. Bitzer and P. van der Smagt, "Learning EMG control of a robotic hand: towards active prostheses," *Proceedings 2006 IEEE International Conference on Robotics and Automation, 2006. ICRA 2006.*, no. May, pp. 2819–2823, 2006.

[217] C. Castellini and R. Kõiva, "Intention Gathering from Muscle Residual Activity for the Severely Disabled," in *IEEE/RSJ International Conference on Intelligent Robots and Systems (IROS 2012), Workshop on Progress, Challenges and Future Perspectives in Navigation and Manipulation Assistance for Robotic Wheelchairs*, Vilamoura, Algarve, Portugal, 2012.

[218] C. Castellini and R. Koiva, "Using a high spatial resolution tactile sensor for intention detection." in *IEEE Rehabilitation Robotics (ICORR)*, Jun. 2013, pp. 1–7.

[219] H. Forssberg, A. Eliasson, H. Kinoshita, R. Johansson, and G. Westling, "Development of human precision grip I: Basic coordination of force," *Experimental Brain Research*, vol. 85, no. 2, pp. 451–457, Jun. 1991.

[220] H. Forssberg, A. Eliasson, H. Kinoshita, G. Westling, and R. Johansson, "Development of human precision grip," *Experimental Brain Research*, vol. 104, no. 2, pp. 323–330, May 1995.

[221] H. Kinoshita and P. R. Francis, "A comparison of prehension force control in young and elderly individuals." *European journal of applied physiology and occupational physiology*, vol. 74, no. 5, pp. 450–60, Jan. 1996.

[222] M. A. Srinivasan, J. M. Whitehouse, and R. H. LaMotte, "Tactile detection of slip: surface microgeometry and peripheral neural codes." *Journal of neurophysiology*, vol. 63, no. 6, pp. 1323–32, Jun. 1990.

[223] R. Johansson and G. Westling, "Signals in tactile afferents from the fingers eliciting adaptive motor responses during precision grip," *Experimental Brain Research*, vol. 66, no. 1, pp. 141–154, Mar. 1987.

[224] M. Schöpfer, C. Schürmann, M. Pardowitz, and H. Ritter, "Using a Piezo-Resistive Tactile Sensor for Detection of Incipient Slippage," *International Symposium on Robotics*, pp. 2–7, 2010.

[225] M. Schöpfer, "Tactile Perception of Cognitive Robots," Ph.D. dissertation, Bielefeld University, 2011.

[226] E. O. Brigham and R. E. Morrow, "The fast Fourier transform," *IEEE Spectrum*, vol. 4, no. 12, pp. 63–70, Dec. 1967.

[227] R. P. Lippmann, "An introduction to computing with neural nets," *ACM SIGARCH Computer Architecture News*, vol. 16, no. 1, pp. 7–25, Mar. 1988.

[228] M. Schöpfer, "Grasp Force Adaption Using Ultra-Fast Tactile Sensors." [Online]. Available: http://www.youtube.com/watch?v=mSq8e4PU90s

[229] Q. Li, R. Haschke, B. Bolder, and H. Ritter, "Grasp Point Optimization by Online Exploration of Unknown Object Surface," *Humanoids*, 2012.

[230] S. J. Lederman and R. L. Klatzky, "Hand movements: a window into haptic object recognition." *Cognitive psychology*, vol. 19, no. 3, pp. 342–68, Jul. 1987.

[231] N. Chen, H. Zhang, and R. Rink, "Edge tracking using tactile servo," *Proceedings 1995 IEEE/RSJ International Conference on Intelligent Robots and Systems. Human Robot Interaction and Cooperative Robots*, vol. 2, pp. 84–89, 1995.

[232] H. Zhang and N. Chen, "Control of contact via tactile sensing," *IEEE Transactions on Robotics and Automation*, vol. 16, no. 5, pp. 482–495, 2000.

[233] Q. Li, C. Schürmann, R. Haschke, and H. Ritter, "A control framework for tactile servoing," in *Robotics: Science and Systems Conference*, 2013.

[234] V. A. Ho, T. Nagatani, A. Noda, and S. Hirai, "What can be inferred from a tactile arrayed sensor in autonomous in-hand manipulation?" *2012 IEEE International Conference on Automation Science and Engineering (CASE)*, pp. 461–468, Aug. 2012.

[235] M. Huber, "A Hybrid Architecture for Adaptive Robot Control," Ph.D. dissertation, 2000.

[236] O. Brock, A. Fagg, R. Grupen, R. Platt, M. Rosenstein, and J. Sweeney, "a Framework for Learning and Control in Intelligent Humanoid Robots," *International Journal of Humanoid Robotics*, vol. 02, no. 03, pp. 301–336, Sep. 2005.

[237] M. Schöpfer, F. Schmidt, M. Pardowitz, and H. Ritter, "Open source real-time control software for the Kuka light weight robot," in *2010 8th World Congress on Intelligent Control and Automation*. IEEE, Jul. 2010, pp. 444–449.

[238] Q. Li, "Video: Tactile servoing." [Online]. Available: http://www.youtube.com/watch?v=TcWipks3qJ0

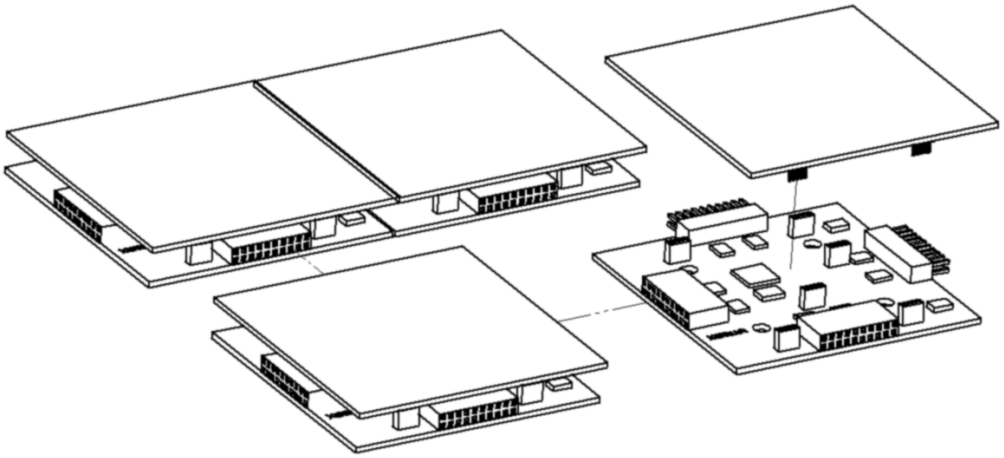

Thanks for reading -
A 2x2 Myrmex array has just the right size for a hand to wave goodbye!